

**CZECH TECHNICAL
UNIVERSITY IN PRAGUE**

**FACULTY OF
MECHANICAL
ENGINEERING**



MASTER'S THESIS

2022

DÁVID MAMRILLA

I. OSOBNÍ A STUDIJNÍ ÚDAJE

Příjmení: **Mamrilla** Jméno: **Dávid** Osobní číslo: **466465**
Fakulta/ústav: **Fakulta strojní**
Zadávací katedra/ústav: **Ústav energetiky**
Studijní program: **Energetika a procesní inženýrství**
Specializace: **Energetika**

II. ÚDAJE K DIPLOMOVÉ PRÁCI

Název diplomové práce:

Perspektivy parního oběhu pro využití biomasy v energetice nízkých výkonů

Název diplomové práce anglicky:

Perspectives of Rankine cycle for the use of biomass in low power generation

Pokyny pro vypracování:

Laboratoř organických Rankinových cyklů a jejich aplikací (LORCA) na ČVUT UCEEB se systematicky věnuje výzkumu a vývoji technologií využívajících biomasu pro decentralizovanou energetiku, zejména v oblasti tzv. mikrokogenerace. V posledních letech se objevily možnosti nasazení objemových expandérů v oblasti teplot pracovních látek přes 200°C, což otevírá dříve omezené možnosti úvah o využití vody jako pracovní látky.

Globálním cílem práce je vyhotovení teoretické studie pro odhad parametrů zařízení využívajícího tepla ze spalování biomasy k transformaci na elektřinu (případně KVET) pomocí Rankinova-Clausiova oběhu využívajícího vodní páru.

Výsledkem práce je detailní vhled do zadané problematiky a doporučení, které budou dále sloužit jako vstup pro navazující koncepční práce.

Práce bude obsahovat:

Rešerše komerčně dostupných technologií na biomasu, které jsou prakticky aplikovatelné pro výrobu elektřiny (případně KVET) z biomasy v oblasti mikrokogenerace, tedy do 50 kW elektrického výkonu

Rešerše vývoje technologií využívajících biomasu pro mikrokogeneraci

Rešerše problematiky vývoje parních oběhů pro vysoké parametry páry, problematika volby materiálu, možnosti přenosu informací do oblasti nízkých výkonů

Rešerše možností nasazení objemových expandérů pro využití vodní páry

Návrh geometrie vybraného expandéru

Vytvoření matematického popisu zvoleného objemového expandéru a zhodnocení možností jeho nasazení pro parní oběh s tepelným výkonem do 250 kW

Diskuse možností propojení studovaného parního oběhu s existujícím ORC oběhem využívaným na ČVUT UCEEB v zařízení Wave

Definování okrajových podmínek pro navazující koncepční práce

Seznam doporučené literatury:

Dle pokynů vedoucího práce, zdroje dostupné branou EIZ.

According to the supervisor's instructions, the resources available through the EIZ gateway.

Jméno a pracoviště vedoucí(ho) diplomové práce:

Ing. Jakub Maščuch, Ph.D. ústav energetiky FS

Jméno a pracoviště druhé(ho) vedoucí(ho) nebo konzultanta(ky) diplomové práce:

Datum zadání diplomové práce: **21.04.2022**

Termín odevzdání diplomové práce: **03.06.2022**

Platnost zadání diplomové práce: **31.12.2023**

Ing. Jakub Maščuch, Ph.D.
podpis vedoucí(ho) práce

podpis vedoucí(ho) ústavu/katedry

doc. Ing. Miroslav Španiel, CSc.
podpis děkana(ky)

III. PŘEVZETÍ ZADÁNÍ

Diplomant bere na vědomí, že je povinen vypracovat diplomovou práci samostatně, bez cizí pomoci, s výjimkou poskytnutých konzultací. Seznam použité literatury, jiných pramenů a jmen konzultantů je třeba uvést v diplomové práci.

Datum převzetí zadání

Podpis studenta

Declaration

I declare that this thesis is my own work, that I have compiled it on my own under the guidance of my supervisor and that I have used only the sources cited in the attached bibliography in accordance with the Guideline no. 1/2009 For adhering to ethical principles when elaborating on academic final thesis.

In Prague on June 3rd, 2022

Bc. Dávid Mamrilla

Anotační list

Jméno autora:	Dávid Mamrilla
Název DP:	Perspektivy Rankinova oběhu pro využití biomasy v energetice nízkých výkonů
Akademický rok:	2021/2022
Ústav / Odbor:	Ústav energetiky / Energetika
Vedoucí DP:	Ing. Jakub Maščuch, Ph.D.
Bibliografické údaje:	Počet stran: 89 Počet obrázků: 55 Počet tabulek: 27 Počet příloh: 6
Klíčová slova:	Rankinův oběh, kogenerace, energetika nízkých výkonů, objemové expandéry
Abstrakt	<p>Tato práce zkoumá možnosti nasazení Rankinova parního oběhu v malé kogenerační jednotce využívající biomasu jako palivo. Jejím hlavním cílem je prozkoumat potenciál použití vysokých parametrů páry v kontextu vývoje nových materiálů pro parní elektrárny. Na základě rešerše komerčních i vývojových technologií je zvolen typ expandéru, kterého chování je popsáno volně dostupným semi-empirickým termodynamickým modelem.</p> <p>Pro několik konkrétních expandérů je provedena citlivostní analýza zkoumající vliv admisní teploty a tlaku na výkon a účinnost kogenerační jednotky. Je prezentována a prozkoumaná i možnost propojení studovaného parního oběhu s existujícím ORC oběhem uplatněným v zařízení WAVE vyvinutým na ČVUT UCEEB.</p> <p>Následně jsou shrnuty dosahované výsledky, jejich srovnání s existujícími technologiemi a doporučené parametry. Závěr obsahuje doporučení dalších cest výzkumu pro navazující práce.</p>

Annotation sheet

Author:	Dávid Mamrilla
Thesis title:	Perspectives of Rankine cycle for the use of biomass in low power generation
Academical year:	2021/2022
Department / specialization:	Department of Energy Engineering / Energy engineering
Thesis supervisor:	Ing. Jakub Maščuch, Ph.D.
Bibliographical information:	Number of pages: 89 Number of figures: 55 Number of tables: 27 Number of appendices: 6
Keywords:	Rankine cycle, cogeneration, micro-scale generation, volumetric expanders
Abstract:	<p>This work explores possibilities of applying the steam Rankine cycle in a small cogeneration unit employing biomass as a fuel. Its main goal is to explore the potential of utilizing high steam parameters in the context of development of new materials for steam power plants. Based on the research of commercial and developmental technologies, a type of expander is selected, and its behaviour is described by a freely available semi-empirical thermodynamic model.</p> <p>Sensitivity analysis is performed for several specific expanders, investigating the influence of admission temperature and pressure on the power output and efficiency of the CHP unit. The possibility of connecting the explored steam cycle with the ORC employed in the WAVE CHP unit developed at CTU UCEEB is also examined and presented.</p> <p>Next, the attained results, their comparison with existing technologies and recommended parameters are summarized. The conclusion includes recommendations for further development pathways for subsequent works.</p>

Acknowledgements

I would like to express my immense gratitude to my supervisor Ing. Jakub Maščuch, Ph.D. for his patience, guidance, and an incredible wealth of knowledge, as well as for his ever-present enthusiasm and passion. His dedication and support are what made writing and completing this thesis not only possible, but also enjoyable and fulfilling.

Great acknowledgement goes also to my colleagues and tutors Ing. Jan Špale and Ing. Václav Novotný, Ph.D. for their kind advice and insights that they have provided me while compiling this work and throughout my studies.

Special thanks goes to my friends Bc. Tomáš Stanovčák, Ing. Miroslav Rathan and Bc. Ondrej Jarina for their help and advice regarding Python and MATLAB programming. To my teachers and classmates at CTU Prague, I am deeply grateful that they have made the final years of my studies so immensely educative and worthwhile.

Last but not least, I would like to thank all of my family and friends for their love and support. They kept me going and this work would not have been possible without them.

Table of contents

Chapter 1: Introduction.....	1
1.1 The Rankine cycle.....	1
1.2 Combined heat and power (CHP) generation	3
Chapter 2: Biomass-fired CHP technologies up to 50 kW _e	5
2.1 Advantages and perspectives of micro cogeneration	5
2.2 Commercially available biomass technologies	5
2.3 Research projects and development regarding biomass micro-CHP technologies	6
Chapter 3: Steam cycles utilizing high-parameter steam	8
3.1 High pressure and temperature steam in high-power applications	8
3.1.1 Current state-of-the-art.....	8
3.1.2 Brief history of development of supercritical plants.....	9
3.2 Materials of components	10
3.2.1 Low-alloyed ferritic and martensitic steel grades	10
3.2.2 High-alloyed martensitic steel grades	11
3.2.3 Nickel-based alloys	11
3.3 Utilising high-parameter steam in low-power applications	12
Chapter 4: Expanders.....	14
4.1 Overview	14
4.2 Demands on a micro-scale cogeneration plant expander	15
4.3 Piston.....	16
4.3.1 General information	16
4.3.2 Modifications	16
4.3.3 Specifications and uses	17
4.4 Screw.....	17
4.4.1 General information	17

4.4.2	Modifications	18
4.4.3	Specifications and uses	20
4.5	Scroll	20
4.5.1	General information	20
4.5.2	Modifications	21
4.5.3	Specifications and uses	21
4.6	Vane	22
4.6.1	General information	22
4.6.2	Modifications	22
4.6.3	Specifications and uses	23
4.7	Evaluation, expander choice, reasoning	23
Chapter 5:	Single-screw expander – description and geometric parameters	28
5.1	Characteristics of the single-screw expander	28
5.2	Geometry and leakage of single-screw machines	29
Chapter 6:	Mathematical modelling of a single-screw expander	32
6.1	Available thermodynamic models of screw expanders	32
6.2	Description of used thermodynamic model	32
6.2.1	Mathematical modelling	34
6.2.2	The calculation environment	37
6.3	Geometry design model	38
6.4	Boundary conditions of the examined steam cycles and desired outputs	43
6.4.1	Boundary conditions for two variants of the Rankine cycle	44
6.4.2	Limitations, assumptions and possible inaccuracies of used models	46
Chapter 7:	Defining the geometry of appropriate expanders for two pressure levels	48
7.1	Expanders for the 100 °C condensation variant (Variant 1)	48
7.1.1	Demands on the expanders and desired outputs	48
7.1.2	Determining how BVR influences the cycle	49

7.1.3	Determining how BVR in combination with V_{sw} influences the cycle	54
7.1.4	Defining expander parameters for further testing	56
7.2	Expanders for the 200 °C condensation variant (Variant 2)	57
7.2.1	Determining how BVR influences the cycle	57
7.2.2	Determining how BVR in combination with V_{sw} influences the cycle	58
7.2.3	Discussion on the impact of leakage losses for Variant 2	61
7.2.4	Determining the behaviour in Variant 2 with constant leakage area	63
Chapter 8:	Obtaining the outputs for a range of working conditions for the examined expanders	67
8.1	Sensitivity analysis for Variant 1	67
8.1.1	Expander A	67
8.1.2	Expander B.....	68
8.1.3	Expander C.....	69
8.1.4	Expander D	70
8.1.5	Exhaust temperature, filling factor and losses	71
8.2	Sensitivity analysis for Variant 2	74
8.2.1	Expander E.....	75
8.2.2	Expander F.....	76
8.2.3	Volumetric performance	77
8.3	Recommended ranges of inlet steam parameters	77
8.3.1	Ranges of viable inlet conditions for Variant 1	78
8.3.2	Ranges of viable inlet conditions for Variant 2	81
Chapter 9:	Evaluation of performance and perspectives of studied expanders	85
9.1	Comparison of obtained results with commercial and research projects	85
9.2	Possibilities of connecting a steam Rankine cycle with a bottoming ORC	85
9.3	Defining boundary conditions and recommendations for subsequent conceptual studies	88
Conclusion	90

List of Figures	92
List of Tables	95
List of graphs	97
Bibliography	99
List of appendices	107
Appendix A Geometry of designed expanders	108

List of symbols

A	area [mm]
a	coefficient for leakage area [m ²] or [m ² ·bar ⁻¹] or distance [mm]
AU	heat transfer coefficient [kW·K ⁻¹]
BVR	built-in volume ratio
b_{nc}	coefficient for losses from natural convection [kW·K ^{-1,25}]
c_p	specific heat capacity at constant pressure [kJ·kg ⁻¹ ·K ⁻¹]
D	diameter [mm]
d	distance [mm]
E	exergy [kW]
FF	filling factor [-]
f	mechanical losses coefficient [m ³] or [m ³ ·s·bar]
H	head [kJ]
h	specific enthalpy [kJ·kg ⁻¹]
i	meshing pair ratio [-]
K	geometric coefficient [m ^{1,8}]
L	length [mm]
ṁ	mass flow rate [kg·s ⁻¹]
n	number of grooves [-]
N	rotational speed [rpm]
Nu	Nusselt number [-]
P	power [kW]
p	pressure [MPa]
Pr	Prandtl number [-]
Q	heat output [kW]
R	radius [mm]
Re	Reynolds number [-]
s	specific entropy [kJ·kg ⁻¹ ·K ⁻¹]
T	temperature [°C]
U	thermal transmittance [kW·m ⁻² ·K ⁻¹]
v	specific volume [m ³ ·kg ⁻¹]

V	volume [m ³]
\dot{V}	volumetric flow [m ³ ·s ⁻¹]
w	width [mm]
x	steam quality [-]
z	number of grooves or teeth
α	angle [rad]
β	angle [rad]
γ	angular spacing of the starwheel teeth [rad]
Δ	difference [-]
ε	pressure ratio [-]
η	efficiency [%]
θ	main rotor or starwheel angle [rad]
λ	thermal conductivity [kW·m ⁻¹ K] or sometimes ratio [-]
μ	dynamic viscosity [Pa·s]
ξ	starwheel tooth width parameter [-]
ρ	density [kg·m ⁻³]
ω	rotational speed [rad·s ⁻¹]

List of subscripts

ad	admission
amb	ambient
CHP	combined heat and power
close	closed
conf	configuration
crit	critical
cycle	cycle
d	discharge
eff	effective
el	electric
eng	engaging
ex	exhaust, exergy
exp	expander
gen	generator
g	groove
hx	heat exchange
in	inlet or inner
int	internal
leak	leakage
load	load
loss	loss
m	mechanical
max	maximum
net	net
open	opened
opt	optimal
ORC	organic Rankine cycle
out	outlet
RC	Rankine cycle
rot	rotation

s	suction
sh	shaft
sr	screw rotor
su	supply
system	system
sw	swept, starwheel
t	tooth
th	thermal
vol	volumetric
w	wall of the isothermal envelope
0	point 0 in the thermodynamic model or the dead state
1 - 6	points 1 – 6 in the thermodynamic model

List of acronyms

A-USC	advanced ultra-supercritical
C	cylindrical
CHP	combined heat and power
HP	high pressure
IP	intermediate pressure
ORC	organic Rankine cycle
P	plate
RC	Rankine cycle
SC	supercritical
SSE	single-screw expander
TS	tensile strength
USC	ultra-supercritical
Var	variant
YS	yield strength

Chapter 1: Introduction

1.1 The Rankine cycle

The Rankine cycle (RC) is a thermodynamic cycle which utilizes phase change of the working fluid. Based on the selection of the working fluid, the RC can be categorized into steam Rankine cycles and organic Rankine cycles (ORC). Nevertheless, the well-known principle of the cycle remains the same. Firstly, liquid is compressed in a pump (1 → 2); then, it runs through a boiler or other heat source where it is turned into vapour or steam and usually superheated (2 → 3); the vapour or steam then enters an expander, usually a turbine, where it expands, doing work in the process (3 → 4); finally, the steam or vapour, which is now at low pressure, is condensed in the condenser and the cycle repeats itself (4 → 1).

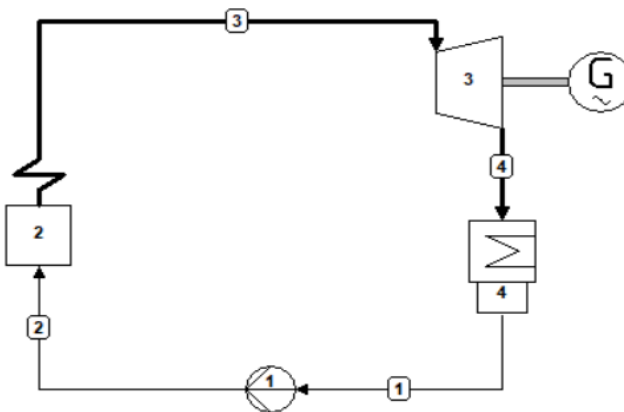


Figure 1 - Scheme of a simple RC

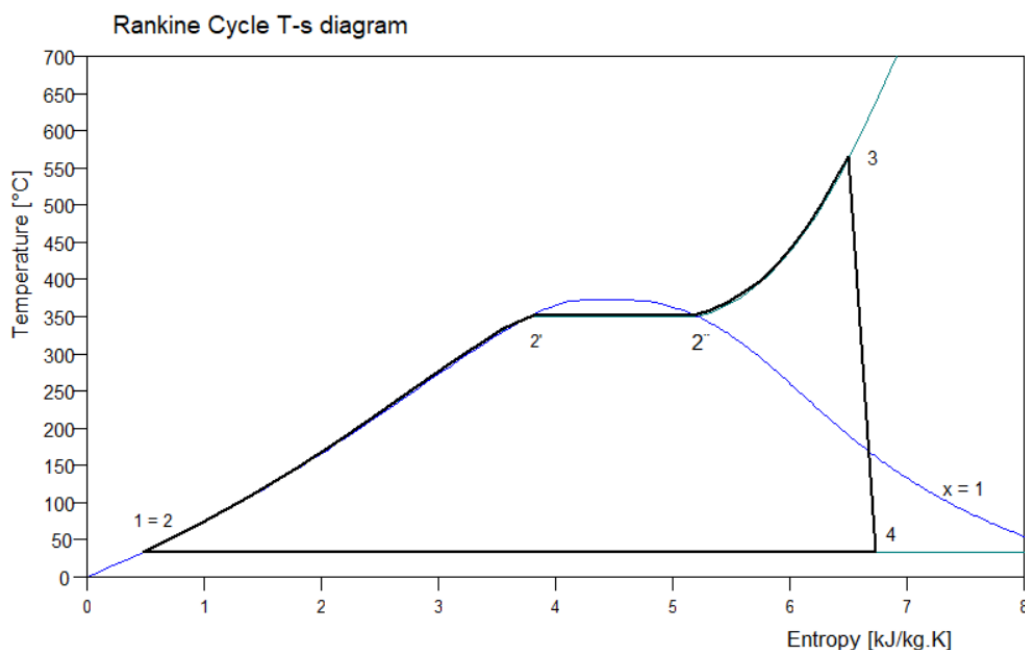


Figure 2 - T-s diagram of a simple RC¹

¹ Figures 1 and 2 were obtained from the Cycle-Tempo software

The Rankine steam cycle is the most widely used thermodynamic cycle in large-scale power generation. While its properties and modifications in high power applications are well studied and understood, utilizing it in low-power applications is not as thoroughly examined. Organic Rankine Cycles (ORC) have been developed in recent years to replace the steam cycle at low power and waste heat recovery applications, thanks to favourable properties of organic fluids such as low boiling point and dry expansion. However, steam has undisputed advantages, especially when a high-temperature heat source such as boiler is available.

Firstly, water has better heat transfer characteristics than organic fluids. This results in lower mass flow rates and therefore smaller heat exchangers and condensers. Secondly, water is a cheaper, more accessible and less dangerous working fluid than its organic counterparts. Furthermore, the problem of wet expansion with steam can be resolved if a high-temperature heat source is available, thus enabling higher superheating on the inlet, or if volumetric expanders, which are not threatened by droplet erosion to a large degree, are used instead of a turbine [1] [2].

It is well-known that the Rankine cycle efficiency increases with increasing steam temperature and pressure at the turbine inlet. For each temperature of the superheated steam, there is a peak in efficiency for a specific pressure as illustrated in Fig. 4.

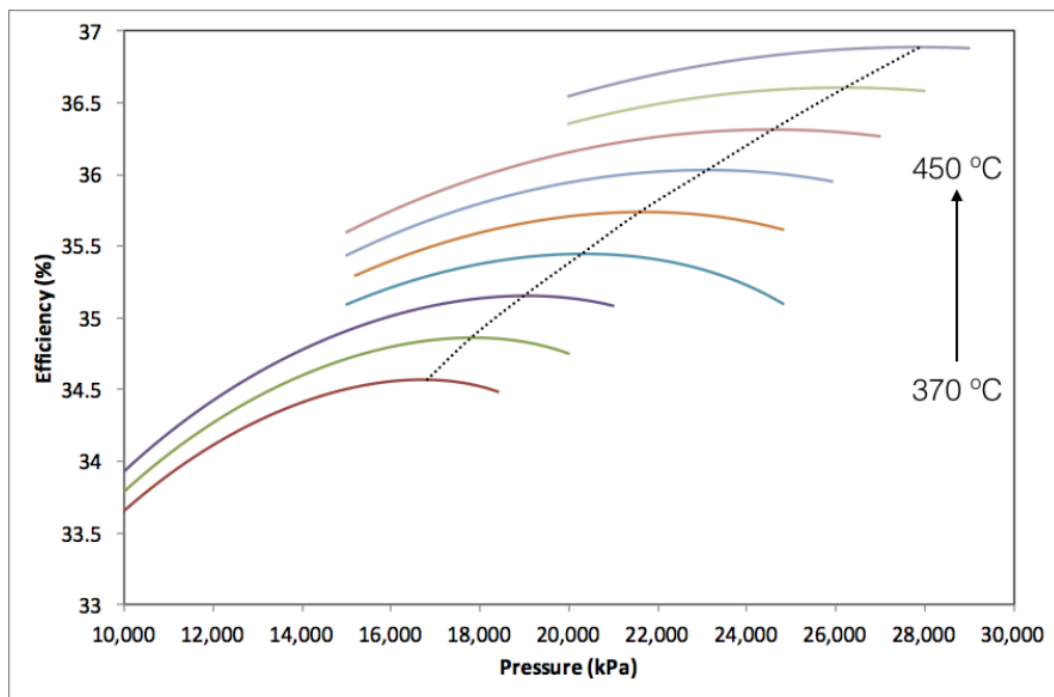


Figure 3 - Efficiency of the RC on steam temperature and pressure from 370 up to 450 C. The condensation pressure is 10 kPa. The dotted line displays the optimum pressure for each temperature [3].

For this reason, utilising high inlet parameters of steam is an important factor when designing any steam cycle. The effort of maximizing the parameters of inlet steam led to the development of modern supercritical and ultra-supercritical power plants which are used in high power generation and are briefly described in chapter 4.

1.2 Combined heat and power (CHP) generation

A combined heat and power plant produces electricity and useful heat simultaneously, boosting the plant's efficiency. Even state-of-the-art steam power plants can reach efficiencies of up to 48% when producing electricity only, while CHP plants often reach up to 80% or higher thanks to utilizing some or all of the exhaust heat that would otherwise go to waste [4].

For efficiency of a plant producing electricity only:

$$\eta_{net} = \frac{W_{el}}{Q_{in}} = \frac{Q_{in} - Q_{out}}{Q_{in}} \quad (1)$$

Whereas for a CHP plant:

$$\eta_{net} = \frac{W_{el} + Q_U}{Q_{in}} = \frac{Q_{in} - Q_{loss}}{Q_{in}} \quad (2)$$

Where η_{net} is the net efficiency, W_{el} is the electric work, Q_{in} is the heat input from the fuel, Q_{out} is the rejected heat, Q_U is useful heat and Q_{loss} represents the heat losses [4].

The size of CHP plants varies widely, from large centralised plants of over 1 GW [5] to small domestic units of 1 kW. Technologies applied in these plants are numerous – from combined cycles, gas and steam turbines, through microturbines, internal combustion engines and organic Rankine cycles (ORCs) to fuel cells and Stirling engines.

Main advantages of CHP plants are therefore high efficiency and high degree of fuel utilization, along with increased energy security, diversity of energy sources, flexibility and affordability [6]. CHP technologies are applied in municipal, district or commercial building heating or in the industrial and marine sector [7].

Large-scale CHP, typically defined as installations over 2 MW, has been used worldwide since the beginnings of the 20th century. In large industrial applications, exhaust gas from a gas turbine is frequently used to heat a process, while back-pressure steam turbines are widely applied in CHP plants for district heating.

However, the widest range of applications for cogeneration falls into small (100 kW – 2 MW) or micro (up to 50 kW) scale. They can be widely applied for domestic, municipal, and industrial uses. The heat for these plants can be provided either by combusting fuel or by utilizing waste heat [6]. A report developed in the frame of the CODE2 project estimates the potential for annual sold micro-CHP systems in the EU for residential applications (up to 5 kW_e) of about 2,9 million and for small and medium business application (up to 50 kW_e) of about 68 000 units in 2030. This would amount to a cost-effective potential for cogeneration to deliver 20% of electricity and 25% of heat in the EU [8] [9].

CHP technology	Approximate power range applied in CHP	Approximate electric efficiency range [%]	Approximate peak CHP efficiency [%]
CCGT	20 MW - 600 MW	30 - 55	85
Gas turbine	2 MW - 500 MW	20 - 45	80
Steam turbine	500 kW - 850 MW	15 - 47	75
Internal combustion engine	5kW - 10 MW	25 - 40	90
ORC	1 kW – 1.5 MW	5 - 15	90
Microturbine	30 kW - 250 kW	25 - 30	75
Fuel cell	5 kW - 1 MW	30 - 40	75
Stirling engine	0,6 kW - 50 kW	10 - 30	95

Table 1 - Overview of main CHP technologies and their characteristics [5] [6] [8]

While large-scale steam CHP technologies are technologically feasible and widely employed, scaling a steam power or CHP plant down below the 500 kW threshold becomes problematic mainly due to difficulties with selecting and designing the appropriate expansion machine. Large power stations use turbines for steam expansion due to their high efficiency, reliability and scalability in a very wide range of power outputs. In a small-scale Rankine cycle below 500 kW, deploying turbines becomes problematic due to low mass flow rates, which causes poor efficiency, high production costs and danger of erosion of the turbine blades due to expansion into wet steam [1].

Chapter 2: Biomass-fired CHP technologies up to 50 kW_e

2.1 Advantages and perspectives of micro cogeneration

Modern trends in energetics are focused on improving sustainability, decreasing the impact of power generation on the environment, and maximizing the efficiency of fuel economy. Micro- and small-scale cogeneration and waste heat recovery hold significant potential for improvement in all of these areas. Their benefits over conventional systems can be summarized as follows:

- Micro- and small-scale CHP produces heat and electricity at point on demand to fulfil the industrial / residential / domestic electric and heating requirements.
- A high utilization of primary energy source is achieved by reducing waste heat.
- Emissions are significantly reduced owing to high overall efficiency of the CHP system.
- A small CHP system can work independently from the grid and thus provide power and heat even during blackouts.
- Local energy sources can be utilised.

Furthermore, small-scale cogeneration provides the opportunity for more people and entities to participate in the energy market and to be also producers of heat and power, not just consumers. Small CHP units are often put forward as key microgrid components. Therefore, they hold tremendous potential for future energy concepts like smart grids and local energy communities [10]–[13].

2.2 Commercially available biomass technologies

Biomass is a very broad term which describes a variety of matter of organic origin such as trees and crops, but also industrial, agricultural and domestic organic waste. All biomass is a product of solar energy which is captured by plants through the process of photosynthesis. The range of technologies which can be used to convert biomass into heat and electricity is also very wide and includes combustion, gasification, pyrolysis, fermentation and anaerobic digestion. Biomass is considered a renewable and CO₂ neutral energy resource due to the relatively short period it takes to form. Burning biomass simply returns to the atmosphere CO₂ that was absorbed by the plant as it grew. Of course, additional emissions produced by transportation or processing must be considered.

Biomass is well-suited for decentralized, small - and micro-scale CHP plants due to its lower calorific values, local availability and often lower costs than fossil fuels [6]. In the micro-scale with power output up to 50 kW_e, the commercially implemented technologies are organic Rankine cycles (combustion), internal combustion engines and Stirling engines (combustion or gasification) [14]. Biomass may become particularly relevant in Europe due to the uncertainty of natural gas deliveries in the coming years [15].

Table 2 summarizes several commercially available biomass micro-CHP technologies and their attributes.

Unit name, manufacturer	Technology	Power output [kW]	Heat output [kW]	CHP efficiency [%]
ENO 10 – 40LT. Enogia [16]	ORC	10 – 40 (~5% el. efficiency)	~ 200	-
WAVE 120, LORCA (UCEEB) [17]	ORC	6,2	120	89
ORChidea, Kaymacor [18]	ORC	3 – 128	-	-
Winno Energy gasification unit [19]	ICE + gasification	40	80	-
Q-PowerGen, NewEnCo [20]	Stirling + gasification	36	120	-
Froling CHP 50, Froling [21]	ICE + gasification	46 – 56	95 – 116	85
Microgen Stirling engine [8] [22]	Stirling + gasification / combustion	1	3 – 24	-
PACK, Orcan Energy [23]	ORC, wide range of fuels cited	50 - 200	-	-
Green Steam + Neumot VEP Fordertechnik [24]	Steam piston engine	30	110	~90

Table 2 - Overview of current commercial biomass CHP technologies with power output up to 50 kW_e.

While the Stirling engine has the potential to be a highly efficient technology even at micro-scale, multiple companies trying to develop them have either discontinued their activities or have been stuck on demonstration and commercialization phase for several years [14] [25] [26]. This is largely due to investment costs, which can be up to 7 500 € / kW [8].

ORCs are becoming a widespread technology because of their numerous advantages over steam cycles such as dry expansion, lower boiling temperatures, and low vaporization heat. On the other hand, water is a much more accessible, cheaper and safer working fluid with a higher heat capacity [6]. Another important aspect is the heat source temperature. While ORCs are much more suitable than steam for utilizing low-temperature heat sources such as waste heat, organic fluids become thermally unstable at high temperatures over 300 °C, where they undergo thermal degradation into methane, alkanes and other substances. Maximum operating temperatures for most organic fluids are around 290 – 320 °C [27].

2.3 Research projects and development regarding biomass micro-CHP technologies

On top of numerous commercial technologies on the market, new technologies are being constantly researched or improved. Their scope is naturally wider, encompassing

internal combustion engines, ORCs, Stirling engines and even unconventional technologies such as thermoelectric generators (TEGs) or hot air turbines. More information is provided in Table 3.

Reference	Technology	Power output [kW]	Heat output [kW]	CHP efficiency [%]
[28]	mobile ICE + gasification	3 – 3,5	8 – 9	47,7 – 51,5
[29]	TEG	0,25	10 - 20	>92
[30]	ORC	3,2 – 4,4	26 - 29	75
[31]	Hot air turbine	47,5 (el. efficiency 15 %)	217	83
[32]	Stirling	0,5	-	65
[33]	Stirling	0,7	2,3	40
[34]	Steam engine	5	20	-
[35]	Steam engine (no testing yet)	23	104	78

Table 3 - Research and development regarding micro-CHP biomass technologies

A microturbine CHP with biomass gasification is sometimes also considered [34] [35]. Company Xcel Energy is actively researching this concept with the aim of developing a 30 kW microturbine. Although the development has been going for around 10 years, the biomass gasification technology has not yet been constructed and tested [38]. The technology is also examined by the microturbine manufacturer Bladon [39].

Chapter 3: Steam cycles utilizing high-parameter steam

3.1 High pressure and temperature steam in high-power applications

3.1.1 Current state-of-the-art

Supercritical power plants are the state-of-the-art among thermal power plants. They take advantage of the fact that the efficiency of the thermodynamic cycle rises with increasing pressure and temperature by employing steam above the critical point ($p = 22,12$ MPa and $t = 374,15$ °C) and can thus achieve an efficiency close to 50%, especially if a very low pressure can be achieved in the condenser. Modern supercritical steam power plants usually operate at steam pressure of 25-28 MPa and temperature up to 600 - 620 °C. Single or, more often, double reheating of the steam is necessary to avoid expanding into wet steam [4][40].

When talking about plants with high steam parameters, the terminology typically used is as follows:

- **Subcritical** plants below the critical point of water at $\sim 540^{\circ}\text{C}$ and 17 – 22 MPa, efficiencies usually up to 38%.
- **Supercritical (SC)** plants that operate slightly above the critical point at 22 – 25 MPa and 600 °C / 615 °C with efficiency up to 42%.
- **Ultra-supercritical (USC)** plants significantly above the critical point at 25 – 30 MPa and 620 °C with efficiency in the range of 42 - 48%. These are the current state-of-the-art plants. Examples – Moorburg (Germany), Patnów (Poland), Wai Gao Qiao (China).
- **Advanced ultra-supercritical (A-USC)** next generation of power plants not deployed for commercial purposes so far. These plants would target steam pressures up to 35 MPa, 700 – 760 °C temperature range and efficiencies over 50% [8] [10].

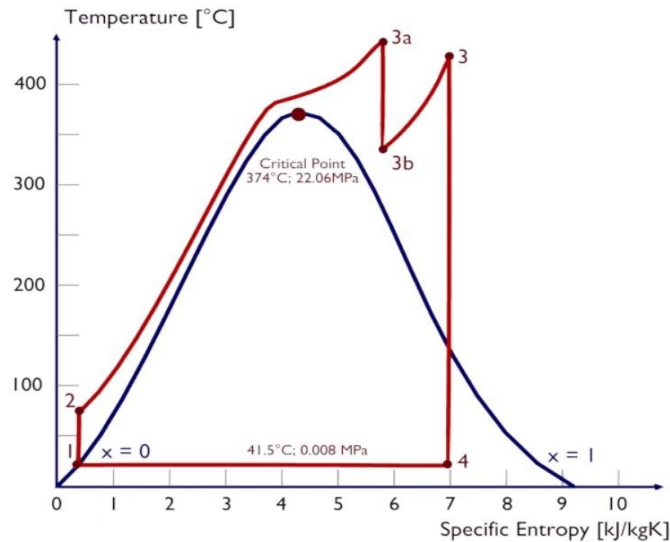


Figure 4 - Supercritical steam Rankine cycle with single reheat [43]

3.1.2 Brief history of development of supercritical plants

Although using supercritical steam in power generation is not a new idea, with first commercial uses dating as far back as 1950s, their operation was problematic, mainly from metallurgic standpoint. They suffered from high costs, low reliability and high failure rate. These were caused mainly by lack of adequate materials durable at high temperatures. What later enabled supercritical plants to attain better feasibility was the development of steel grades 91 and 92 and durable nickel-based alloys for heavy section tubular components and derivatives for the cast and forged components [41]. Highly durable steel like the T91 and T92 and their derivatives P91 and P92 thus enabled the reliable running of USC plants, but to make A-USC plants possible and thus achieve the threshold of 50% efficiency, a new generation of materials would be required.

To develop new materials, multiple research programs were launched on the national and international level in late 1990s and early 2000s. One such notable program was the AD700, which was comprised by over 40 companies and funded by the European Commission. Its goal was the research and development of materials for A-USC plants. The project was divided into several phases and culminated in building the COMTES700 (COMponent TEST facility for a 700°C power plant) demonstration site at the E.ON coal fired Scholven plant in Germany in 2005, which aimed to test the limits of using supercritical steam at the 700 °C temperatures. The main concerns were naturally the materials required for such application [44]. The test facility used steam from the Scholven plant and achieved 17 000 hours of operation from 2005 until 2009. It tested boiler components such as tubes, valves and superheaters at 705 °C and 22.6 MPa. The components were made of alloys T24, HCM12, Alloy 617, Inconel 740 and others. Following the successful component test facility, a full-scale demonstration was planned to begin in 2014 at E.ON's plant at Wilhelmshaven. Although the project got suspended and the demonstration never took place [45][44][46], a list of candidate materials for various components of the demonstration plant, shown in Table 4, was worked out.

Components		Candidate alloys
Walls	Membrane walls	T23, T92, similar ferritic steels
Pipes and tubing	Superheaters	T92, Alloy 617m, Alloy 174, Inconel 740
	Reheaters	Alloy 617m, S304, T91
Turbine casing	Outer casing	Cast steel (9-10% Cr)
	Inner casing	Alloy 625 (cast), welded with 9-10% martensitic steel
Valves	Casing	Alloy 625 (cast)
	Weld-on ends	Alloy 617m
Turbine rotor	HP and IP	Alloy 617 welded with 10Cr steel
Turbine blades	HP and IP	Martensitic steels, Nimonic80, Waspalloy

Table 4 - Components and their candidate materials for a A-USC plant as a result of the COMTES700 and AD700 programmes [47]

3.2 Materials of components

The most important factor that determines the use of higher pressure and temperatures is the availability and cost of materials to withstand these conditions [41]. There are a number of other demands on these materials, depending on what they're used for – boiler membrane walls, heat exchangers, pipes, turbine components etc.

The first SC plants used austenitic steels, but this caused difficulties, mainly because of their higher thermal expansion coefficient and low thermal conductivity. That's why focus was later shifted to ferritic and martensitic steels and then to nickel-based alloys [41]. However, austenitic steels do have an advantage over their counterparts in terms of better weldability [48].

In the following chapters, some of the most widely used generations of materials used for high-temperature steam are presented.

Material type	Thermal conductivity	Coefficient of thermal expansion
Ferritic steel	High (~50W/m°C)	Low (~11 × 10 ⁻⁶)
Austenitic steel	Low (~16W/m°C)	High (~18 × 10 ⁻⁶)
Nickel alloy	Moderate (~24W/m°C)	Moderate (~14.7 × 10 ⁻⁶)

Figure 5 - Thermo-physical properties of ferritic and austenitic steels and nickel alloys [41]

3.2.1 Low-alloyed ferritic and martensitic steel grades

After austenitic steels were no longer a candidate material for high-temperature applications, development efforts focused on 9-12% Cr ferritic steels. This resulted in the T23 (2.25Cr-1.6WVNb), T24 (2.5CR-1MoVBTi) and later T91 and T92 (X10CiMoVNB) steels with maximum working temperatures 560 - 625 °C. These steels are mostly annealed and used in boiler membrane walls and steam generator components, headers and heat pipes. T92 has also been used in superheater tubes [49][48]. They're weldable, with necessary

preheating in the temperature range 150–250°C to prevent cold cracking. T23 is an exception, tests showed that no cracking occurred even under room temperatures [41].

Steel	YS/TS at room temperature [MPa]	Max. recommended work temperature (in power engineering applications) [°C]
T23	400/510	580
T24	415/585	590
T91	415/585	600
T92	440/620	625

Table 5 - Mechanical properties of several low-alloyed steels. The properties may vary depending on the type of heat treatment process applied [41][50]

3.2.2 High-alloyed martensitic steel grades

High tensile and creep strength, good corrosion and oxidation resistance, high thermal conductivity, and low thermal expansion in combination with relatively low cost make martensitic 9–12% Cr steels ideal for use in the hottest parts of steam boilers [51].

The P91 steel (X10Cr-MoVNb) was first used in Europe in 1997 with steam parameters of 28 MPa and 580 °C. It has since been widely applied in construction of USC plants in steam pipes and outlet heaters along with its close derivatives, such as the CB2 and X20 alloys.

P92 is currently the strongest commercially available steam pipe steel, and it has enabled the construction of several USC power plants with steam parameters up to 30 MPa and 600°C, and sizes up to more than 1 GW [41].

Steel	YS/TS at room temperature [MPa]	Max. recommended work temperature (in power engineering applications) [°C]
P91	415/585	625
P92	430/620	650
X20	480/650	620
CB2	500/670	650

Table 6 - Mechanical properties of several high-alloyed martensitic steels. The properties may vary depending on the type of heat treatment process applied [52][53][54][55]

3.2.3 Nickel-based alloys

The current USC operation temperature limit for 9-12% Cr steels is around 650°C. It is unlikely that steels will ever have sufficient creep strength and oxidation resistance to operate beyond 680 °C. Only nickel alloys are likely to maintain sufficient high-temperature properties. Many nickel-based alloys have been tested and developed, such as the Inconel X-750 (used for gas turbine blades), Inconel 740H (which was the direct result of the COMTES700 tests [46]) and Haynes 282, which can be used for steam temperatures up to 800 °C [41][48][55].

Alloy	YS/TS at room temperature [MPa]	Max. recommended work temperature (in power engineering applications) [°C]
Inconel 740H	750/1120	780
Inconel X-750	815/1200	780
Haynes 282	700/1130	800

Table 7 - Mechanical properties of several high-alloyed martensitic steels. The properties may vary depending on the type of heat treatment process applied [41][56][57]

3.3 Utilising high-parameter steam in low-power applications

A wide range of installed power in SC and USC plants can be noted. While in China, the trend is building large plants, European and American units have scaled down to 600-900 MW. According to studies conducted by Siemens and Alstom, the effect of plant size on efficiency is negligible, less than 0.5% when comparing 400 and 800 MW blocks [58] [47]. Furthermore, a study between Sandia National Laboratories and Siemens confirmed the feasibility of adapting the Siemens SST-900 turbine for supercritical steam with parameters of 23 – 26 MPa and ~ 550 °C in a CHP plant with power output of 140 MWe [59]. However, applications of supercritical steam at smaller scale have not been attempted.

Steam turbines with inlet parameters of around 290 °C and 4 MPa can be deployed for low-power CHP applications, although commercially available turbines in this area are usually not primarily designed for this purpose. They are often used in marine or industrial applications [60][61]. A US-based company CyclonePower claims to have developed a highly efficient small CHP unit consisting of six piston expanders utilizing steam at almost critical conditions [62]. However, they have not yet published any proven test results. While there are concepts considering a steam turbine of under 100 kW_e [63], they are yet to be tested in real applications.

Volumetric expanders can be a viable choice thanks to their ability of easily handling low mass flow rates and working under a wide range of conditions [64]. While it would be difficult to deploy and utilize supercritical pressure due to heavy pressure losses, leakage and possible stability issues, high temperature is limited mainly by the available materials. The components, such as casing, piping, valves etc. can be designed with materials discussed in this chapter. In fact, for a given temperature, it is possible that less costly materials than the ones used in SC plants could be theoretically deployed owing to the lower pressure. In Figure 6, it is observed that each material can be used for a slightly higher temperature at a lower pressure. Therefore, in a small, decentralized steam unit with a high inlet temperature but lower inlet pressure, it should be researched whether the T92 and P92 steel grades could be replaced by the T22 or T23 or by similar, cost-efficient materials.

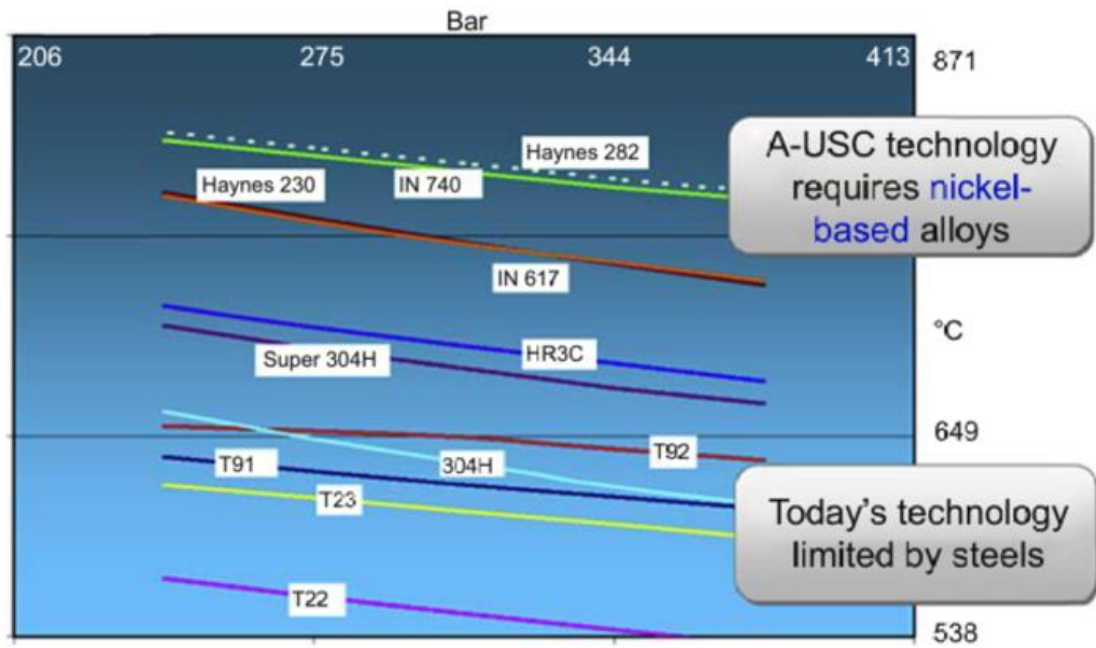


Figure 6 - Maximum working temperatures of different materials based on operating pressure [41]

Chapter 4: Expanders

Expander is a crucial component of the Rankine cycle. The overall performance of the entire plant depends heavily on its efficiency. This chapter discusses the different types and categories of expanders, their characteristics, and applications.

4.1 Overview

Expanders can be broadly divided into two categories – volumetric (sometimes called positive displacement) expanders and dynamic expanders.








volumetric expanders				dynamic expanders		
$work = \int v dp$				$work \sim u^2$		
						
piston	screw	scroll	vane	axial	cantilever	radial

Figure 7 - Types of expanders [65]

Dynamic expanders, referred to as turbines, convert the dynamic pressure or high-velocity fluid momentum into mechanical energy while passing through a series of blades. They can be divided into main three categories based on the direction of the incoming fluid – axial, radial and cantilever, with axial turbines being the most commonly used. They are standard for larger machines with output $> 500 \text{ kW}_e$ [66].

Volumetric expanders are periodically operating machines that don't use blades to generate mechanical energy. Instead, relative position of the stator and rotor defines a one or several working chambers where the fluid expands. Volumetric expanders have a specific built-in volume ratio and can be classified into many types. The most usual volumetric expanders, and the ones discussed in this work, are the piston, screw, scroll and vane type. Other, more niche and less common expanders include the Roots expander or the Wankel turbine. The advantage of volumetric expanders is that they are suitable for low volumetric flow rates, achieve decent efficiencies and low rotational speeds. Therefore, they are used in smaller plants, such as steam and ORC units for geothermal plants or waste heat recovery systems [64].

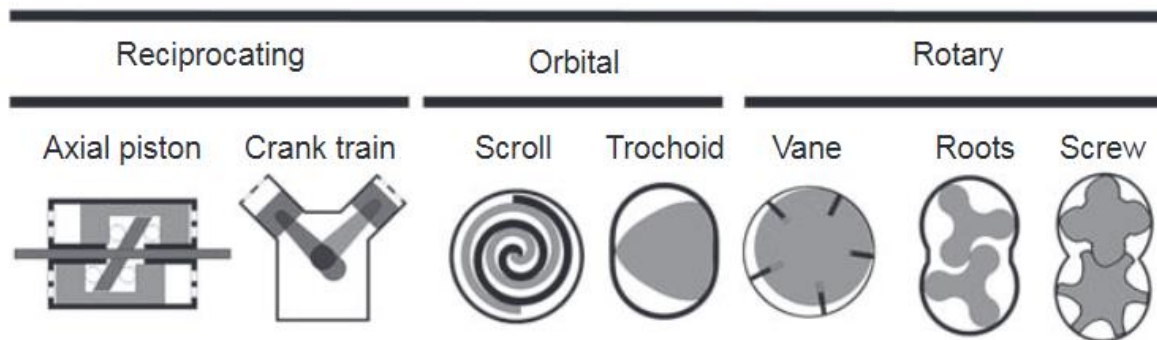


Figure 8 - Different types of volumetric expanders sorted by their rotor motion [64]

While dynamic expanders can achieve much greater efficiencies and are widely deployed in large-scale thermal plants, they are designed for high flow rates and scaling them down below the 500 kW_e threshold is difficult due to both technical issues and high cost. Technical issues include difficulty when working with low mass flow rates, and high rotational speed (up to tens of thousands rpm). These high speeds mean that it is more difficult to connect the turbine directly to the generator. Special high-speed generators or gearboxes are then needed. Bearings are also burdened by the high speeds due to mechanical stresses and there is a danger of higher leakage between the stator and the rotor [67][68]. At the same time, volumetric expanders have low cost, low rotational speed, ability to work with low mass flow rates and can better withstand two-phase working fluids. Most of the uses and applications of volumetric expanders nowadays can be found in ORC or CO₂ systems [64].

4.2 Demands on a micro-scale cogeneration plant expander

Small- and micro-scale power units have received a heightened attention in the previous years. However, their mode of operation often differs from the classical turbines that work with high flow rates, high steam parameters and are mostly held at the optimum power level. Thus, there can be different factors that will influence decision-making apart from obvious factors such as efficiency and reliability of the machine.

Firstly, a small-scale CHP machine is expected to be subject to varying power demands depending on the application and the time of the year. Therefore, good off-design performance is an important factor.

Secondly, small-scale units are more sensitive on the complexity and investment costs. An expander that is difficult to manufacture or requires costly materials can easily drive the investment cost per installed kW too high up where commercial deployment of such a machine would be no longer feasible.

Other technical-economic factors that are of less importance in larger machines can also come into consideration. A decentralised machine is likely to be installed closer to habited areas and therefore low noise will be desirable. Compactness is also important as the machine will likely be placed in industrial or living areas. Availability of materials and components will also play a larger role. However, properties of volumetric machines can make certain aspects of design easier, such as lower rotational speeds and ability to handle two-phase expansion, which are discussed elsewhere in this work [69][70][71].

Finally, for this particular work, the ability of the expander to withstand high pressure and temperature of the expanding steam will also be desired. The expected power output of the unit employing the expander is around 10 - 50 kW_e.

4.3 Piston

4.3.1 General information

The piston is among the oldest expanders, having been widely used since the 18th century until the early years of the 20th century, most notably during the industrial revolution. Interest in this technology was renewed in recent years for small-scale steam or ORC systems, waste heat recovery from internal combustion engines and even as means of propulsion for automobiles [72]. This is due to numerous advantages such as large built-in volume ratio, high achievable operating pressures and temperatures, low rotational speed, and even compactness.

Piston expanders work best with low displacement at a relatively high volume ratio. They are best suited for low power applications because of their ability to work well with high inlet temperature and a high pressure ratio. Some of its drawbacks, however, are relatively low power range and limited wet expansion [73].

4.3.2 Modifications

Reciprocating piston

The reciprocating piston is the simplest and oldest type of piston. The piston is contained in a cylinder and moves in and out as the working fluid expands and is then exhausted.

Swash-plate piston

The swash-plate piston is the most popular choice among modern experimental units. A cylinder block containing multiple pistons is attached to a shaft. As the fluid expands, the pistons move against a stationary plate that sits at an angle to the cylinder. Thus, the shaft rotates.

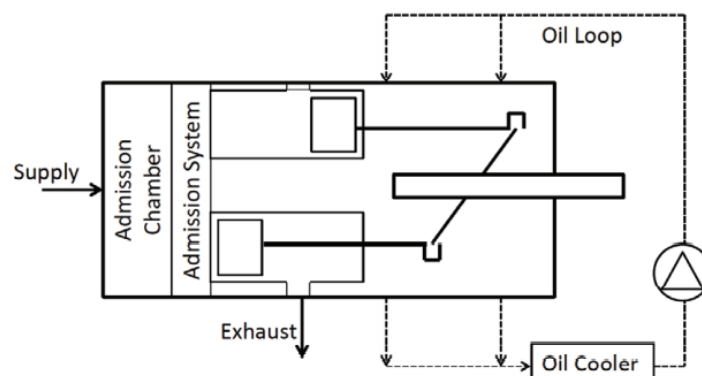


Figure 9 - An experimental swash-plate piston configuration [72]

Rolling piston

The rolling piston is a rarer configuration which is used in CO₂ refrigeration cycles. Both the stator and the rotor are of a cylindrical shape. The rotor (which is attached to a

crankshaft) is placed inside the stator and rotates eccentrically. A single vane separates the suction and the exhaust part. This machine then represents a sort of combination of a piston and a vane expander [74].

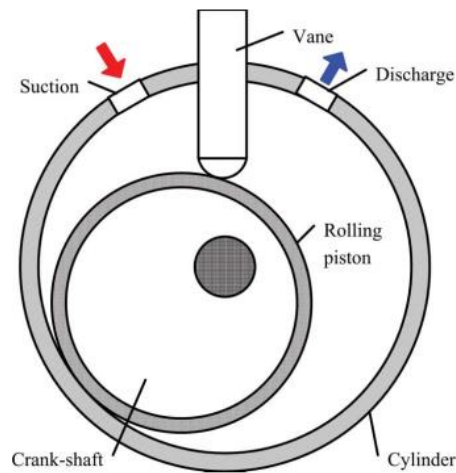


Figure 10 - The rolling piston

4.3.3 Specifications and uses

The piston is the only expander which uses linear motion instead of rotational, which means that a crankshaft needs to be used, which introduces additional losses. When compared with other volumetric expanders, piston has lower speed of 600 – 2000 rpm [64].

One notable disadvantage of the piston against other expanders is the necessity for complicated valve-timing gears, which makes it more complex and costly. Wet expansion is also not recommended [65] [68].

Ref	Working fluid	Isentropic efficiency [%]	Power output [kW]	Volume ratio	Rotational speed [rpm]	Inlet pressure [MPa]	Inlet temperature [°C]
[24]	Steam	-	30	-	-	3,2	350
[72]	R245fa	53	2	-	1000	3	-
[75]	steam		14	-	1500	3,2	380
[76]	R245fa	53	2,7	4,7	1000 - 4000	3	153
[77]	CO ₂	45	1,1	2,3	800 - 2000	-	48
[78]	steam	-	2,1	-	200 - 800	1	-

Table 8 - Results from studies and investigations of piston expanders

4.4 Screw

4.4.1 General information

The screw expander is comprised of one or two rotating helical rotors with the grooves serving as chambers. It is often a favourite choice for ORC plants because of its wide range of power output applications, ranging from units of kW all the way to units of MW

[79]. Another used application is WHR. Aside from its excellent scalability, its advantages over other volumetric expanders are high isentropic efficiency (reaching as high as 80% in test conditions) and balanced load distribution of the rotor. All variants of the screw machine generally have a higher relative manufacturing cost than other expanders due to complexity of their geometry and the need of precise machining [80].

This chapter provides only generalised description of the screw machine. Its attributes and geometry (especially that of the single-screw variant) is elaborated upon in greater detail in later chapters.

One area where it has established its dominance are ORC geothermal plants [64]. However, it is reported that the twin-screw becomes unstable for high pressure ratios due to bearing forces associated with pressure distribution across rotor. This makes it difficult to work with a higher potential fluid and the screw is therefore used for utilizing low grade heat. Thanks to low fluid velocities, screw expander can work with a two-phase fluid much better than dynamic expanders [81] [82].

4.4.2 Modifications

Single- and twin-screw

Two broad variants of the screw machine can be distinguished:

- a) The twin-screw. This type of configuration is broadly used in vapor compression, ORC applications or geothermal plants. It consists of two rotors - male and female. As their grooves mesh, working chambers are created in which the fluid is expanded, as is visible in Figure 12.

The rather complex geometry of the twin-screw machine allows for a very wide range of different rotor profiles. The geometry has a serious impact on leakage and friction as well as overall performance of the expander. The early screw compressors had a symmetric profile, which is easier to design, but leaves a leakage path when the machine is repurposed as an expander due to a large blow-hole area. This can be fixed with an asymmetric design at the cost of higher friction and complexity [64].

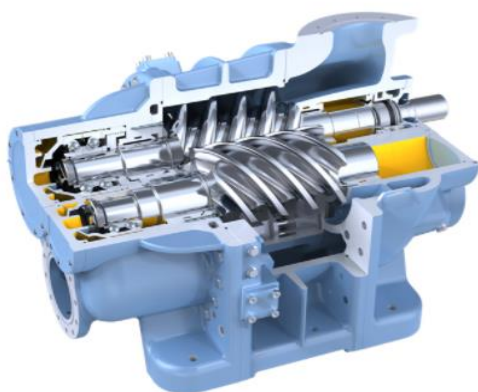


Figure 11 - Example cross section of a twin-screw expander [81]

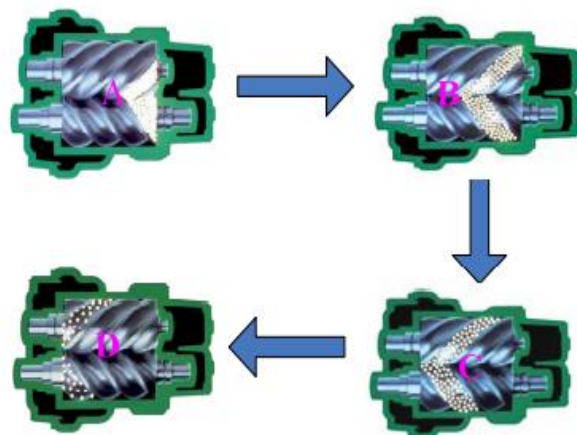


Figure 12 - Operating principle of the twin-screw. A - suction; B and C - expansion; D - discharge

- b) The single-screw. Although the single-screw has a simpler geometry, it is a newer and less widely used design, both in compression and expander application. However, multiple experiments have been conducted to confirm the viability and advantages of this configuration [80][83][84]. It consists of a single helical rotor, while the female rotor is replaced by two or more gate rotors (sometimes also referred to as starwheels). This eliminates problems with increased leakage area described above and allows for greater pressure ratios at the cost of more moving parts and larger dimensions of the expander configuration. Major advantages of the single-screw variant over the more conventional twin-screw are cited in literature – a more balanced loading of the helical rotor, low leakage even at high pressure ratios, lower noise and vibrations [80].

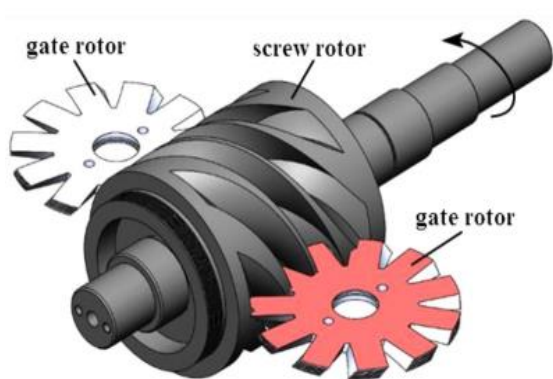


Figure 13 – Cylindrical-plate, the most common configuration of the single-screw expander [85]

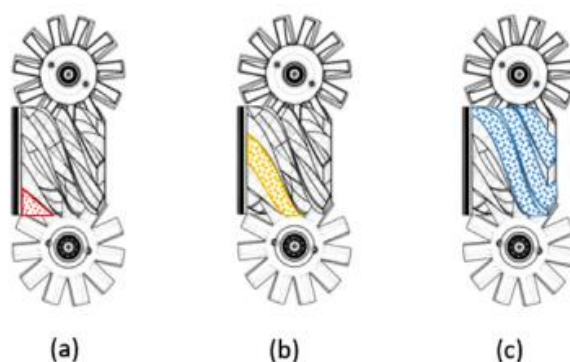


Figure 14 - Expansion process of the single screw expander. a) suction, b) expansion, c) end of expansion and discharge [80]

Dry screw and flooded screw

- a) The dry screw. Also referred to as synchronized, operates without any lubrication being injected inside the working chambers. This is the simpler variation, without the need of an external oil loop. Naturally, this comes at the cost of friction, leakage and stress. To prevent contact between the rotors, external timing gears are required.
- b) The flooded screw. Injecting oil into the working chamber and thus lubricating the rotor and the bearings solves the problems of the dry screw. An external oil loop is required, increasing the complexity, but reducing friction and leakage losses. A major downside is that it is impossible to completely extract the oil from the working fluid. For this reason, the oil is sometimes replaced with water as a lubricant. Further sealing and timing gears are required for this [64][86].

4.4.3 Specifications and uses

Ref	Working fluid	Isentropic efficiency [%]	Power output [kW]	Volume ratio	Rotational speed [rpm]	Inlet pressure [MPa]	Inlet temperature [°C]
[76]	R245fa	65	1,3	2,5	up to 12450	1	130
[82]	Steam	70	-	5	-	4	-
[87]	Steam	-	100 - 1600	-	-	3	-
[88]	Steam	-	50 - 1500	-	1500 - 4000	0,15 - 3	300
[89]	R245fa	-	1000	-		1,4	~100
[64]	Steam	22 - 45	200 - 800	-	2500 - 3300	0,3 – 1,4	177
[90]	steam	40 - 46	Up to 850	-	2500	0,69 – 1,5	-
[91]	R123	80	100 - 300	3	up to 6000	0,5	65 - 80
[92]	Air	55	22	-	2800	1,6	-

Table 9 - results from studies and investigations of screw expanders

The screw has been long been used in air or CO₂ compressors. In recent years, it also is frequently recommended as a viable expander for ORC, steam or air-based systems utilizing low grade heat, such as in waste heat recovery or geothermal plants. This is mainly due to a very wide range of power outputs, good efficiency, compactness, and the ability to handle two-phase working fluid well.

Drawbacks are mainly difficulties when working with higher temperature and pressure fluids, as well as possibly high leakage losses for the twin screw. Single-screw could therefore be a viable alternative [93].

An interesting project regarding new possible fields of screw expanders deployment is a micro-CHP Brayton cycle unit which is being developed by company BraytonEnergy LLC in cooperation with City University of London. The CHP unit utilizes a twin-screw expander with inlet temperature as high as 1100 – 1200 °C. To withstand such conditions, the expander is made of a ceramic material. At the time of writing this work, the project is nearing the end of its testing phase [94].

4.5 Scroll

4.5.1 General information

The scroll expander has a more complicated geometry than the other devices mentioned here. It consists of two spirals – an orbiting scroll (rotor) and a fixed scroll (stator). When the scrolls rotational movement of the orbiting scroll is the same as the direction of the swirl, the space between them decreases and the machine works as a compressor. When the wrap rotates in the opposite direction, the gap increases, and the machine works as an expander [95].

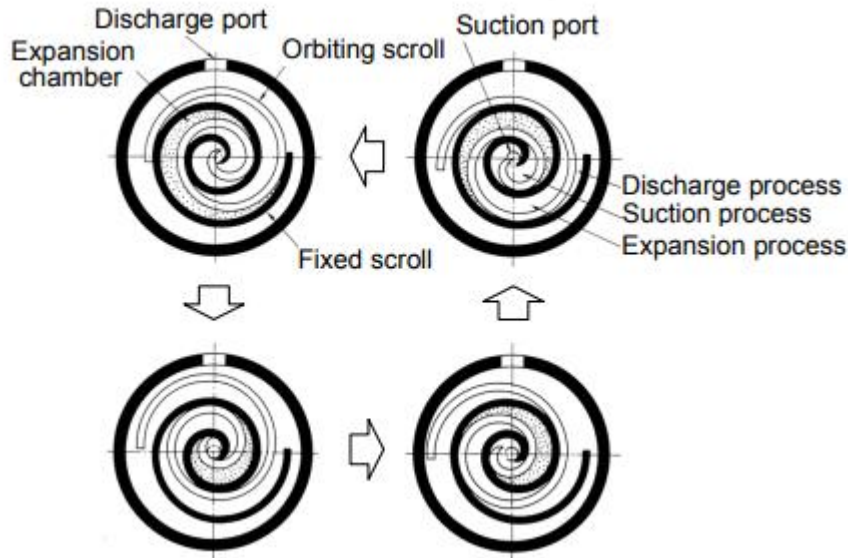


Figure 15 - Operating principle of the scroll expander [95]

Scroll expanders report some of the highest efficiencies among volumetric expanders. They are suited for micro-power applications up to 12 kW. They are generally designed for lower pressure ratios, and are characterized by low flow rates and rotational speeds, good efficiency and flexibility [64][96].

Thanks to these qualities, scrolls are generally applied as compressors in air conditioners and cooling systems.

4.5.2 Modifications

Scroll expanders can be generally divided into two types – compliant and kinematically constrained. The compliant variation needs lubrication through an external oil loop to prevent mechanical wear. This also reduced the leakage losses. For constrained scroll expanders, radial leakages are reduced by low friction material tip [64].

4.5.3 Specifications and uses

The scroll device can work very efficiently as both compressor and expander. As expander, it is applied only in very low power units below 15 kW. Some of the main drawbacks of this machine are complicated geometry and production, but also possibly high leakage losses. Danger of cavitation at high pressures and high velocity of the working fluid has also been reported [64]. Although the scroll has very good isentropic efficiency and probably the best partial load performance out of all the volumetric expanders, literature recommends it for only very small units and reserves power outputs of above 15 kW for other machines [97].

From the studies in Table 10, it's clear that scroll expanders are seriously considered for commercial use only in ORC cycles and not in steam systems. The presented data all comes from experimental units, with only one exception where commercially available scroll expander is referenced, specifications cited from the manufacturer's website [98].

Ref	Working fluid	Isentropic efficiency [%]	Power output [kW]	Volume ratio	Rotational speed [rpm]	Inlet pressure [MPa]	Inlet temperature [°C]
[76]	R245fa	76	1,5	2,19	1137 - 7920	1,4	125
[95]	R113	63	0,45	-	1800	-	136
[99]	Steam	34	15	-	1200	1,38	145
[98]	Steam		11	4,5	3600	1	170
[100]	R245fa	50 - 74	20		3600	2,2	140
[101]	R245fa	75	1,5	2,9	3000	0,7	-

Table 10 - Specifications of various experimental and commercial scroll expanders

4.6 Vane

4.6.1 General information

The vane rotor has slots in which several vanes are set. Their number can vary from 2 to up to 30, but most expanders will have five to ten vanes. These vanes then define the working chambers. High pressure vapour enters through the inlet, expands between the vanes and the housing and is then released through the outlet, as shown in Figure 16. Similarly to the scroll, vane is preferred in ORC systems.

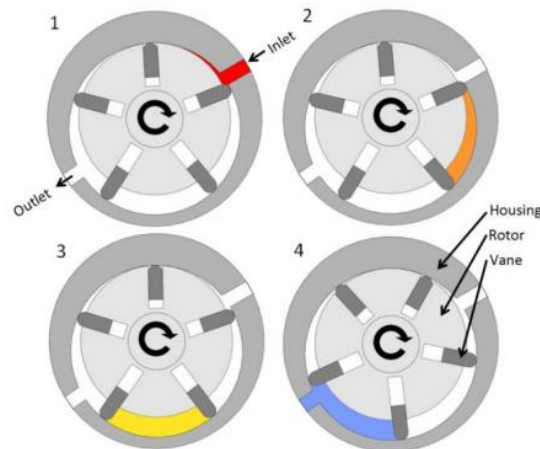


Figure 16 - Working principle of the rotary vane. 1- inlet; 2-3 - expansion; 4- exhaust [97]

The vanes can move freely in their slots and are pressed to the stator by the centrifugal force. The vane expander is less complex and costly than the screw and scroll expanders, but poses higher risks of significant leakage and frictional losses and therefore lower efficiency [102]. The number of vanes influences these losses – more vanes will mean lower leakage losses due to lower pressure ratio between two neighbouring working chambers. On the other hand, more vanes will mean more contact with the stator, which will increase frictional losses.

4.6.2 Modifications

The rotary vane expander (or compressor) can be constructed with either circular or non-circular (elliptical) geometry, with the former being the more prevalent solution. Circular

geometry is naturally less costly and easier to manufacture, while elliptical geometry can be used to balance pressure forces acting on the rotor and are better suited for working with higher pressure fluids than the circular geometry [67].

4.6.3 Specifications and uses

Ref	Working fluid	Isentropic efficiency [%]	Power output [kW]	Volume ratio	Rotational speed [rpm]	Inlet pressure [MPa]	Inlet temperature [°C]
[10]	C ₉ H ₁₂	-	0,8	-	-	0,78	265
[17]	MM	52	6,2	3,1	3034	0,52	180
[71]	MM	46	2	-	-	0,5	176
[103]	steam	20	2	-	840 - 1900	1,03	188
[104]	steam	<1	0,03	-	1500	0,15	-
[105]	R141b	1,7	0,2	-	2000 - 3000	-	90
[106]	R245fa	42	0,61	-	1533	1,01	90,7
[106]	R245fa	43	0,47	-	1524	0,85	74,5

Table 11 - Specifications of various experimental and commercial vane expanders

The vane expander is successfully used in the commercially available WAVE 120 CHP unit utilizing an ORC cycle. A study [103] conducting experiments with a steam vane expander found, however, that the vane had relatively high frictional losses, reducing the efficiency by 40 – 60%. Higher frictional and leakage losses are also reported by other studies. To lower friction, a small quantity of lubricating oil is usually added to the working medium [107]. Price of the vane expander is lower than the screw or scroll thanks to its simple construction [67].

4.7 Evaluation, expander choice, reasoning

In section 4.2, demands on a desired expander were set. Then, in sections 4.3 – 4.6, each respective expander is explored. Table 12 shows a summary of the knowledge from these chapters and from [64] and [65]. The rated power ranges may differ, especially in the case of the scroll and vane, as these are less explored expanders and the mentioned sources often studied small experimental units, not commercially deployed ones.

	Piston	Screw	Scroll	Vane
Isentropic efficiency [%]	< 50	20 - 70	< 80	< 70
Maximum pressure [MPa]	4	3	2,2	1,03
Maximum temperature [°C]	380	300	170	265
Volume ratio	6 - 14	2 - 8	1,5 - 5	2 - 8
Pressure ratio	Up to 40	2,5 - 15	2 – 10,2	2 – 4,5
Rotational speed [rpm]	600 - 2000	1200 - 4000	1200 - 3600	1000 - 3000
Leakage losses	Low	Medium	Medium to high	Medium to high
Frictional losses	Medium	Low	Low	Medium to high
Power range [kW]	1 - 30	1 - 2000	Up to 13	Up to 10
Flexibility	Low	Best	Good	Good
Complexity	High	Medium	Medium	Simple
Reliability	High	High	Medium	Medium
Compactness	Good	Average	Average	Good
Noise	High	Medium	Low	Low
Cost and manufacturing difficulty	Medium	Medium to high	Medium	Low

Table 12 - Comparison of different volumetric expander types. Based on information summarized in previous chapters. Some parameters taken from [64] and [65]

Turbomachinery manufacturer Barber-Nichols takes a more complex approach. They recommend an appropriate expander based on a dimensional analysis, by introducing several similarity parameters, namely the specific speed N_s and specific diameter D_s .

$$N_s = N \sqrt{\frac{\dot{V}}{H_{ad}^{3/2}}} \quad (1)$$

$$D_s = D \sqrt{\frac{H_{ad}^{1/2}}{\dot{V}}} \quad (2)$$

where N is the rotational speed in rpm, \dot{V} is the volumetric flow rate in m^3/s , Δh is the enthalpy drop in kJ/kg and D is the diameter of the expander in meters. These parameters should account for factors such as parasitic losses and the effect of the Reynolds and Mach number. Based on these parameters, a selection map for several types of piston and turbomachines was created [108].

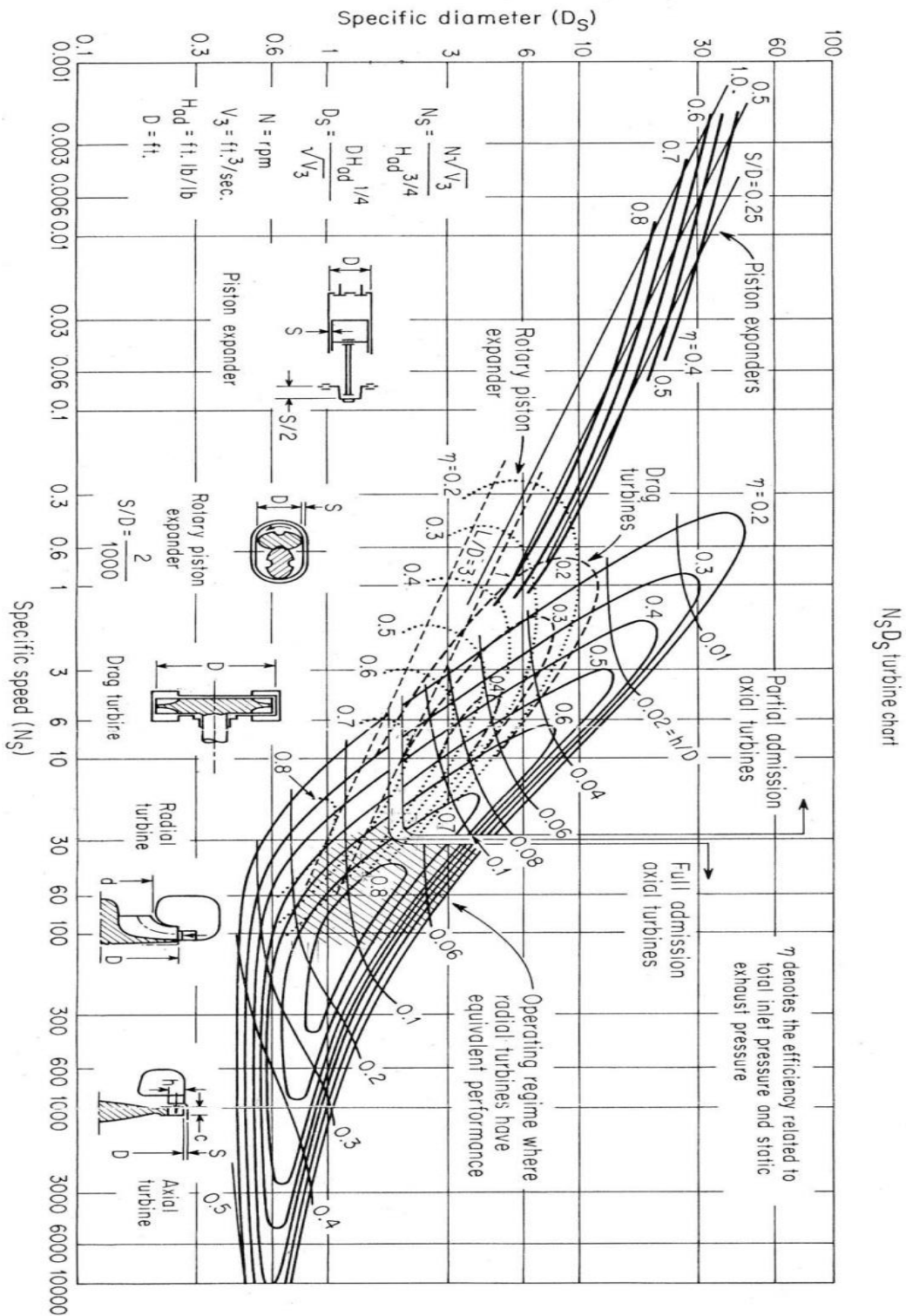


Figure 17 - Selection map for pistons and turbomachines [108]

Another interesting point of reference can be the map of power ranges for various volumetric expanders used in ORC systems, put together by Vodička in [67] from the Zenodo ORC database.

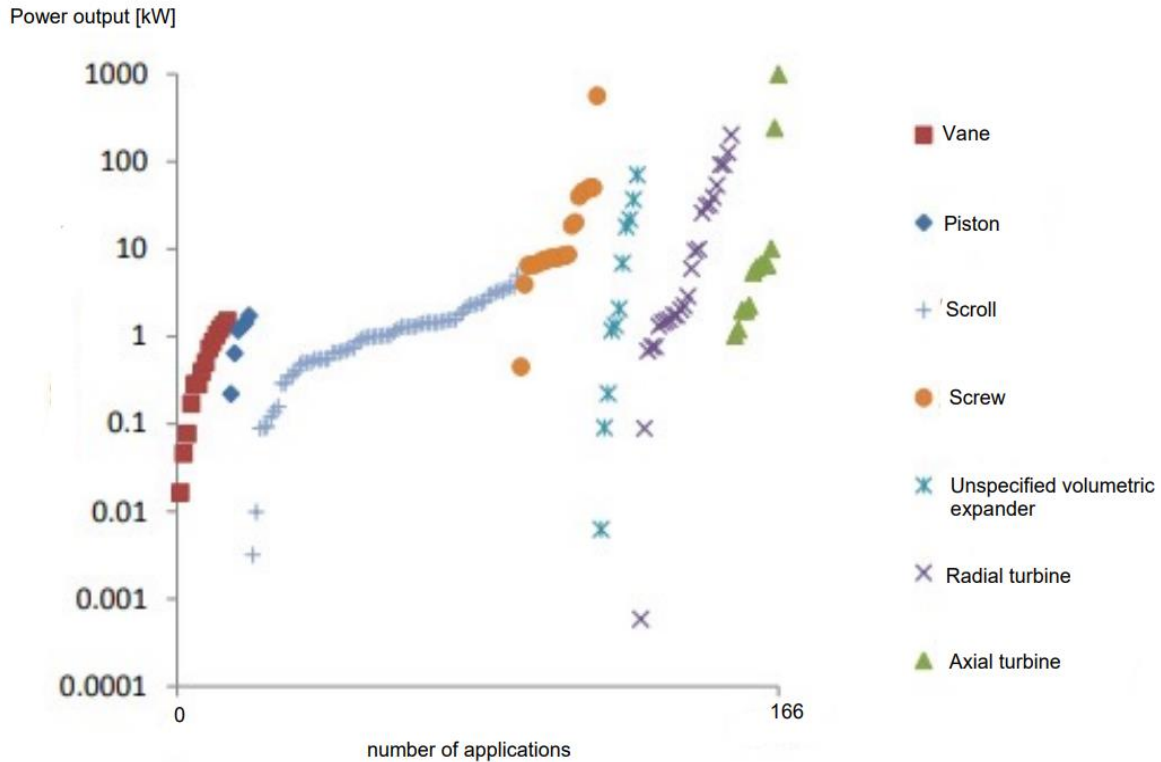


Figure 18 - Power output of installed volumetric expanders in ORC systems [67]

Putting together the above-mentioned information, the demands listed in section 2.2. and comprehensive studies on various types of volumetric expanders such as [64] by Imram et. al. or [76] by Dumont et. al., several conclusions can be made:

- I. Performance of all volumetric expanders with steam above 300 °C is largely unexplored. No matter the final expander choice, extensive testing and experimenting will be required.
- II. While the piston seems like the best candidate for handling high parameter steam due to its robustness and reliability, it might not be suitable as a decentralised machine. This is mainly because of its poor off-design performance, high noise and complexity.
- III. While the scroll appears as an attractive choice thanks to high efficiency, it seems to be poorly suited for high pressures and larger than micro-scale machines.
- IV. Both the vane and screw can be a viable choice. The LORCA laboratory already has experience with design and manufacture of vane expanders that would prove useful. However, it is likely that the vane would suffer higher leakage losses when exposed to higher pressures and the screw seems to be better suited to work with high-parameter fluids in general. Furthermore, it has a larger power range and similar, if not better, off-design performance.
- V. Based on the reasons stated above, the screw expander, specifically the single-screw variant, is chosen as the best candidate for a small-scale unit utilizing high parameter steam with heat output of 200 – 250 kW and electric power output of 10 – 50 kW. A mathematical description based on semi-empirical models found in

literature will be used to predict the best conditions for the use of a single-screw expander in a micro-scale CHP unit.

Chapter 5: Single-screw expander – description and geometric parameters.

5.1 Characteristics of the single-screw expander

Single-screw expanders (SSEs) show considerable potential in the power range of units of kW up to hundreds of kW. As outlined in Chapter 4, they show multiple advantages compared to the twin-screw variant. A number of both theoretical and experimental studies have been published which examine the performance of SSEs with a wide range of working fluids. These mostly include organic fluids [109]–[111], but also compressed air [52] [59], ammonia-water mixture [112] and steam [80] [113].

The single-screw machine consists of a single helical rotor and two or four gate rotors, called also starwheels. As the rotors rotate, the volume of the groove changes and the fluid is expanded or compressed. Depending on the shape of the helical rotor and number and positions of the starwheels, four different configurations can be distinguished. The first letter abbreviates the rotor shape and the second letter the starwheel shape.

- Plate-Cylindrical (PC) – a planar main helical rotor and two cylindrical starwheels which mesh with the grooves on the face of the rotor. The working process occurs only on one side.
- Cylindrical-Plate (CP) – by far the most common configuration. The main rotor is cylindrical while the starwheels positioned at the sides are planar. Expansion occurs on both sides.
- Plate-Plate (PP) – the only configuration involving four starwheels. The planar starwheels are positioned on either side of the helical planar rotor and expansion therefore occurs on both sides at the cost of a more complicated machine.
- Cylindrical-Cylindrical (CC) – both the helical rotor and the starwheel are cylindrical. Expansion takes place on both sides [80].

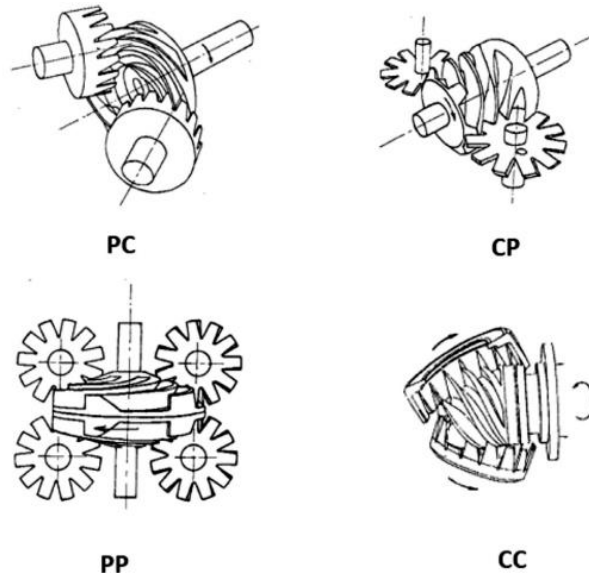


Figure 19 - Different configurations of the SSE based on the shape and number of rotors [114]

In [78] by Wang et. al, several organic fluids were calculated along with steam to be used in a low-power system utilizing an SSE.

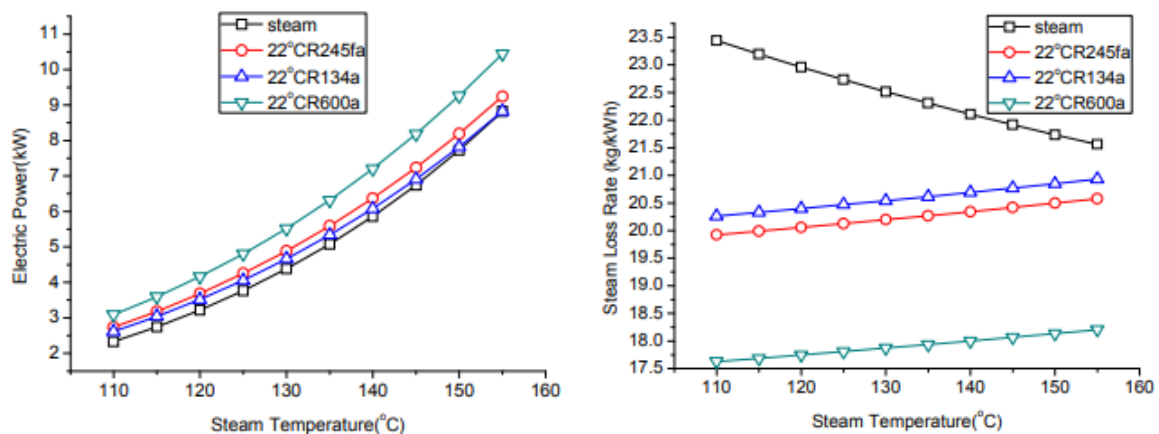


Figure 20 - Compared performance of a SSE when organic fluids and water are used as working fluid [113]

While steam has the lowest produced power and the highest steam loss rate at a low temperature, it gradually catches up with its counterparts. Higher temperature range should be therefore explored to determine its further performance.

5.2 Geometry and leakage of single-screw machines

Scroll and screw machines are geometrically among the more complex positive displacement machines. The single-screw expander or compressor usually consists of one helical rotor and two starwheels (the CP configuration). The meshing profile and conditions therefore need to be determined and the helical rotor precisely machined to prevent deformations and leakage. The manufacture of these machines is particularly difficult since the helical profile cannot be produced or measured by usual machining tools. Single-screw machines are usually manufactured by contouring machining methods, but even these can have significant errors. Inaccuracies in the meshing profiles result mainly in reduced lifespan, increased leakage, and noise of the machine. This can be considered as one of the biggest

drawbacks when compared with other volumetric machines [92] [111]. Casting and high precision CNC grinding can be adopted when ceramic materials are used [94].

The geometry is influenced mainly by the number of grooves on the helical rotor, the number of starwheel teeth, the main rotor diameter, and the ratio of the diameters of the helical rotor and the starwheel. This is shown in greater detail in following chapters. A combination of 6 grooves on the main rotor and 11 teeth on the starwheel is most commonly adopted for the CP configuration [80].

As for leakage, the screw machines generally have good volumetric efficiency among the positive displacement machines. This means that the relative share of the leakage mass flow is small in comparison with the entire mass flow. Volumetric efficiencies of 75 – 85 % are achievable, or even over 90 % for low rotational speeds [110].

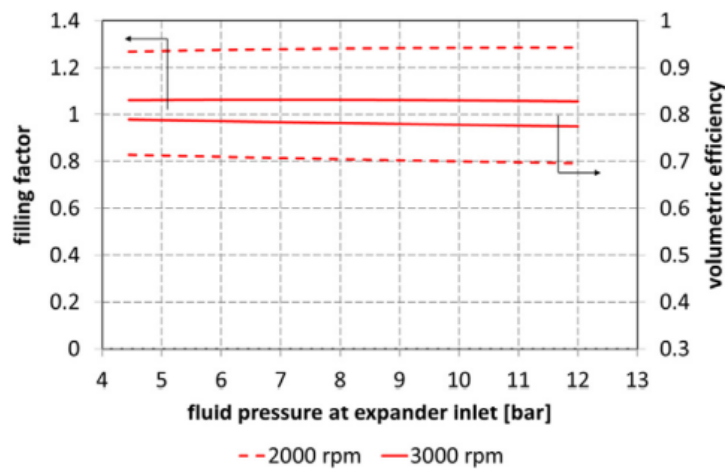


Figure 21 - Filling factor and volumetric efficiency on inlet pressure (working fluid is R245fa) [110]

The leakage flow in an expander will be divided among several leakage paths. Single-screw expander leakage paths were classified and described in detail by Shen et al [85]. In total, 9 different leakage paths were identified and described as functions of the rotor rotation angle. They were classified into three main categories:

- Fitting leakage paths. These are between the shell and the screw rotor.
- Meshing leakage paths. These involve the meshing sides of the main rotor grooves and the starwheel teeth.
- Splitting leakage paths. These are between the shell and the starwheels [85].

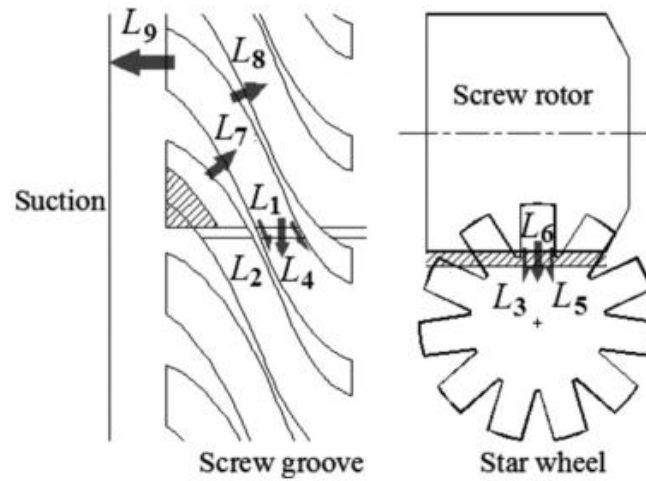


Figure 22 - Leakage paths within a single-screw expander – fitting (L7 – L9), meshing (L1 – L5) and splitting (L6) [85]

Despite this complex leakage model, a single constant leakage area is usually assumed in thermodynamic models of single-screw machines. This method was validated by multiple experiments and is considered to have good accuracy [79] [84] [85].

Chapter 6: Mathematical modelling of a single-screw expander

In order to assess the performance of the single-screw expander as accurately as possible, mathematical models were used to model the geometry and the expansion process. This chapter presents detailed description of the performed calculations and assumptions.

6.1 Available thermodynamic models of screw expanders

The single-screw machine started to be considered for use as an expander only recently. While a lot of professional (and expensive) modelling software exist for the twin-screw machine, such as SCORG, SCCAD or KaSim [117]–[119], this cannot be said for the single-screw. The mathematical models that exist were published in scientific studies which often resulted in tested prototypes and there is so far no commercial program for calculating either the geometry or the thermodynamics of single-screw expanders. The modelling work done on SSEs so far focuses only on compressed air or organic fluids [52] [59] [80] [109]–[111]. A prototype has been tested and validated also for the Kalina cycle [112].

Multiple models for volumetric expanders have been developed in recent years. Most of the models are proposed by researchers from the University of Liège, Belgium. Lemort et al first designed a model for a scroll expander [120]. The model described the processes during expansion in several steps, taking into account the suction pressure loss, heat losses into the environment and also leakage losses. The expansion was divided into two parts – an isentropic and isochoric part. After it was proven that the model had very good agreement with measurements (maximum deviation of 5% for the shaft power), subsequent models for volumetric expanders were derived from these ideas, though each model uses different methods to approximate the various losses and relations within the system [110] [120] [121]. These models are semi-empirical, meaning that the coefficients and relations are derived from experimental testing of prototype expanders.

The only publicly available software for predicting the behaviour of volumetric machines is the open-source software package PDSim developed by Ziviani and Bell [109], [115]. This is a python-based software used for simulation of positive displacement machines. It has been validated with experiments multiple times. This tool would have been useful to compare results with, but unfortunately, the single-screw expander templates are currently missing from the template library and only the scroll and piston expander models are available [122]. A request to add the SSE templates was submitted to Mr. Bell via the PDSim’s Github page [123]. Hopefully, the templates will become available in the future.

6.2 Description of used thermodynamic model

This work uses single-screw expander thermodynamic model proposed by A. Giuffrida in 2017 [110] as it is the most recent SSE model with revised and more complex

computational methods for some of the aspects of the model. While Ziviani et. al proposed their versions of the SSE model over multiple papers [50] [84] [86], many of the relations for losses and heat transfer are identical to the scroll models. Giuffrida proposes new relations for the pressure, frictional and ambient heat losses and good agreement with experimental results is demonstrated. For example, it takes into account the thermo-physical properties of the working fluid during heat losses unlike the older scroll models, where the heat losses depend only on the mass flow rate [110].

While the relations for pressure, frictional and heat losses were adjusted according to experimental data, the structure of the model remains the same or similar to thermodynamic models of other volumetric expanders mentioned at the start of this chapter.

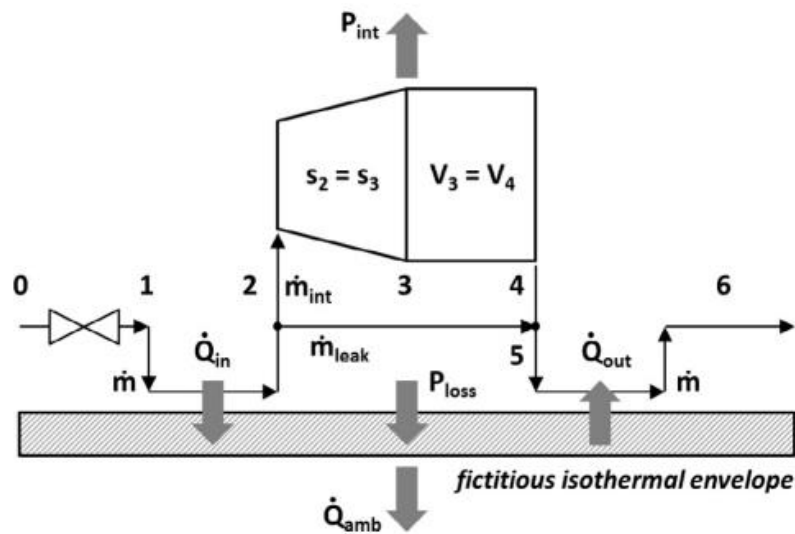


Figure 23 - Schematic of the screw expander model [110]

The expansion of the working fluid is described in six steps:

- 0 → 1 represents the supply pressure drop during filling of the chamber
- 1 → 2 represents isobaric cooling of the working fluid by a fictitious envelope
- 2 → 3 represents the first stage of the expansion, which is considered as isentropic
- 3 → 4 is the second stage of expansion, which is considered isochoric
- 4 → 5 is adiabatic mixing of the main flow and the leakage flow
- 5 → 6 represents the heating or cooling of the exiting fluid by the envelope [110].

6.2.1 Mathematical modelling

The flowchart in Figure 24 shows the inputs and outputs of the thermodynamic model.

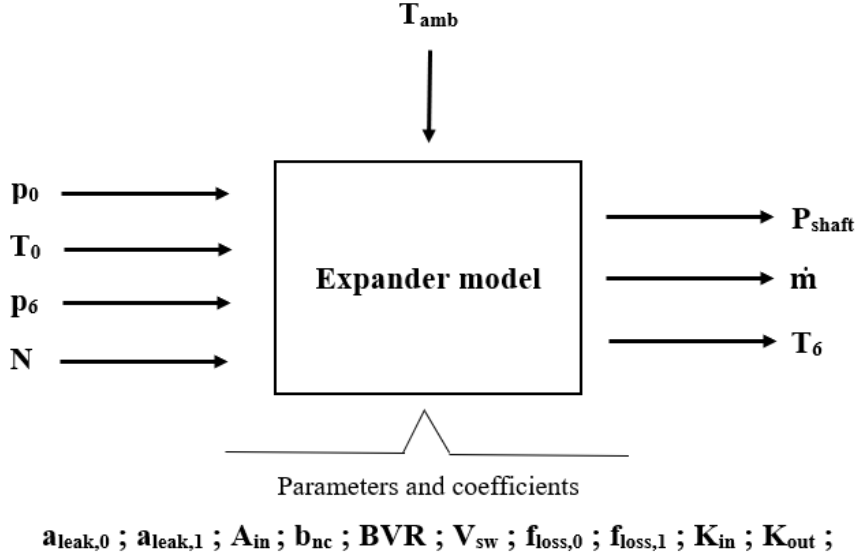


Figure 24 - Inputs and outputs of the SSE model

The four main inputs are the characteristics of the expansion process, where p_0 and T_0 are the inlet pressure and temperature, p_6 is the outlet pressure and N is the rotational speed. Ambient temperature also needs to be specified in order to calculate the temperature of the fictitious isothermal envelope.

The model then gives three outputs: the shaft power P_{shaft} , the mass flow rate \dot{m} and the outlet temperature T_6 . Other parameters and coefficients, shown in the bottom, need to be specified as well. These will be explained as the steps of the calculation are reviewed.

Supply pressure drop

The steam is throttled at the expander inlet as it enters the working chamber. An isentropic flow through a converging nozzle with a cross sectional area of A_{in} is assumed:

$$\dot{m} = \rho_{1,is} \cdot A_{in} \cdot \sqrt{2 \cdot (h_0 - h_{1,is})} \quad (3)$$

The pressure p_1 is calculated iteratively based on this equation. The enthalpy h_1 is equal to h_0 because of the throttling process.

Isobaric cooling-down of the steam

Heat transfer occurs between the steam and isothermal envelope of the expander. The heat transfer is modelled as:

$$Q_{su} = \dot{m} \cdot (h_1 - h_2) = \left[1 - e^{-\frac{AU_{in}}{\dot{m}C_p}} \right] \cdot \dot{m} \cdot C_p \cdot (T_1 - T_2) \quad (4)$$

where AU_{in} is the supply heat transfer coefficient expressed as follows:

$$AU_{in} = K_{in} \cdot \lambda \cdot \left(\frac{\dot{m}}{\mu}\right)^{0,8} \cdot Pr^m \quad (5)$$

where K_{in} is a geometric constant. The exponent m is equal to 0,4 if the fluid is heated by the wall and 0,3 if it is cooled down by the wall.

Internal leakage

Not all of the entering mass flow is usefully expanded in the chambers of the expander; a part of the mass flow leaks and does no useful work on the shaft. Shen et. al described in detail the different leakage paths in the SSE which can be obtained by numerically solving differential equations related to the angles of the main rotor and the starwheels [85]. However, in this model, a single hypothetical area is used to account for all the leakage paths. This area is then used to simulate the leakage as an isentropic flow through a converging nozzle, similarly to equation (3).

$$\dot{m}_{leak} = \rho_{leak} \cdot A_{leak} \cdot \sqrt{2 \cdot (h_2 - h_{leak})} \quad (6)$$

While the pressure on the inlet of this nozzle is p_2 (see Figure 23), the outlet pressure is the highest out of p_4 and the critical pressure $p_{crit,leak}$ which is calculated from p_2 by assuming the medium to be an ideal gas.

$$p_{crit,leak} = p_2 \cdot \left(\frac{2}{k+1}\right)^{\frac{k}{k-1}} \quad (7)$$

where k is the isentropic exponent (1,33 assumed for steam as a 3 atomic gas).

The leakage area is usually regarded as a constant. In this model, however, it is a function depending on the expander load:

$$A_{leak} = a_{leak,0} + a_{leak,1} \cdot p_{load} \quad (8)$$

where p_{load} is the mean absolute pressure on the rotating parts and is obtained as follows:

$$p_{load} = \rho_3 \cdot (h_2 - h_4) + p_6 \quad (9)$$

The utilized mass flow needs to rotate the shaft at a specified speed and needs to fill the grooves of the rotor, which are characterized by swept volume. Therefore, the relation for the entering and exiting mass flow is finally defined as:

$$\dot{m} = \rho_2 \cdot \frac{V_{sw}}{BVR} \cdot N + \dot{m}_{leak} \quad (10)$$

Isentropic expansion

The non-leaked part of the fluid expands in two stages. In the first stage, it expands isentropically to the adapted pressure which is defined by s_3 and v_3 , where $s_3 = s_2$ and:

$$v_3 = BVR \cdot v_2 \quad (11)$$

Adiabatic expansion at constant volume

The second stage of the expansion occurs adiabatically at constant machine volume. The model assumes that some fluid flows out or into the chambers instantly as they open up at the discharge. The discharge is then defined by $p_4 = p_5 = p_6$ and by h_4 from the relation:

$$h_3 - h_4 = v_3 \cdot (p_3 - p_4) \quad (12)$$

The adapted pressure p_3 can be either lower or higher than the system outlet pressure p_4 . Based on this, under- or over- expansion occurs, as illustrated on Figure 25.

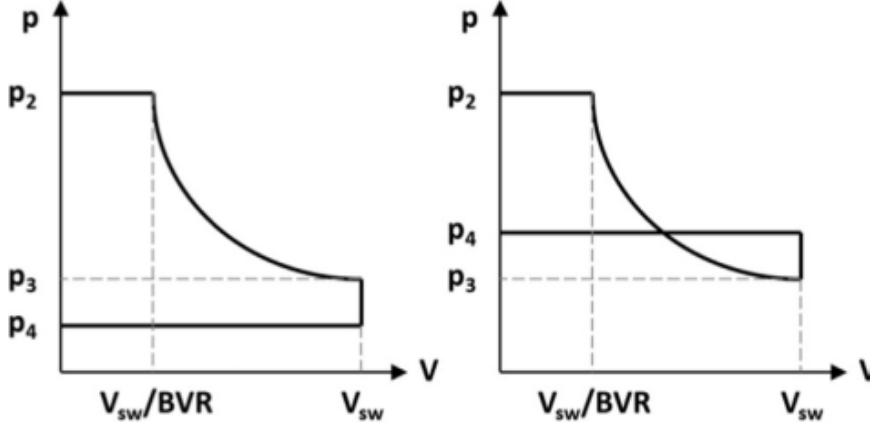


Figure 25 - Under- and over-expansion in the p-V diagram [110]

For both under- and over-expansion, equation (12) applies. For over-expansion, the term $p_3 - p_4$ will be negative and therefore the shaft power will be lower. Both cases mean losses, but the losses associated with over-expansion are cited to be higher [111].

Adiabatic mixing

After the expansion, the main mass flow and the leakage are again joined into one flow. They mix together and the enthalpy is increased as a result between points 4 and 5.

$$h_5 = \frac{(\dot{m} - \dot{m}_{leak}) \cdot h_4 + \dot{m}_{leak} \cdot h_2}{\dot{m}} \quad (13)$$

Isobaric heating up or cooling down on the exhaust

The last stage is heat transfer to or from the environment. Similarly to the heat transfer on the supply side, heat is exchanged between the fluid being exhausted from the expander and the isothermal envelope:

$$Q_{ex} = \dot{m} \cdot (h_5 - h_6) = \left[1 - e^{-\frac{AU_{out}}{\dot{m}C_p}} \right] \cdot \dot{m} \cdot C_p \cdot (T_5 - T_w) \quad (14)$$

Geometric constant K_{out} is introduced and AU_{out} is calculated just like AU_{in} in equation (5).

Heat losses

There will naturally be an imbalance between the heat flows on the supply and exhaust side of the expander. On top of that, the model assumes all mechanical losses to be injected as heat into the envelope. This will cause that heat to be transferred from the

expander envelope to the environment which is assumed to be at constant temperature T_{amb} . This heat can be calculated either from the envelope temperature:

$$Q_{amb} = b_{nc} \cdot (T_w - T_{amb})^{\frac{5}{4}} + b_{ra} \cdot (T_w^4 - T_{amb}^4) \quad (15)$$

where both convection and radiation are taken into account, or from the energy balance for heat transfer between the system of the expander and the environment:

$$P_{loss} + (1 - \eta_{gen}) \cdot P_{sh} + Q_{su} - Q_{amb} \pm Q_{ex} = 0 \quad (16)$$

Power output and power losses

After determining the thermodynamic states in steps 0 – 6, the expander internal power can be calculated:

$$P_{int} = (\dot{m} - \dot{m}_{leak}) \cdot (h_2 - h_4) \quad (17)$$

Next, a power loss accounting for friction must be introduced. The method of calculating it is different throughout the various expander models. The followed model calculates it as a function of rotational speed and the pressure p_{load} from equation (9):

$$P_{loss} = \left[f_{loss,0} + f_{loss,1} \cdot \frac{N}{p_{load}} \right] \cdot p_{load} \cdot N \quad (18)$$

Thus, the shaft and subsequently electric power can be obtained:

$$P_{sh} = P_{int} - P_{loss} \quad (19)$$

$$P_{el} = P_{sh} \cdot \eta_{gen} \quad (20)$$

Finally, the expander efficiency can be calculated. Since mechanical losses were already subtracted in equation (19), the expander efficiency as defined here means the mechanical efficiency of the expander and its shaft:

$$\eta_{exp} = \frac{P_{sh}}{\dot{m} \cdot (h_0 - h_{6,is})} \quad (21)$$

6.2.2 The calculation environment

The described model was implemented in MATLAB, where CoolProp and Refprop libraries were used to obtain the state properties of water and steam. While Coolprop has a simpler interface in MATLAB, it has difficulties obtaining state properties from certain combinations of inputs, such as density and entropy. Therefore, it was supplemented with Refprop where necessary.

An iterative approach was used to obtain the pressure drop, the flow rates and the envelope temperature, similarly to the approach taken by Rathan in his modelling of a scroll expander [124].

The model has several nodes where the iteration and the new result is compared and, if needed, recalculated. The model can then be used to calculate a wide range of input parameters of the inlet steam. Figure 26 shows the schematic of the calculation approach.

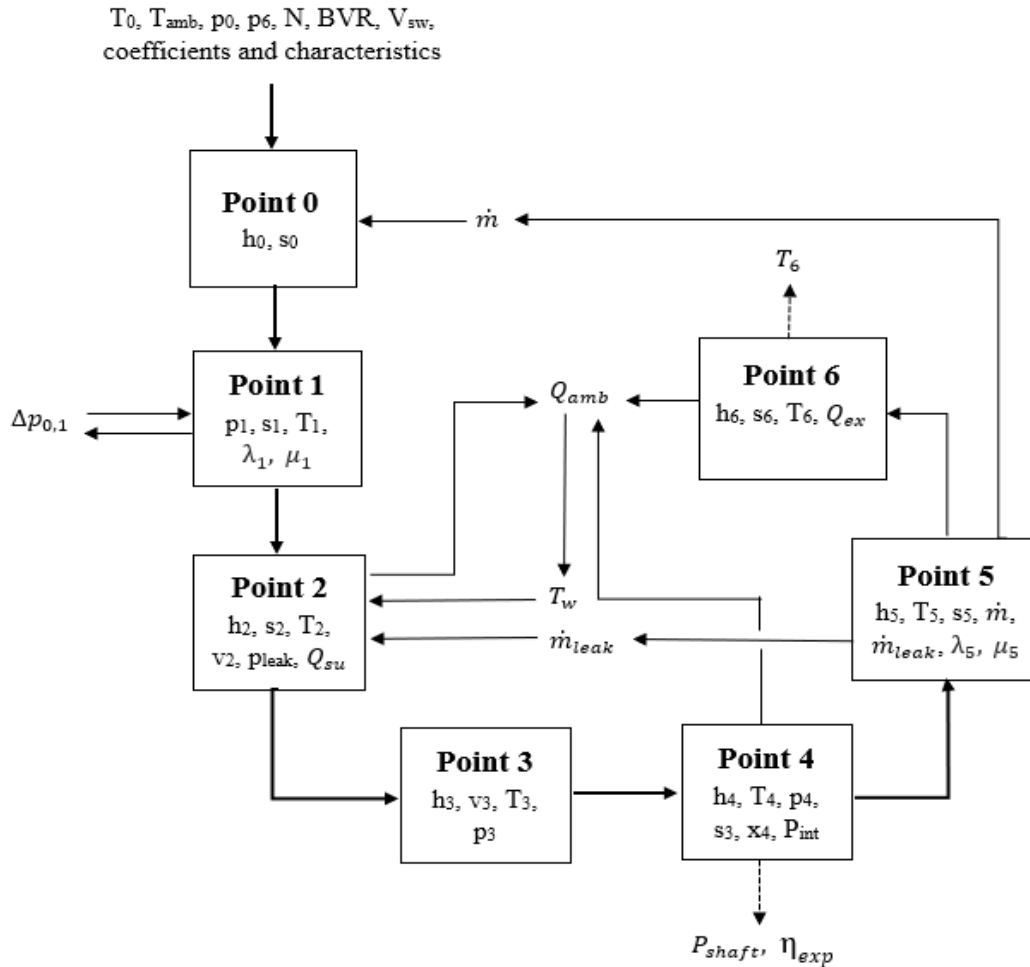


Figure 26 - Flowchart of the iterative calculation of the expansion

6.3 Geometry design model

The thermodynamic model described in the previous section depends on the geometric properties and design of the expander. The most notable of these characteristics are the swept volume V_{sw} and the built-in volume ratio BVR. Built-in volume ratio is the ratio of volumes at the beginning and the end of the expansion. Swept volume is the volume of liquid that can be displaced in a single rotation [80]. A geometry model is introduced to estimate the dimensions of the examined expander and to determine whether V_{sw} and BVR can be chosen independently or not.

Geometry model presented by Ziviani and Bell in [80] and [114] is used to obtain the angles and dimensions. The model presents geometric relations for a cylindrical-plate single-screw expander, in other words, one helical rotor and two starwheel rotors whose shafts are parallel to each other and perpendicular to the rotation axis of the main screw.

The input properties of the model are the main rotor diameter D_{sr} , number of grooves of the rotor z_{sr} , number of teeth of the starwheels z_{sw} and two lambda coefficients λ_d and

$\lambda_{opt} \cdot \lambda_d$ is the ratio of the starwheel diameter D_{sw} and main rotor diameter D_{sr} , while λ_{opt} is the ratio of the distance between the center axes of the main rotor and starwheels $d_{sr,sw}$ and D_{sr} . Based on these inputs, the entire geometry of the expander can be designed. In this work, the focus will be mainly on obtaining the swept volume, the built-in volume ratio through calculation of the groove volumes at suction and discharge points.

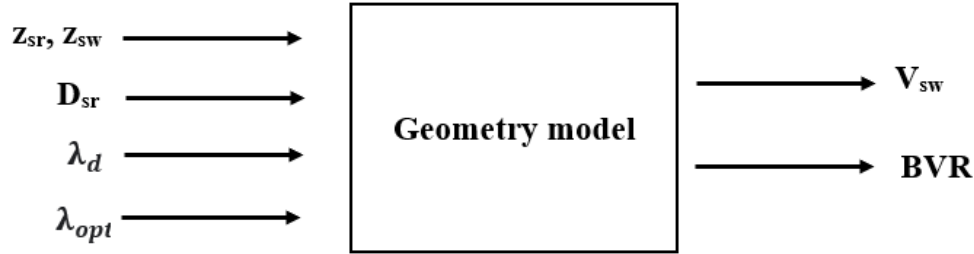


Figure 27 - Scheme of the inputs and desired outputs of the geometry model

Starwheel angles and main rotor section lengths

Firstly, the meshing pair engaging ratio is defined as:

$$i = \frac{z_{sw}}{z_{sr}} = \frac{\theta_{sw}}{\theta_{sr}} = \frac{\omega_{sw}}{\omega_{sr}} \quad (22)$$

The degree of penetration of the tooth into the groove is given by the distance of the axes of the main rotor and the starwheel:

$$d_{sr,sw} = \lambda_{opt} \cdot D_{sr} \quad (23)$$

The last input parameter that needs to be defined is the starwheel inner diameter, where for obvious structural reasons:

$$R_{sr} - (R_{sw} - R_{sw,in}) > R_{sr,sh} \quad (24)$$

Finally, the meshing angles can be calculated. Figure 28 shows where the respective angles are located in regard to the fixed coordinate systems of both the starwheel and the main rotor.

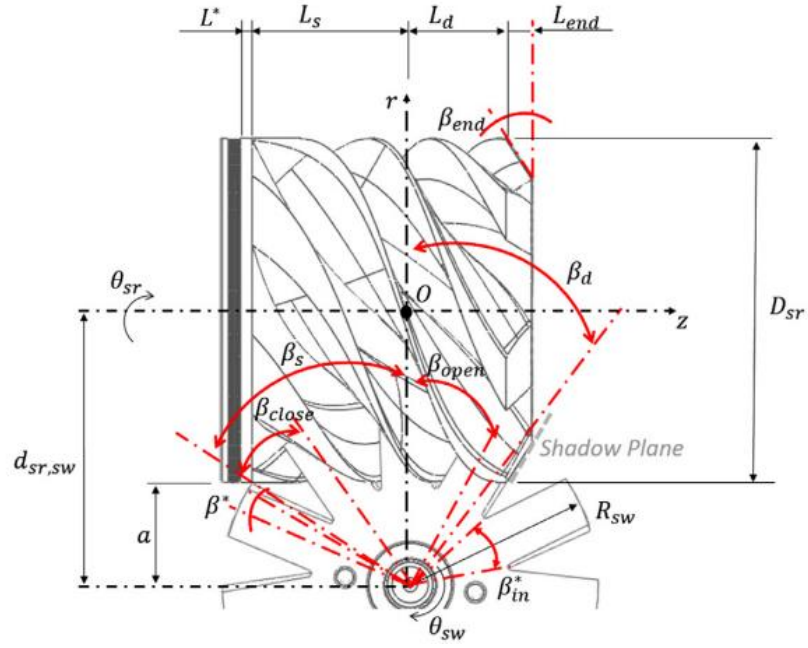


Figure 28 - Main geometric parameters of the SSE [80]

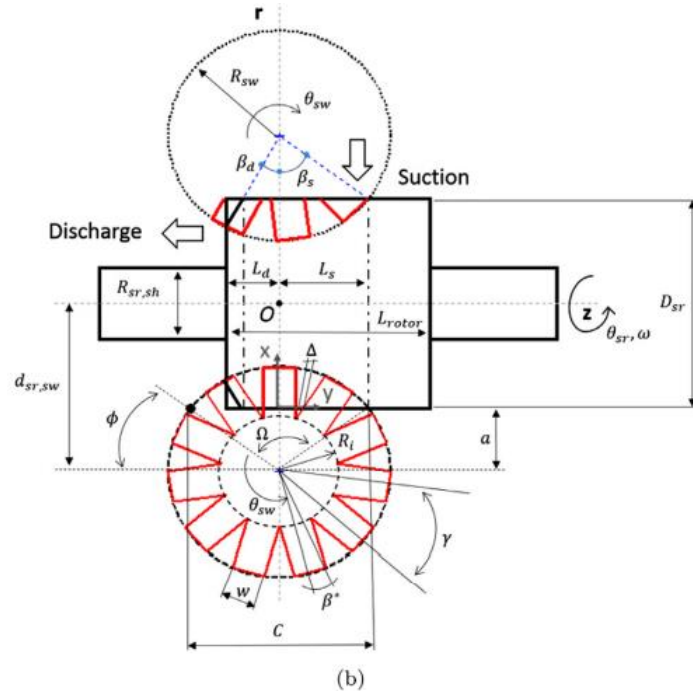


Figure 29 - Schematic view of the rotor meshing, suction and discharge side [80]

For the angles starwheel angles and rotor section lengths, the following relations are followed:

$$\beta_s = \cos^{-1} \left(\frac{d_{sr,sw} - R_{sr}}{R_{sw}} \right) \quad (25)$$

$$\beta^* = \sin^{-1} \left(\frac{w}{2R_{sw}} \right) \quad (26)$$

$$\beta_{in}^* = 2\sin^{-1} \left(\frac{w}{2R_{sw}} \right), \beta_{in}^* < \frac{2\pi}{z_{sw}} \quad (27)$$

$$L_s = R_{sw} \cdot \sin\beta_s \quad (28)$$

$$L_d = R_{sw} \cdot \sin\beta_d \quad (29)$$

$$L^* = (0,1 - 0,15) \cdot D_{sr} \quad (30)$$

The effective length of the expander that participates in the expansion is then obtained by simply adding the suction and discharge lengths:

$$L_{rot,eff} = L_s + L_d \quad (31)$$

Since $\alpha_{sw} = 90^\circ$, relation for the angle corresponding to the point of the discharge opening can be obtained:

$$\alpha_{sw} = \beta_{open} + \beta^* + \beta_s \quad (32)$$

While the relation for β_{close} is not given, we can approximate it from the ratio of the suction and discharge angles:

$$\beta_{close} = \beta_{open} \cdot \frac{\beta_s}{\beta_d} \quad (33)$$

However, it would be more accurate to obtain the angle from a CAD model.

The tooth width can also be calculated:

$$w = 2 \left(d_{sr,sw} - \frac{D_{sr}}{2} \right) \sin \frac{\gamma}{2} - \xi D_{sr} \cos \frac{\gamma}{2} \quad (34)$$

Where $\gamma = \frac{2\pi}{z_{sw}}$ and $\xi = 0,017 \sim 0,025$.

Groove volume

Using the cylindrical coordinates from Figure 28 and 29, and the angles and dimensions from equations (25) – (35), the variational groove volume can be calculated. Three approaches exist to obtain the groove volume: the polygon approach, the differential approach, and the analytic approach. In this work, the analytic approach is used. It is obtained by performing a numerical integration of functions describing the groove are during rotation. For full process of the integration, see [80].

The solution gives lengthy relations for two parts of the groove, V_{g1} and V_{g2} . V_{g1} is the groove volume during the suction, when $\theta_{sw} < \beta^*$, while V_{g2} is the volume of the groove on before the discharge open $\beta^* < \theta_{sw} < \beta_{open}$.

$$V_{g1}(\theta_{sw}) = i \left\{ d_{sw,sr} \left(R_{sw}^2 \beta^* + \frac{w}{2} \sqrt{R_{sw}^2 - \frac{w^2}{4}} \right) (\beta_s - \beta^* - \theta_{sw}) \right. \\ \left. - \left(\frac{R_{sw}^2 w}{2} - \frac{w^3}{12} \right) [\sin(\beta_s - \beta^*) - \sin\theta_{sw}] \right. \\ \left. - \frac{1}{4} \left[(d_{sw,sr} + R_{sr}) aw + \frac{w^3}{12} \right] \left[\log \frac{1 + \sin(\beta_s + \beta^*)}{1 - \sin(\beta_s - \beta^*)} \right. \right. \\ \left. \left. - \log \frac{1 + \sin\theta_{sw}}{1 - \sin\theta_{sw}} \right] \right\} \quad (35)$$

$$V_{g2}(\theta_{sw}) = \frac{i(\beta_s - \beta^* - \theta_{sw})^3}{12\beta^*} \left[R_{sw}^2 \beta^* + \frac{w}{2} \sqrt{R_{sw}^2 - \frac{w^2}{4}} - aw \frac{1}{\cos(\beta_s - \beta^*)} \right] \times \left\{ R_{sr} - \frac{1}{8\beta^*} [R_{sw} \cos(\beta_s - \beta_{2^*}) - a](\beta_s - \beta^* - \theta_{sw}) \right\} \quad (36)$$

Now the groove volume at discharge opening can be obtained as:

$$V_g = V_{g1} + V_{g2} \quad (37)$$

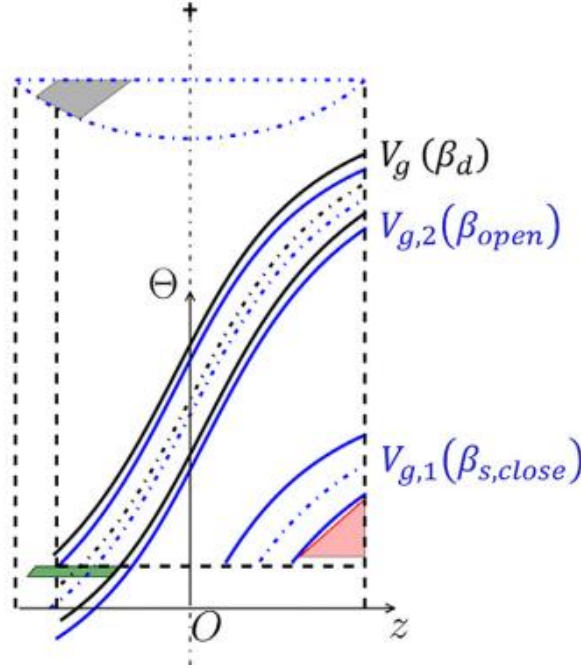


Figure 30 - Representation of V_{g1} and V_{g2} volumes [80]

The built-in volume ratio can then be obtained as the ratio of the groove volumes at suction closure and discharge opening [80].

$$BVR = \frac{V_g(\theta_{sw} = \beta_{open})}{V_g(\theta_{sw} = \beta_{close})} \quad (38)$$

The swept volume can be approximated from the sum of the groove volumes at suction closure and discharge opening also. The relation between $V_{g,max}$ and V_{sw} presented by Giuffrida is used here [110]. The real swept volume will be slightly larger however, owing to the limitations of the analytic method. To obtain a more accurate result, the polygon approach would need to be modelled or a CAD model made.

$$V_{sw} = \frac{2n_g V_{g,max}}{BVR} \cong \frac{2n_g [V_g(\theta_{sw} = \beta_{open}) + V_g(\theta_{sw} = \beta_{close})]}{BVR} \quad (39)$$

where n_g is the number of grooves, and it is multiplied by 2 because the expansion takes place on both sides of the rotor. The width of the entire expander configuration can be also calculated to estimate how much space it will take:

$$w_{exp,conf} = D_{sw} + 2a + D_{sr} \quad (40)$$

The model was set up in Microsoft Excel. Through experimentation, it became apparent that the swept volume and built-in volume ratio can be chosen independently. This is because BVR depends only on the λ_d coefficient and V_{sw} depends in turn only on BVR and the initial chosen rotor diameter. Therefore, BVR and V_{sw} , in this order, can be selected in a wide range of reasonable values and the geometry is then calculated in reverse by the solver function.

6.4 Boundary conditions of the examined steam cycles and desired outputs

The expander models described above are set into Rankine cycles to determine the overall efficiency and heat output. In this section, boundary conditions and assumptions for the cycles are listed. Both variants assume cogeneration. Simple cycle consisting only of a pump, a heat exchanger / boiler, the expander, and a condenser is assumed, as visualized at the beginning of this work in Figure 1.

Variant 1 is intended to transfer heat into supply or process water. Therefore, the condensation temperature is chosen at 100 °C, which corresponds to atmospheric backpressure of 0,1 MPa.

Variant 2 is intended to be connected to a bottoming ORC based on the WAVE 120 CHP unit developed by the Laboratory of Organic Rankine Cycle Applications (LORCA) at UCEEB CTU. The unit uses MM (hexamethyldisiloxane) as working fluid with evaporation temperature at 170 °C and superheating to 180 °C [17]. Temperature difference in the heat exchanger between the two cycles is estimated at 20 - 30 °C. The condensation temperature of the topping Rankine cycle is therefore chosen at 200 °C, which corresponds to backpressure of 1,55 MPa. This configuration (topping RC + bottoming ORC) was considered also in [125] and tested in [126] for larger CHP systems with 189 kW and 260 kW respectively in net power output. The results indicate that this combined cycle achieves better heat source temperature matching than a single ORC or RC and with more generated power.

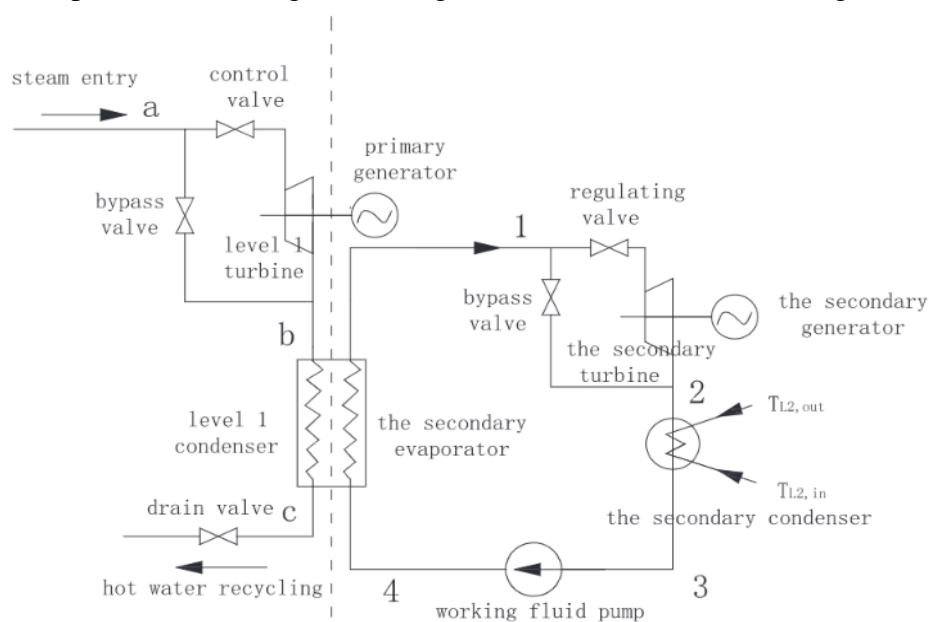


Figure 31 - Schematic of RC + ORC combined cycle system tested in [126]

6.4.1 Boundary conditions for two variants of the Rankine cycle

While Variant 1 uses backpressure equal to one atmosphere, Variant 2 assumes backpressure of 1,55 MPa. The range of inlet parameters is adjusted accordingly. The generator efficiency is assumed at 91,2 % [127] and the pump efficiency at 48 % [128]. The suction port area and the hypothetical leakage area are taken from [110].

For Variant 1, pressure ratios between 2,5 and 15 will be considered, following the knowledge gained in Chapter 4. Considering that new ceramic materials could be used to manufacture this expander, the temperature range can go up. Inlet temperatures from 180 °C up to 600 °C will be considered.

The second variant works under fundamentally different conditions. Pressure corresponding to condensation temperature of 200 °C is 1,55 MPa. That means that using pressure ratios as high as in the first variant becomes difficult. As outlined in Chapter 4, the highest inlet pressure found in literature for any volumetric expander was 4 MPa (piston) and for screw it was only 3 MPa, which would correspond to pressure ratio of only $\frac{3}{1,55} = 1,94$. However, since losses associated with high pressure are all accounted for in the model, it will be attempted to produce results for pressures up to 5 MPa ($\epsilon_{\max} = 5/1,55 = 3,2$).

The high-temperature ceramic screw expander developed by BraytonEnergy [94] is purposed for a gas cycle and therefore likely for lower pressures. However, the goal of this work is to assess the potential of low power steam cycles in a wide context and therefore, even higher pressures will be considered, although a combination of high temperature and pressure could turn out to be not possible for a real application. Subsequent prototyping and testing will be required to establish the limits of the assumed materials.

BVR is considered in the range dictated by literature (see Chapter 4). For the swept volume, the dimensions of the expander need to be taken into account.

Cycle properties		Variant 1	Variant 2
Symbol	Name [unit]		
p_6	Exhaust pressure [MPa]	0,1	1,55
T_0	Inlet temperature [°C]	180 – 600	280 – 600
η_{gen}	Generator efficiency [%]	91,2	
η_{pump}	Pump efficiency [%]	48	
ΔT_{sup}	Minimum superheating [°C]	10	
ϵ	Pressure ratio [-]	2,5 – 15	1,4 – 3,2
x_4	Minimum exhaust steam quality [-]	0,9	
Δp_{cycle}	Pressure losses outside the expander (pipes, heat exchangers, boiler) [kPa]	0	

Table 13 - Boundary conditions for cycle properties of two variants of examined Rankine cycles

Expander properties		Variant 1	Variant 2
Symbol	Name [unit]		
BVR	Built-in volume ratio	2 - 7	
V_{sw}	Swept volume [cm ³]	200 - 2000	
A_{in}	Expander suction port area [mm ²]	93	
$a_{leak,0}$	Nominal leakage area [mm ²]	17	
$a_{leak,1}$	Coefficient for leakage area [m ² bar ⁻¹]	$0,76 \cdot 10^{-6}$	
b_{ra}	Coefficient of heat losses for radiation [W K ⁻⁴]	$3,14 \cdot 10^{-8}$	
B_{nc}	Coefficient of heat losses for natural convection [W K ^{-1,25}]	1,32	
$f_{loss,0}$	Coefficient for mechanical losses [m ³]	$103,2 \cdot 10^{-6}$	
$f_{loss,1}$	Coefficient for pressure and speed dependent mechanical losses [m ³ s bar]	$3,03 \cdot 10^{-6}$	
K_{in}	Heat transfer coefficient at the inlet [m ^{1,8}]	1,12	
K_{out}	Heat transfer coefficient at the outlet [m ^{1,8}]	1,12	
T_{amb}	Ambient temperature [°C]	20	

Table 14 - Expander properties and coefficients

Only two rotational speeds will be considered – 3000 and 1500 rpm, to eliminate the need for a gearbox between the shaft and the generator. Where possible, 3000 rpm will be maintained.

The coefficients, leakage area and suction port area in Table 14 are adopted from [110]. BVR and V_{sw} will be selected based on analysing how they influence the expansion process.

Furthermore, for the single-screw expander geometry outlined in 6.3, recommended values for some of the coefficients are adopted. If the recommended value is in a range, the middle value is chosen. Namely, a standard configuration of 6 grooves on the main rotor and 11 starwheel teeth will be used. Starwheel inner diameter is chosen to be half the outer diameter. All of the chosen parameters and coefficients for the expander geometry are stated in Table 15.

Coefficients		Value
Symbol	Explanation [unit]	
z_{sr}	Number of grooves on the main rotor [-]	6
z_{sw}	Number of starwheel teeth [-]	11
λ_{opt}	Ratio of distance between the rotor axes and the main rotor diameter [-]	0,8
β_d	Starwheel discharge angle [°]	$0,7 \cdot \beta_s$
$D_{sw,in}$	Starwheel inner diameter [mm]	$0,5 \cdot D_{sw}$
L^*	Length of the initial section of the expander before the grooves [mm]	$0,125 \cdot D_{sr}$
ξ	Tooth width parameter [-]	0,02

Table 15 - Assumed geometry coefficients of the expanders [80]

Therefore, for the expander geometry model, the defining input parameters that determine the expander swept volume and built-in volume ratio will be the main rotor

diameter D_{sr} (influences the swept volume) and the ratio of starwheel and main rotor diameter λ_d (influences the built-in volume ratio). The largest dimension of the entire machine will be its width across both the starwheels and the main rotor. The upper limit value for this width was chosen at 1 meter, as a decentralised expander machine cannot be too big and size is an important factor when designing and considering a decentralised CHP unit [6]. Width of 1 meter across the starwheels corresponds to about 2000 cm³ swept volume, depending on the built-in volume ratio.

6.4.2 Limitations, assumptions and possible inaccuracies of used models

The previous sections outlined in detail how the single-screw geometry and expansion process are modelled to obtain results for a single-screw expander in a steam Rankine cycle operating under a wide range of inlet conditions. However, since the model does not account for factors such as strength of the materials under high temperatures or mechanical deformations caused by a high pressure or vibrations, the model will naturally have some limitations. The thermodynamic model was also originally designed for an organic working fluid, so the differences for water need to be taken into account. Firstly, the assumptions and limitations of the thermodynamic model are as follows:

- The kinetic energy of the fluid is neglected in comparison with its internal energy. No pressure drop is assumed at the expander outlet. Fluid leakage through the clearance is assumed to be adiabatic and the presence of lubricating oil is neglected [110].
- The inputted inlet pressures and pressure ratios will be used in the ranges as cited in literature in Chapter 4.
- When initially testing the model, it was noted that at some combinations of the inlet parameters, such as high V_{sw} and low BVR, the model could not iterate the pressure loss at the expander inlet (process 0 → 1, see section 6.2). This is because the model calculates pressure p_1 through an isentropic pressure drop first in equation (3). This becomes problematic when the isentropic point 1 drops below the saturation curve and the model is unable to find a point under the saturation curve, whose enthalpy would satisfy equation (3). These cases will therefore be omitted from the results, and it will likely not be possible to test all of the expanders designed in further chapters on the entire range of inputs.

Secondly, the results will be inadvertently subjected to various inaccuracies:

- The models themselves have an inherent inaccuracy. For the thermodynamic model, mean absolute percentage errors for the mass flow rate, electric power output and exhaust fluid temperature are cited as 0,69%, 1,77% and 0,33% respectively [110].
- For the geometry model, error of up to 3,66% for the maximum groove volume $V_{g,max}$ is stated [80].
- A possibly larger error can be caused by taking the suction inlet port area and the leakage area as fixed values without regards to the dimensions of the expander, while in real applications, these would go up with the size of the expander.
- Approximating $V_{g,max}$ in equation (39) will also yield an inaccuracy, since the real $V_{g,max}$ will always be slightly larger. These errors could be eliminated by constructing CAD models for all of the single-screw expanders designed in the later sections and

obtaining these values from them. However, as this is outside of the scope of this work, the above-stated assumptions will be taken and suction port and leakage area values from [110] assumed as fixed values in all considered expanders.

Chapter 7: Defining the geometry of appropriate expanders for two pressure levels

Two important characteristics influence the behaviour of a volumetric expander, as outlined in previous chapters. These are the built-in volume ratio and the swept volume, as outlined in the previous chapter.

A wide range of combinations of BVR and V_{sw} can be achieved, as BVR depends mainly on the ratio of the rotor and starwheels diameter while V_{sw} depends mainly on the rotor diameter D_{sr} . In this chapter, dependencies of expander and cycle efficiency, delivered power and outputted heat on these two properties will be determined.

As outlined in previous chapters, to aim of this work is to model expanders for two different Rankine cycles:

- Variant 1 with condensation temperature 100 °C (corresponding to pressure of 0,1 MPa)
- Variant 2 with condensation temperature 200 °C (corresponding to pressure of 1,55 MPa)

Based on the data presented in this chapter, 1 - 5 expanders will be modelled along with their geometry for both of the variants. It is expected that for each pressure ratio and temperature, there will exist a different appropriate expander. This chapter will propose expanders that perform well in a range of conditions and these machines will then be tested under a wide range of pressure ratios and temperatures in future chapters.

The dependence of four outputs is evaluated as the key factors when defining expanders for further testing – expander efficiency, heat output, net electric power output and electrical efficiency. Net electric power output is evaluated as the shaft power multiplied by generator efficiency and reduced by the pump work. The net electrical efficiency is then calculated as the net electric power divided by the heat input into the cycle. As for the thermal output, it is assumed that all of the rejected heat from the cycle can be utilized.

$$P_{el,net} = P_{sh} \cdot \eta_{gen} - P_{pump} \quad (41)$$

$$\eta_{el,net} = \frac{P_{el,net}}{Q_{cycle,in}} \quad (42)$$

7.1 Expanders for the 100 °C condensation variant (Variant 1)

7.1.1 Demands on the expanders and desired outputs

The single-screw expander can be designed in a number of ways and can operate under a wide range of working conditions. Therefore, demands have to be set as to what is expected from the machine.

As the system is designated to work as a cogeneration device, the most important demand is the heat output. For the variant with exhaust pressure equal to atmospheric, heat output ranging between 200 and 250 kW is determined. Built-in volume ratios will range from around 2,4 to 7. Very low BVRs result in pressure losses and they are omitted (see 6.4.2).

Owing to low efficiencies of the expander, the expansion often ends in superheated steam, or very slightly in wet steam (for high pressure ratios).

Firstly, the influence of BVR on the stated outputs will be determined and a specific value or a range will be selected. Next, the effect of increasing or decreasing swept volume will be studied and finally, several combinations (and therefore expander geometries) of BVR and swept volume will be selected for further testing under various conditions.

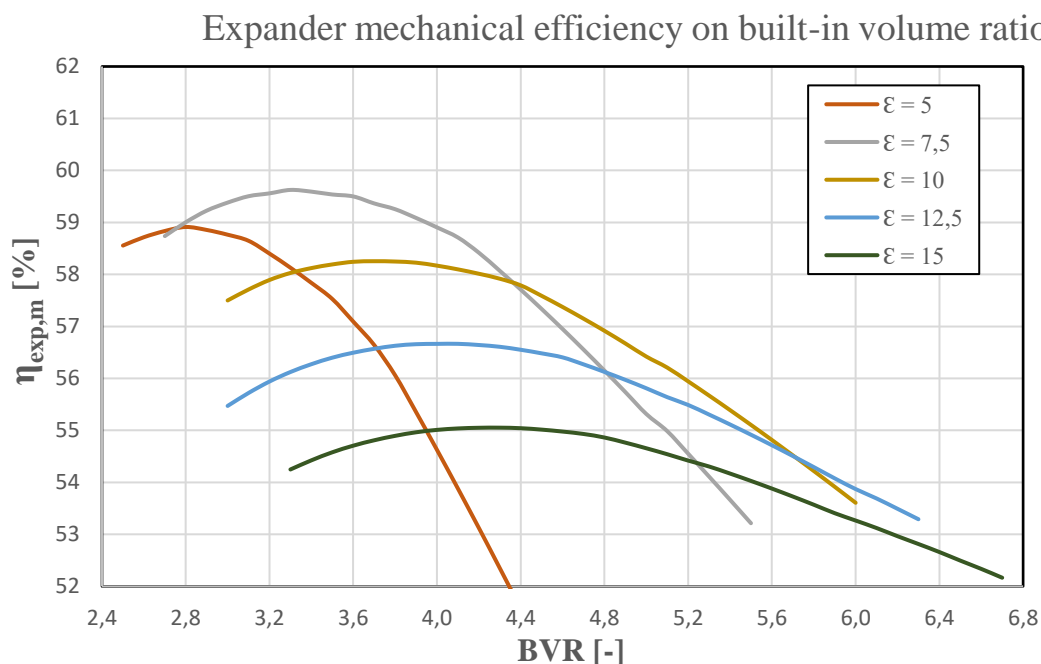
7.1.2 Determining how BVR influences the cycle

Firstly, let us determine how a lower or greater built-in volume ratio influences the performance of the expander with other input parameters set at fixed values. Here, we have set the following starting conditions:

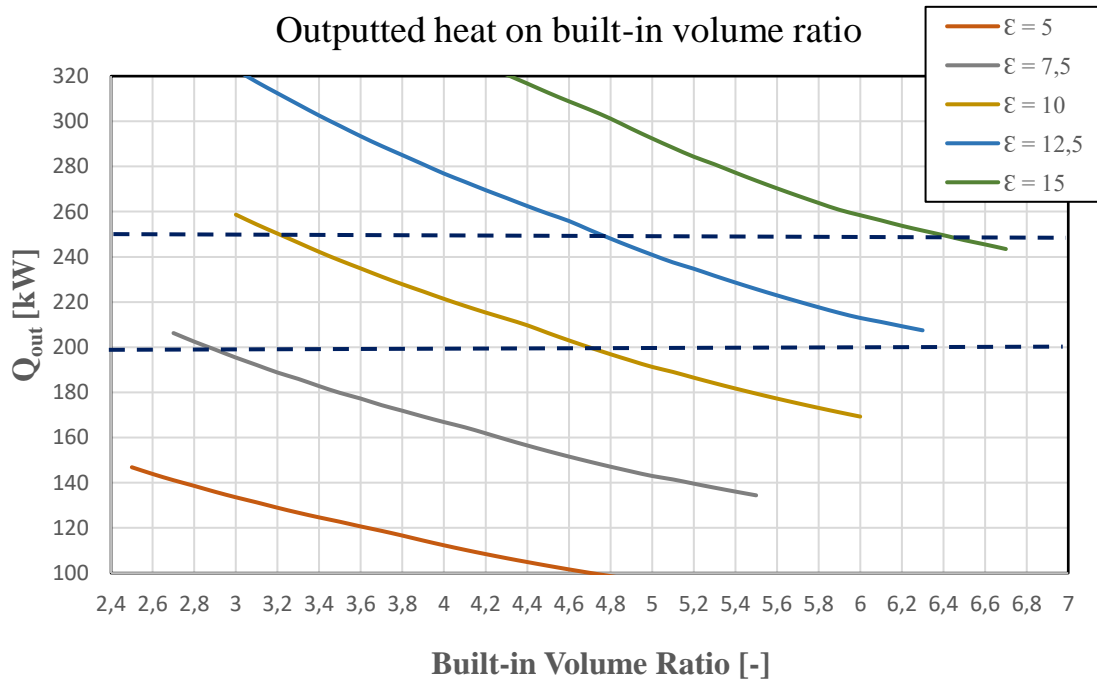
T_{ad} [°C]	ε [-]	N [rpm]	V_{sw} [cm ³]
220	5 - 15	3000	1400

Table 16 - Conditions for determining influence of BVR, T = 220 °C, Var 1

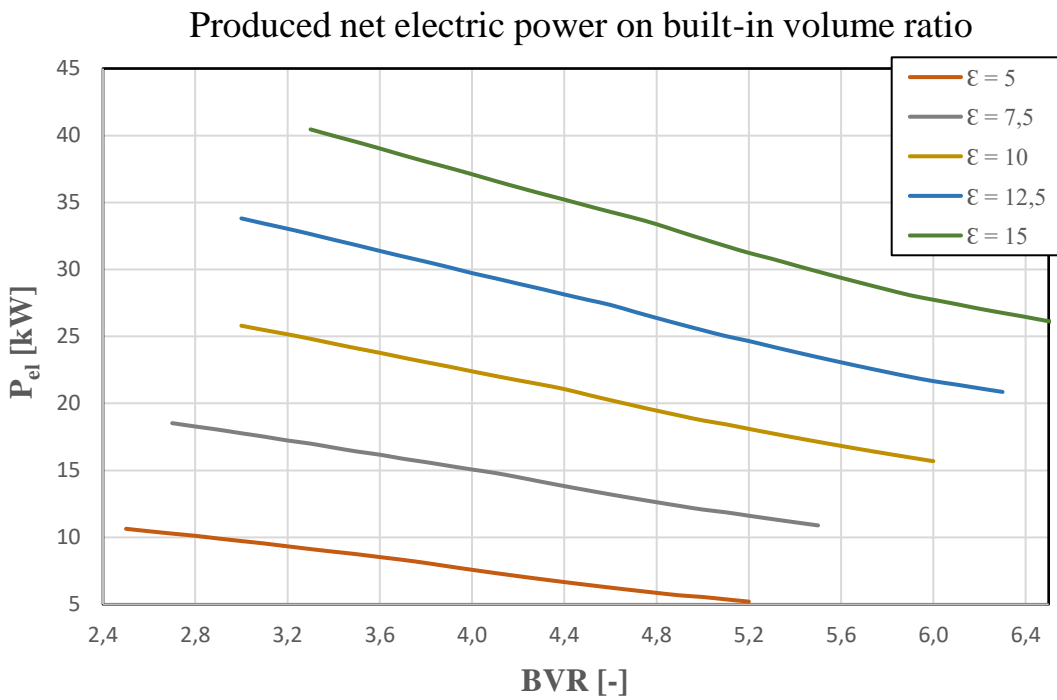
The outputs are evaluated for five different pressure ratios from 5 to 15 with a step of 2,5. Since exhaust pressure remains the same (0,1 MPa), it is only the admission pressure that changes (so $p_a = 0,5$ Mpa for $\varepsilon = 5$ and so on). Originally, lower ε of 2,5 was also studied. However, its performance in all observed outputs was much poorer than its counterparts and was therefore eliminated.



Graph 1 - Expander efficiency on BVR, T = 220 °C, Var 1

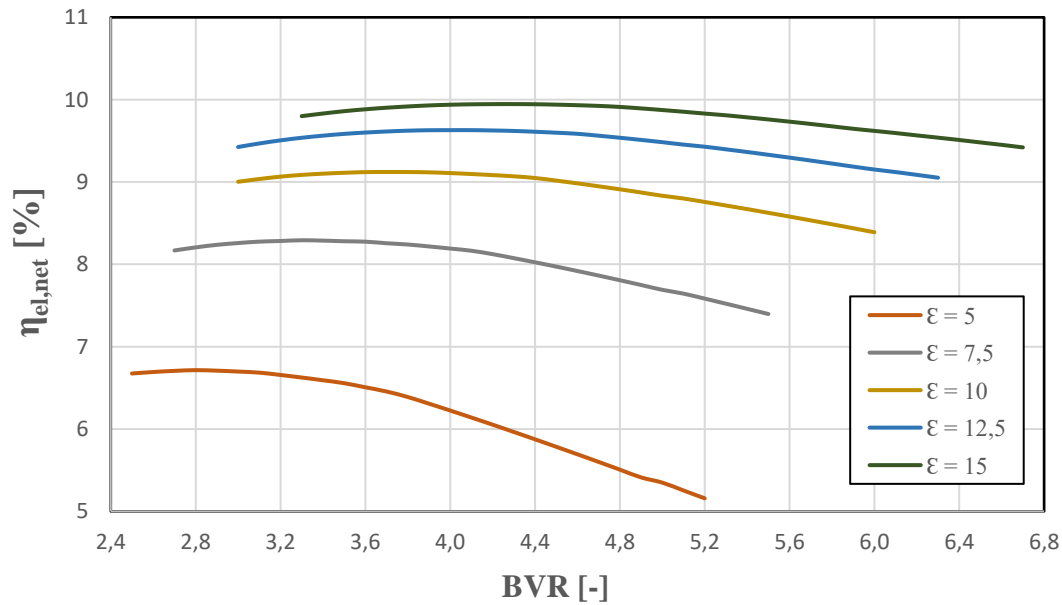


Graph 2 - Outputted heat on BVR, T = 220°C, desired range of outputs highlighted, Var 1



Graph 3 - Net electric power electric power on BVR, T = 220°C, Var 1

Net electrical efficiency on built-in volume ratio



Graph 4 - Electrical efficiency of the cycle on BVR, T = 220°C, Var 1

We can observe that while lower BVRs seem to produce significantly more useful heat and electricity, the efficiency of the cycle peaks slightly towards higher BVR. It is also notable that in terms of efficiency, higher pressure ratios will peak at higher built-in volume ratios. This is because the nature of the model – naturally, for each pressure ratio, the most efficient built-in volume ratio will be the one that will extend the isentropic part of expansion and suppress the isochoric part.

Despite greater pressure and leakage losses and therefore lower expander efficiency, higher inlet pressures will result in a higher system efficiency.

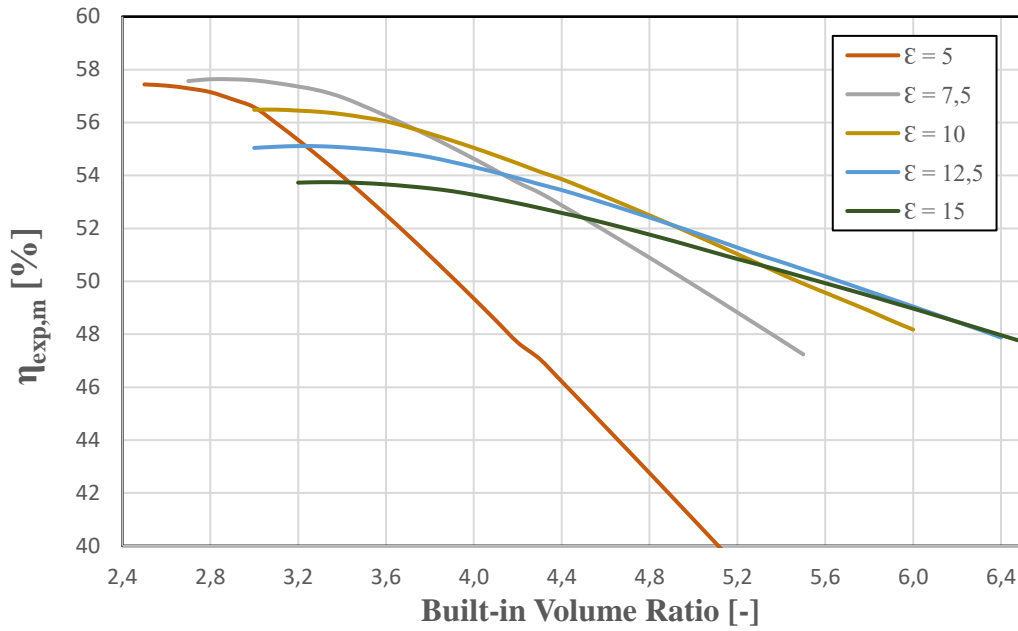
The decline in power and heat output as the BVR grows is because the model tends towards a lower mass flow rate with increasing BVR (see equation (10)).

One more run of the model will be made with a higher temperature to determine whether the relations will be different. Therefore, the inputs for the following graphs will be:

T _{ad} [°C]	ε [-]	N [rpm]	V _{sw} [cm ³]
450	5 - 15	3000	1400

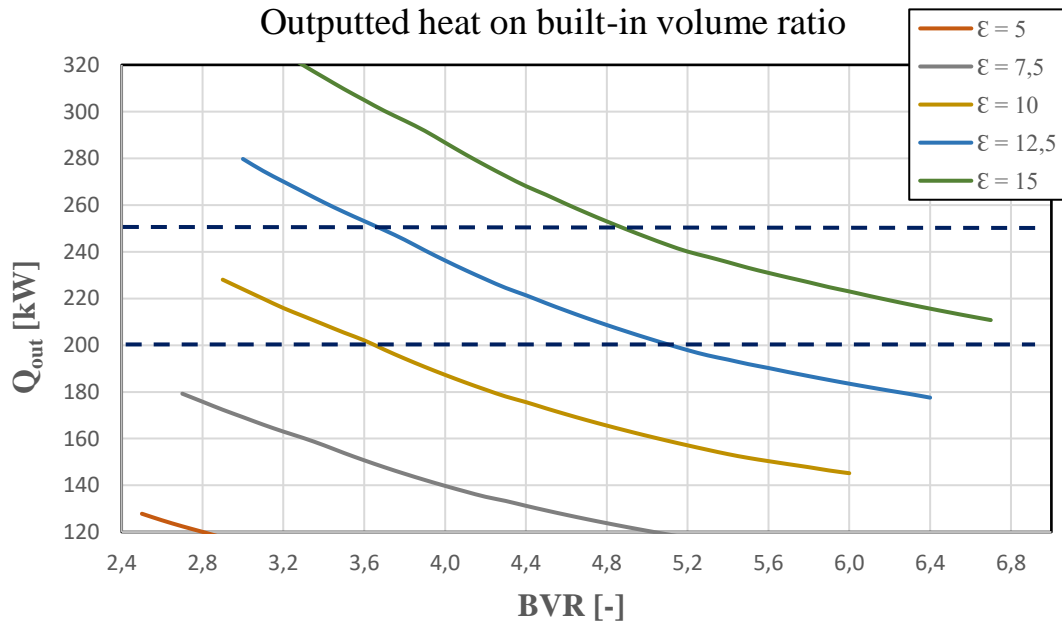
Table 17 - Conditions for determining influence of BVR for Var 1, T = 450 °C

Expander efficiency on built-in volume ratio



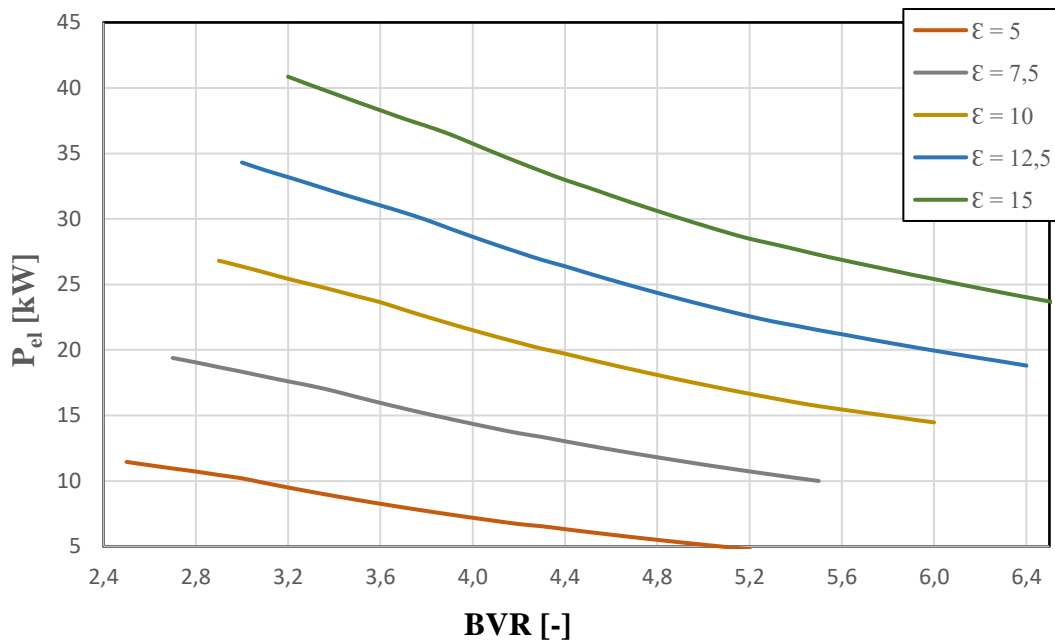
Graph 5 - Expander efficiency on BVR for Var 1, T = 450 °C

Outputted heat on built-in volume ratio



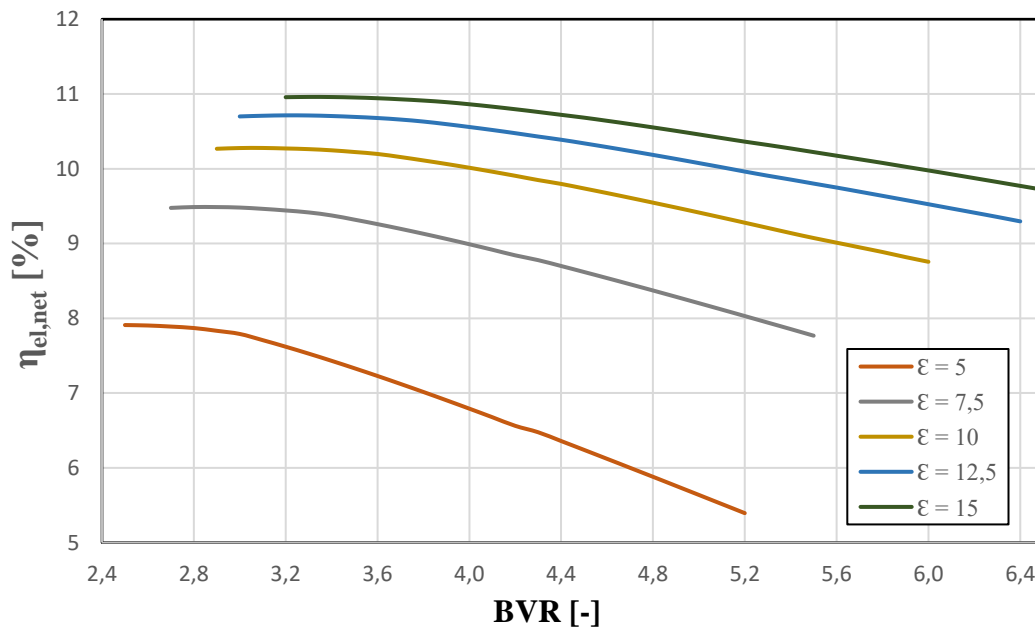
Graph 6 - Heat output on BVR, T = 450 °C, with the desired range highlighted, Var 1

Net electrical power on built-in volume ratio



Graph 7 - Electric power on BVR for Var 1, T = 450 °C

Net electrical efficiency on built-in volume ratio



Graph 8 - Electrical efficiency on BVR for Var 1, T = 450 °C

The expander efficiency is lower because at higher inlet temperatures, the relative leakage mass flow rate becomes greater. The curve of the decreasing η_{exp} is much steeper than for the lower temperature. A greater range of BVRs is possible, as pressure drops that would have ended in wet steam below the saturation curve (see limitations in 6.4.2) end in superheated steam instead and can therefore be calculated. Despite a decline in expander efficiency, the overall system efficiency is greater thanks to the increased temperature.

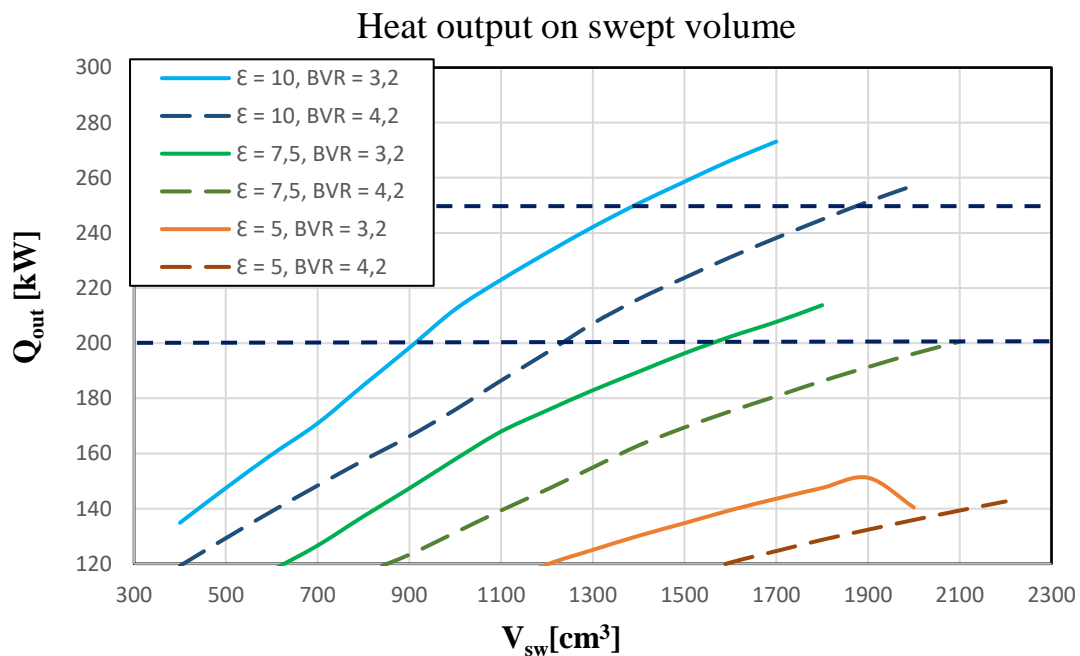
The heat and power curves are similar to the lower temperature variant. The heat output is even somewhat lower. There are several reasons for this. At higher temperatures, the model will lean towards lower mass flow rates at the same swept volume; the ambient heat loss is greater; larger fractions of the inputted heat are converted into electricity. Therefore, dependence of the outputs on changing swept volume should be examined next.

7.1.3 Determining how BVR in combination with V_{sw} influences the cycle

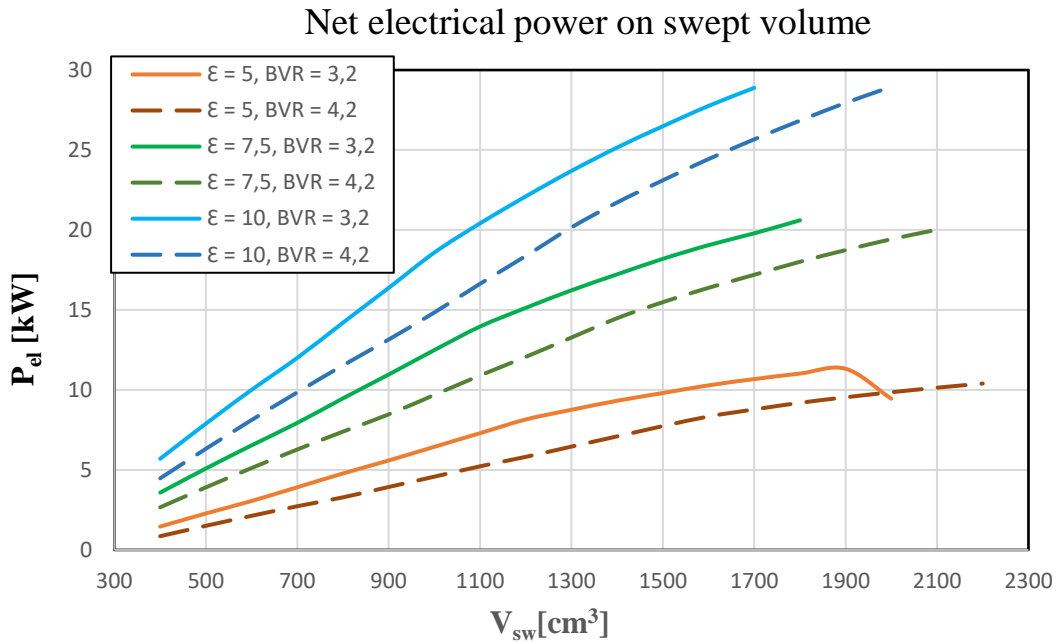
These relations are now observed when the swept volume of the expander is changed along with the BVR. On the graphs below, three different pressure levels with two different BVRs are shown for the following conditions:

T_{ad} [°C]	ϵ [-]	N [rpm]	BVR [-]
220	5 - 10	3000	3,2 and 4,2

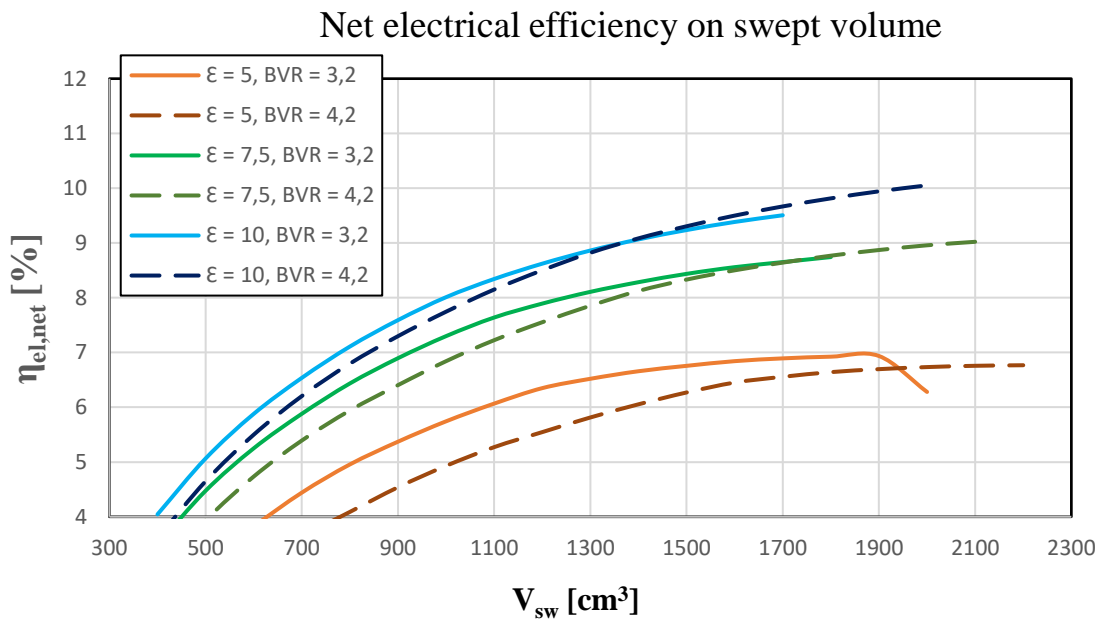
Table 18 - Parameters for determining the influence of swept volume on the performance for Var 1



Graph 9 - Heat output on swept volume for Var 1



Graph 10 - Power output on swept volume for Var 1



Graph 11 - Power output on swept volume and volume ratio for Var 1

While lower BVRs still push the system towards better performance, larger expander has a positive effect on all observed outputs. An interesting point in the above-shown graph occurs for the “ $\epsilon = 10$ ” lines where at a large swept volume, the higher BVR achieves a better electrical efficiency, which is something that wasn’t apparent when examining the BVR alone with V_{sw} fixed. This increase is only fractions of a percentage point. For a combination of higher BVR and V_{sw} , the model is also capable of calculating a wider range of operating conditions. This is because a combination of low BVR and high V_{sw} leads to a high mass flow, which in turn results in a greater pressure loss, which, if it gets so high that the computational nodes drop below the saturation curve, exit the boundary of this model.

7.1.4 Defining expander parameters for further testing

Knowledge from this subchapter can be summarized as follows:

- A lower BVR favours the production of work and heat. However, in order to stay within the boundaries of the model, there is a minimum required BVR for each pressure ratio (see graphs in 7.1.2)
- For each admission pressure, there exists a peak in both expander and overall efficiency on a specific BVR value.
- Taking these two points into account, the ideal range of BVRs is between 3 and 6,4. A very wide range of BVRs satisfies the demand of heat output between 200 and 250 kW when pressure ratios of 5 – 15 are considered.
- A high V_{sw} positively affects all observed outputs owing to greater mass flow rates and lower relative leakage flow rates. Increasing BVR along with V_{sw} affects the work and heat output negatively but can increase cycle efficiency.
- Combinations of a low BVR and high V_{sw} should yield strong performance with high efficiency and high power outputs. However, the range of acceptable conditions for such a combination is expected to be smaller because of higher mass flow rates that will lead to pressure drops which are problematic for the model.

Based on these standpoints, four expanders are defined for further analysis under different pressures and temperatures:

	Expander A	Expander B	Expander C	Expander D
BVR [-]	3	4,4	6,2	3,5
V_{sw} [cm³]	1300	1800	2000	2000

Table 19 - Selected expanders and their swept volumes and volume ratios for Var 1

Expanders A, B and C all have a swept volume defined proportionally to their BVR, which will allow for a wide range of operating conditions to be tested. They are expected to work under a wide range of conditions and provide the desired outputs while maintaining good efficiency. It will be examined whether expander A will achieve better efficiency thanks to a low BVR, expander C thanks to a high swept volume or expander B in the middle and how well they will be able to satisfy the stated demands. The width of expander C slightly exceeds 1 meter, but the properties are kept to explore whether the machine will give a better performance as compensation.

Expander D was chosen with a relatively low BVR and a high V_{sw} . This will make the range of acceptable inputs for this expander smaller, but since both lower BVR and higher V_{sw} increase the work and heat output and to a certain point efficiency, a good performance is expected even at lower pressure ratios.

Based on their respective BVR and V_{sw} , geometry of these expanders can be designed based on the model presented in section 6.3. A reverse approach is used – BVR and V_{sw} are chosen, and the geometric parameters are calculated from them. The respective geometries of the expanders can be found in Appendix A.

7.2 Expanders for the 200 °C condensation variant (Variant 2)

Next, Variant 2 with exhaust pressure of 1,55 MPa will be examined and the influence of BVR and V_{sw} determined, building on knowledge from the previous chapter. Lower efficiencies are to be expected from this setup because a higher pressure will inevitably lead to higher pressure, leakage and friction losses. However, this variant is proposed with the assumption that a bottoming ORC cycle would be installed and therefore all of the exhaust heat utilized.

While the pressure is limited, inlet temperature can be studied for much wider range. The only limitation is that of materials. However, as outlined in Chapter 3, very high steam temperatures can be deployed in modern supercritical plants and steels such as P91 and P92 can be employed up to 600 °C. Therefore, temperature range of 350 - 600 °C can be considered.

It is expected that the swept volume will need to be lowered to decrease the mass flow rate and therefore minimize the pressure losses. Finally, it has been noted during the first initial runs of the model for this variant that rotational speed also needs to be decreased, otherwise either the pressure loss is too great, or the heat output greatly exceeded the defined 200 – 250 kW range. Therefore, $n = 1500$ rpm is used instead of 3000.

When it comes to determining the expander geometry, similar approach to the previous variant will be used. First, the effect of built-in volume ratio on different pressure ratios and inlet temperatures will be studied. Then, change in swept volume will be introduced. The results and trends will be evaluated and, if the desired heat output can be achieved, one or more expanders will be defined for further testing.

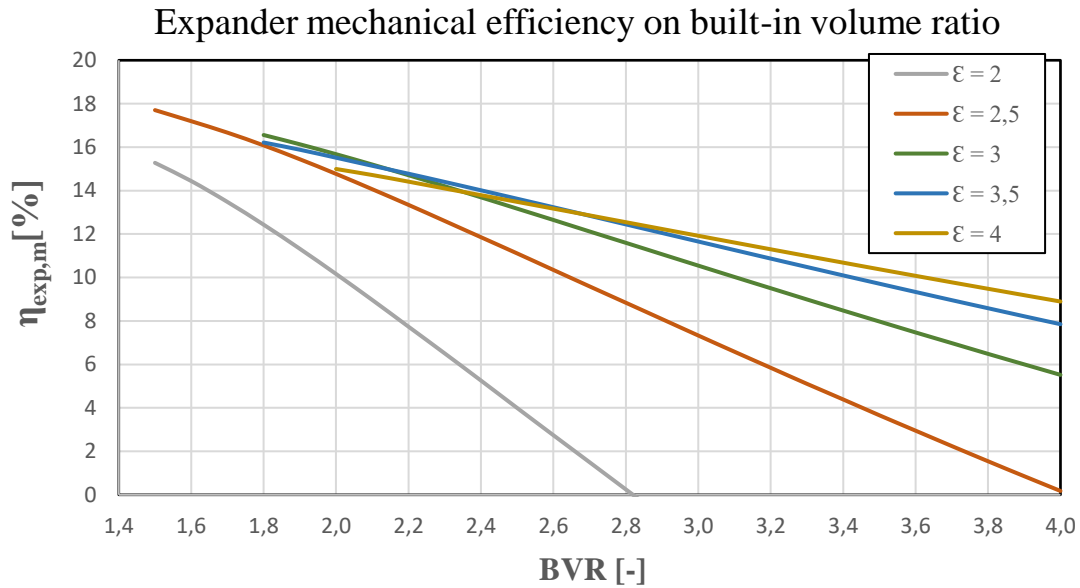
7.2.1 Determining how BVR influences the cycle

Admission temperatures up to 600 °C will be considered, as in Variant 1. Temperature of 450 °C is chosen again as a starting point.

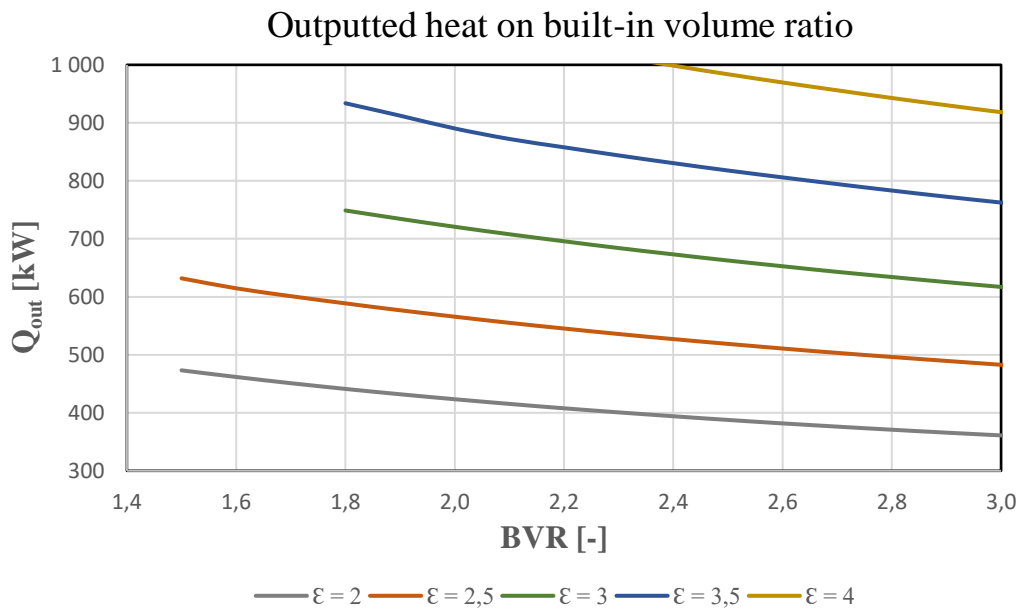
T_{ad} [°C]	ϵ [-]	N [rpm]	V_{sw} [cm ³]
450	2 - 4	1500	500

Table 20 - Boundary conditions for a second iteration of BVR evaluation for Var 2

The heat output range and expander efficiency were evaluated first. It is apparent that the heat output exceeds the desired range, despite running the model on low rotational speed and swept volume. Heat output can be decreased with decreasing pressure ratio and increasing BVR. This, however, affects the already-low expander efficiency and it begins to dip below 10% and towards zero. Even negative values were returned from the calculation since the model still takes friction and over- and under-expansion losses into account. It is known from the previous chapter that changing the admission temperature does not affect the heat output enough to make a significant difference in this case.



Graph 12 - Expander efficiency on BVR for Var 2



Graph 13 - Heat output on BVR for Var 2, T = 450 °C

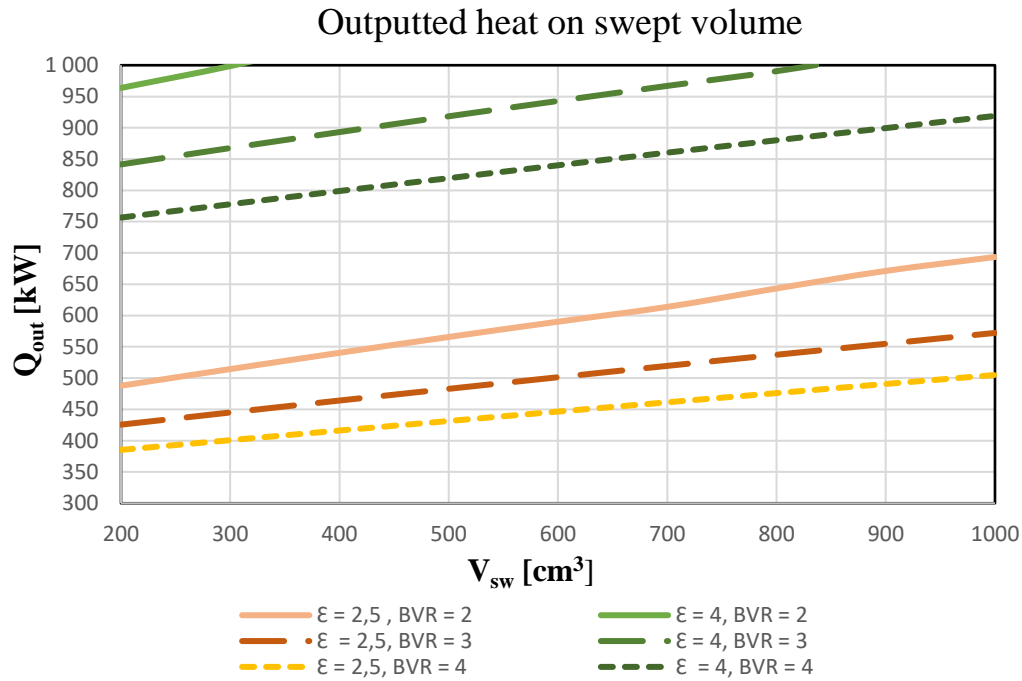
To reduce the heat output, pressure ratio and BVR need to be lowered, but that inevitably decreases the expander efficiency, which drops below zero long before the heat output reaches even 300 kW.

7.2.2 Determining how BVR in combination with V_{sw} influences the cycle

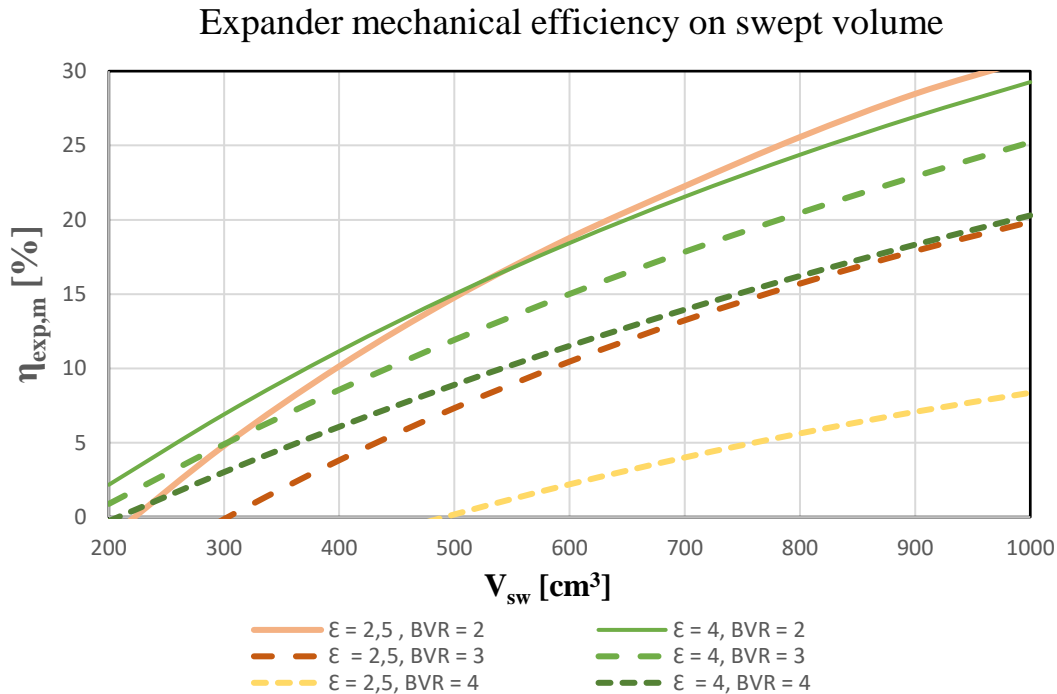
The influence of swept volume will be determined next to see if there is a reasonable value that would produce the desired results.

T_{ad} [°C]	ϵ [-]	N [rpm]	BVR [-]
450	2,5 and 4	1500	2 - 4

Table 21 - Boundary conditions for determining the influence of swept volume on the expander performance, Var 2



Graph 14 - Outputted heat on V_{sw} for different BVRs, Var 2



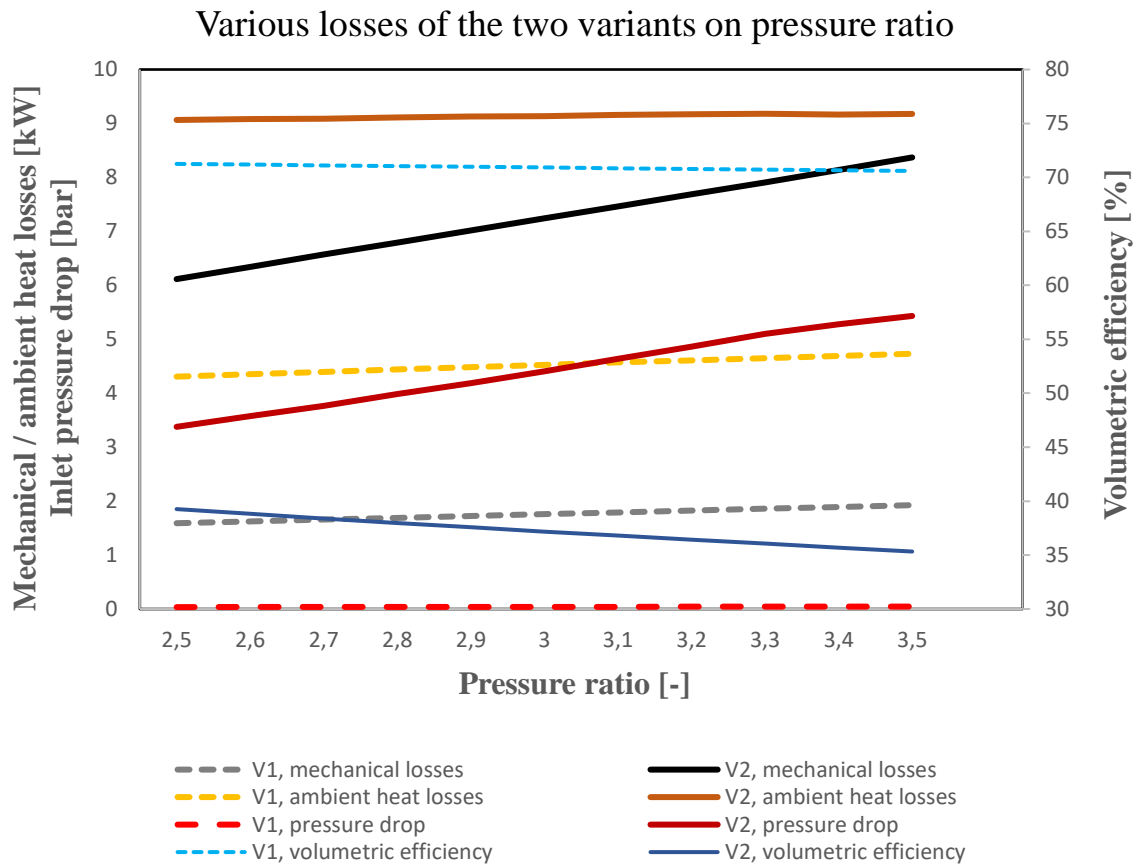
Graph 15 - Expander efficiency on V_{sw} for different BVRs, Var 2

Changing the swept volume does not improve the results. The model would theoretically return the desired heat output for very low swept volume but at that point, the expander efficiency would be already close to zero or even negative. Therefore, it is

examined why the expander efficiency comes out so low. Below, losses for Var 1 and Var 2 are compared for matching conditions.

	T_{ad} [°C]	ϵ [-]	N [rpm]	BVR [-]
Variant 1	450	2,5 – 3,5	3000	3
Variant 2			1500	

Table 22 - Boundary conditions for testing the losses for both variants

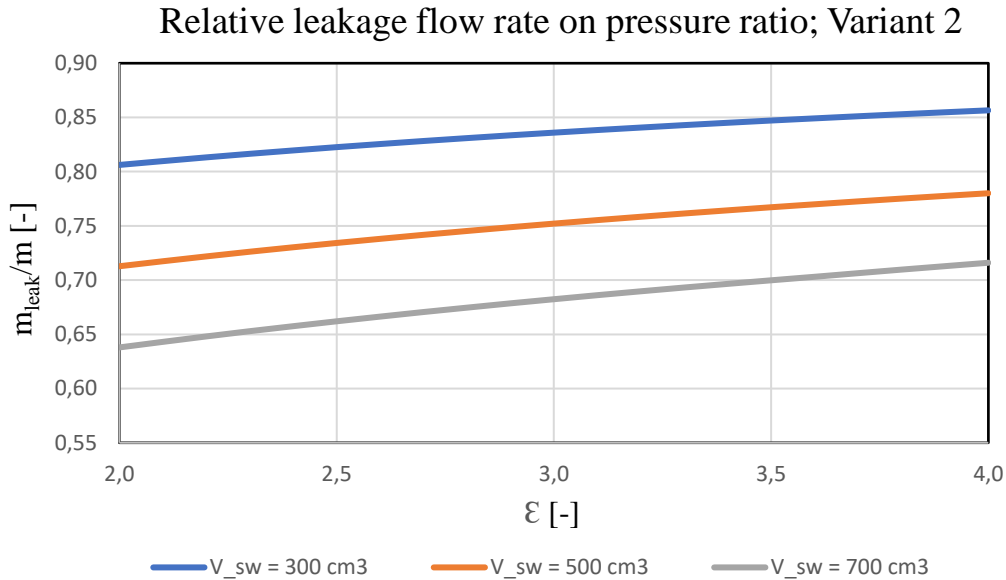


Graph 16 - Dependence of various losses on pressure ratios for Var 1 and Var 2

Graph 16 displays the various losses for both variants and their dependence on the pressure ratio. The performance of Variant 2, which works with much greater pressure levels, is significantly worse. The most notable difference is in the expander volumetric efficiency, only 30 – 40% for Variant 2. This means that only around third of the total mass flow rate usefully expands and does work, the rest leaks outside of the working chambers. The rate of growth of the respective losses is also greater for Variant 2. This is because the same incremental increase in pressure ratio translates to a higher absolute inlet pressure than for Variant 1 because of the higher backpressure. However, as seen in the previous graphs, the growth in overall expander efficiency with increasing pressure ratio is roughly the same for both variants. Similar trend can be observed for pressure loss on the expander inlet, which is over 100 times larger for Variant 2.

7.2.3 Discussion on the impact of leakage losses for Variant 2

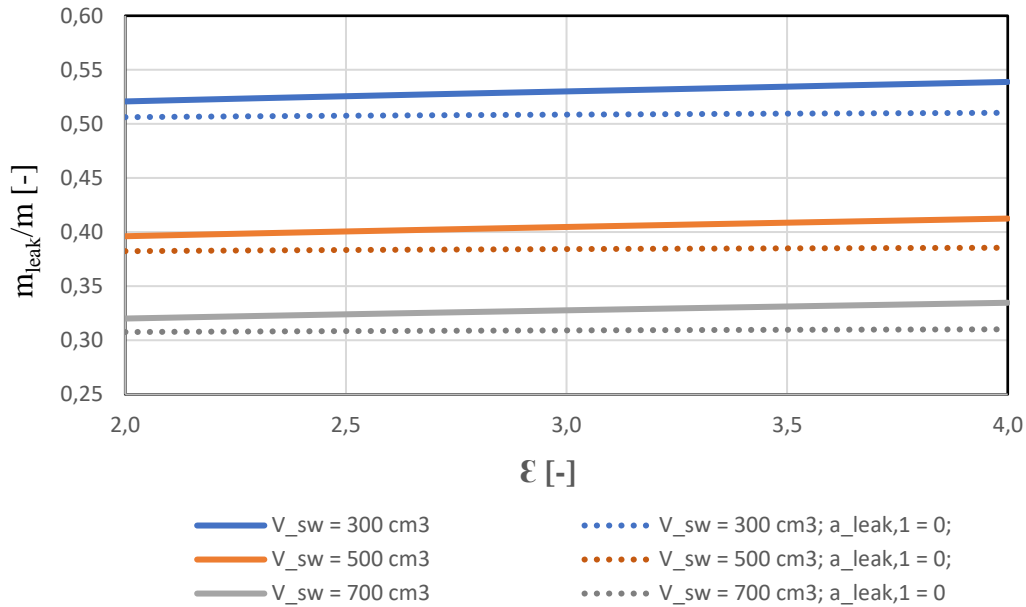
The most detrimental loss in Variant 2 is the leakage loss. The volumetric efficiency is only 35 – 40 % compared to 70 – 75 % for Variant 1 for the same conditions. The dependence of the share of leakage flow in the overall flow pressure ratio for $V_{sw} = 300 - 700 \text{ cm}^3$ for Variant 2 is shown.



Graph 17 - Relative leakage flow rate on pressure ratio, Var 2

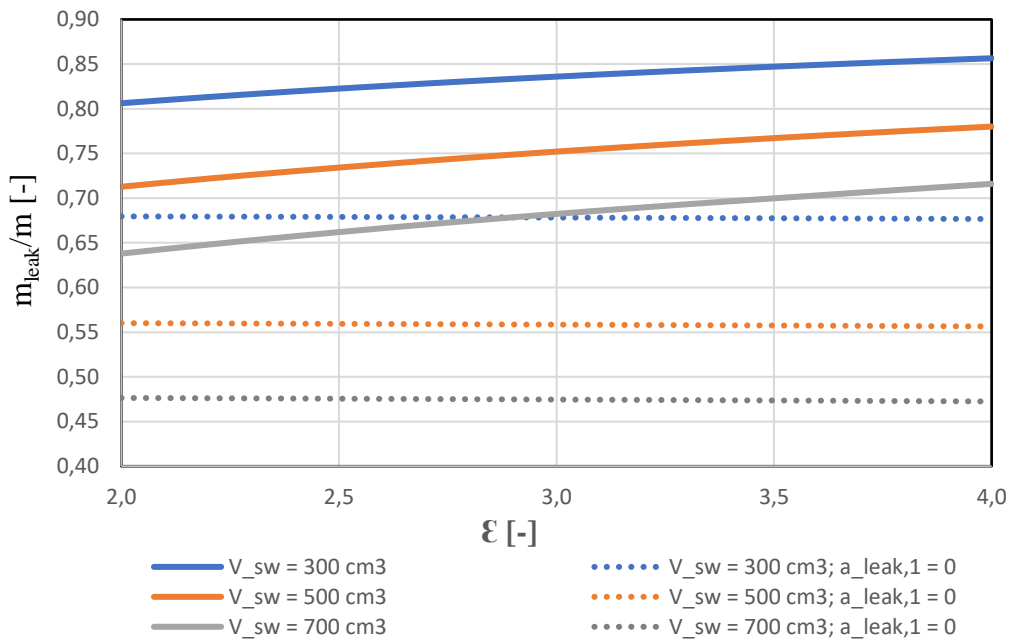
The leakage area depends linearly on the mean absolute pressure on the rotating parts p_{load} in equation (8) with coefficient $a_{leak,1}$, and p_{load} in turn depends on the exhaust pressure in equation (9). However, the exhaust pressure for Variant 2 is over 15 times higher and the effect of this relation becomes disproportionately larger for Variant 2, resulting in extremely high leakage. The coefficient $a_{leak,1}$ is likely put in place to correct the initial model for slightly higher inlet pressures. But since the model was likely not considered for calculating such high inlet parameters, it becomes questionable whether the relation between the leakage area A_{leak} remains linearly dependent on p_{load} . It is examined how the relative leakage flow changes when the coefficient $a_{leak,1}$ is set as equal to 0, in both variants for matching conditions.

Relative leakage flow on pressure ratio with constant leakage area; Variant 1



Graph 18 - Comparison of the relative leakage flow with and without the correction coefficient, Var 1

Relative leakage flow on pressure ratio with constant leakage area; Variant 2



Graph 19 - Comparison of the relative leakage flow with and without the correction coefficient, Var 2

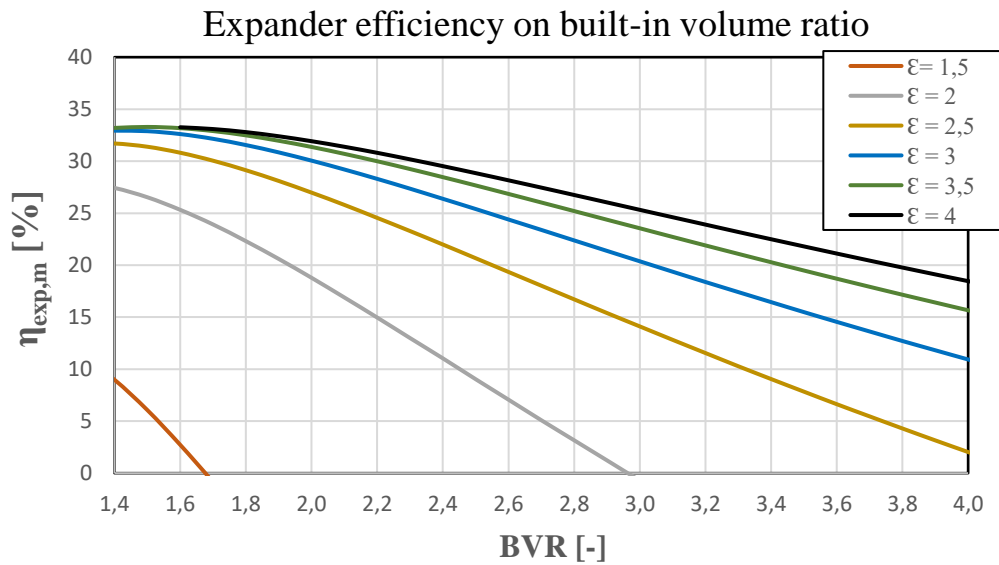
The linear dependence of the model has a significant effect on the leakage loss. For Variant 1, it accounts for a relatively small correction, whereas for Variant 2, it alters the behaviour of the mass flow more profoundly. Since it is not clear that the model [110] was considered for use at higher absolute pressures, the leakage area coefficient $a_{leak,1}$ will be neglected in further analysis of Variant 2 and the theoretical leakage area A_{leak} will equal $a_{leak,0}$. In other words, it will remain at a constant value of 17 mm².

7.2.4 Determining the behaviour in Variant 2 with constant leakage area

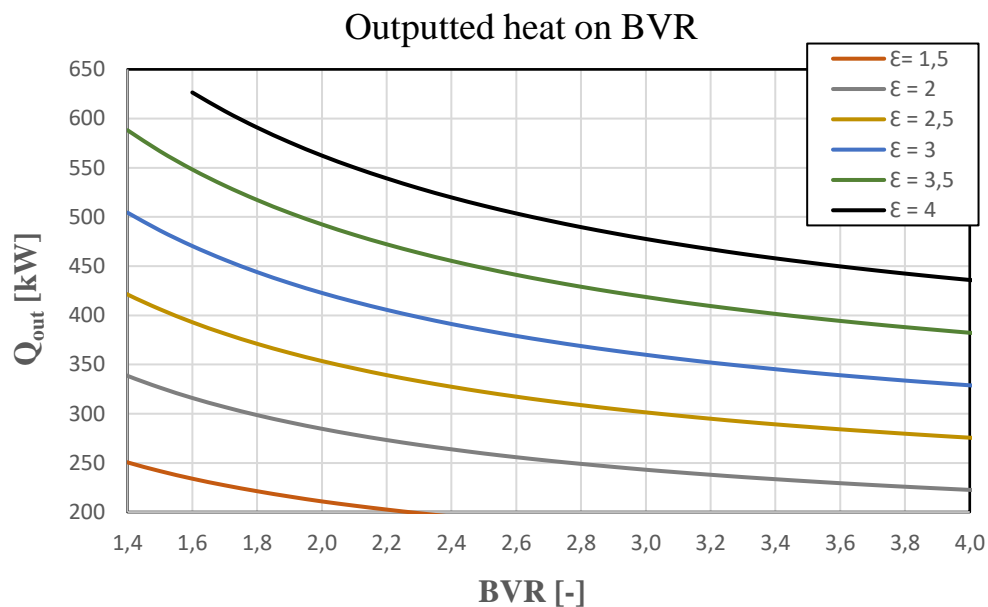
The same methodology is applied and the effect of BVR on the expander and cycle outputs is determined.

T_{ad} [°C]	ϵ [-]	N [rpm]	V_{sw} [cm ³]
450	1,5 - 4	1500	500

Table 23 - Boundary conditions for determining the influence of BVR on the expander behaviour, Var 2, constant leakage area

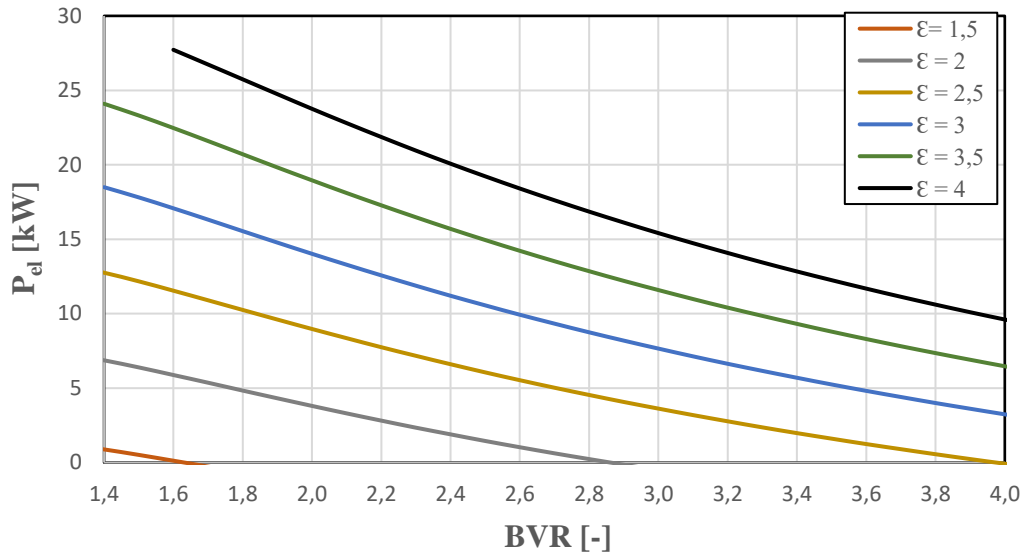


Graph 20 - Expander efficiency on BVR, Var 2, constant leakage area



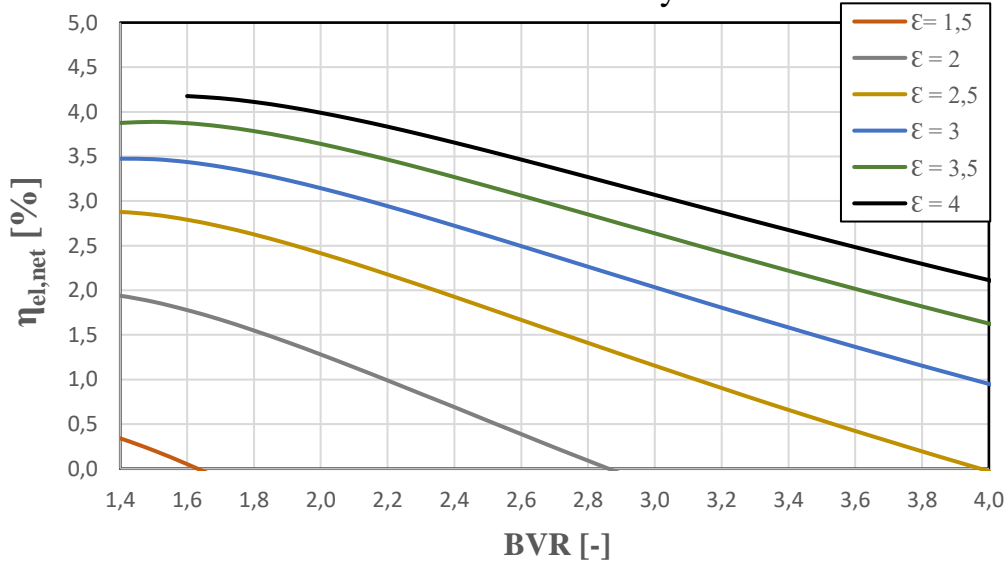
Graph 21 - Thermal output on BVR, Var 2, constant leakage area, desired range of heat outputs highlighted

Net electric power on built-in volume ratio



Graph 22 - Net electric power output on BVR, Var 2, constant leakage area

Net electrical efficiency on BVR



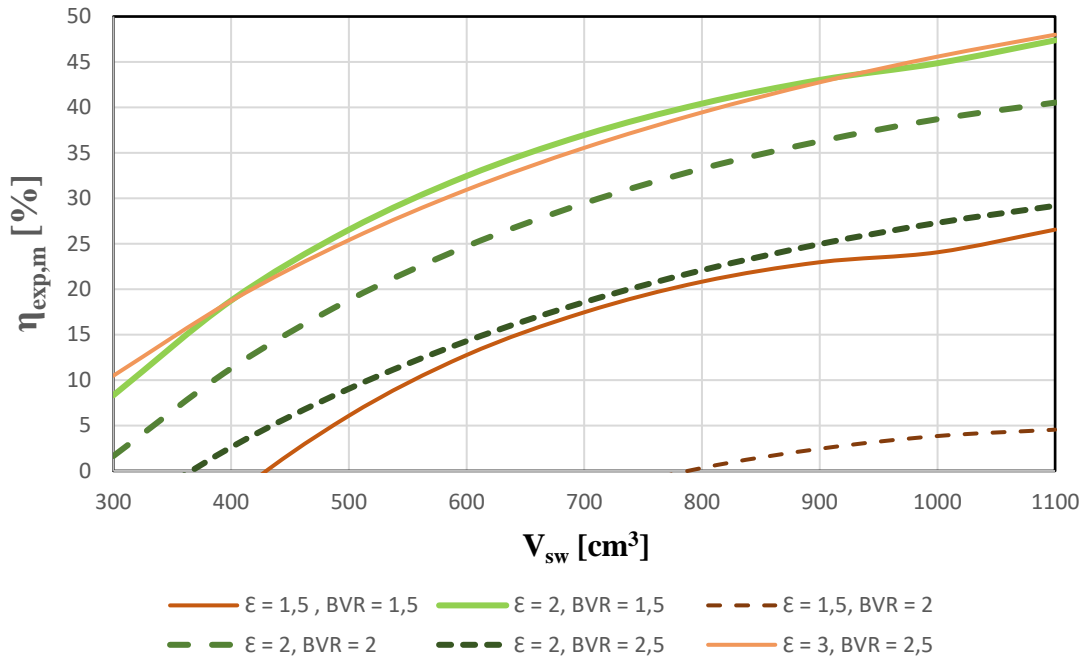
Graph 23 - Net electrical efficiency on BVR, Var 2, constant leakage area

Even with constant leakage area assumed, expander efficiencies are relatively low, not even reaching 35% at these conditions. Influence of swept volume will be determined next for several pressure and built-in volume ratios.

T_{ad} [°C]	ϵ [-]	N [rpm]	BVR [-]
450	1,5 - 3	1500	1,5 - 2,5

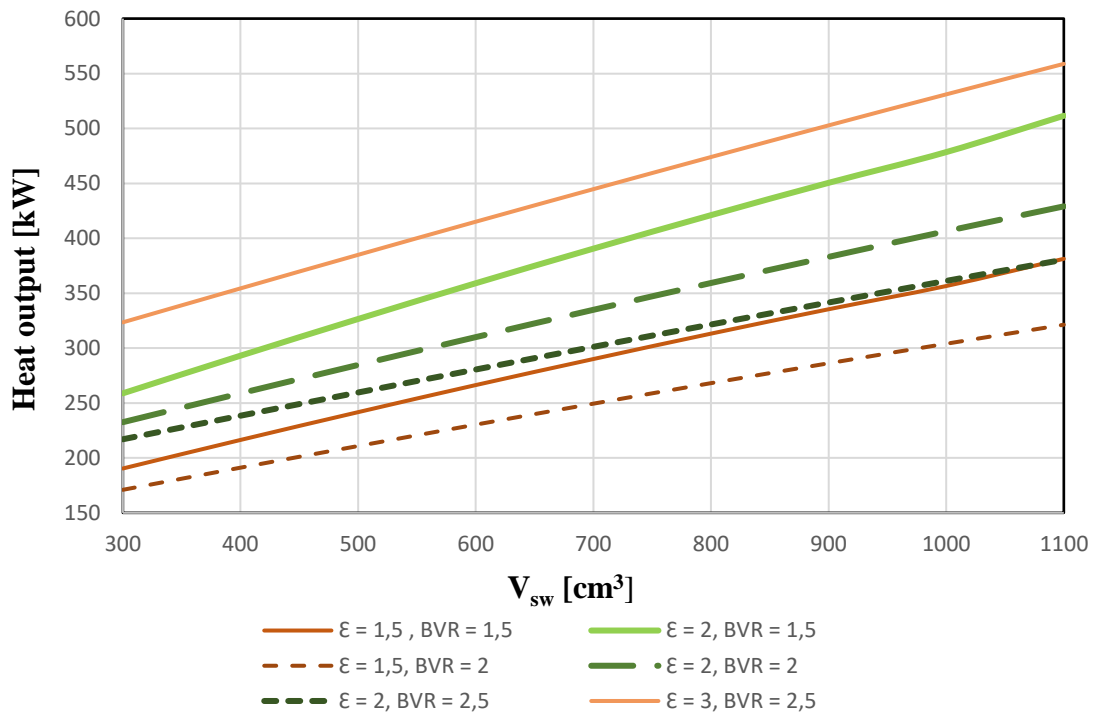
Graph 24 - Boundary conditions for determining the influence of both V_{sw} and BVR on the expander and cycle, Var 2, constant leakage area

Expander efficiency on swept volume



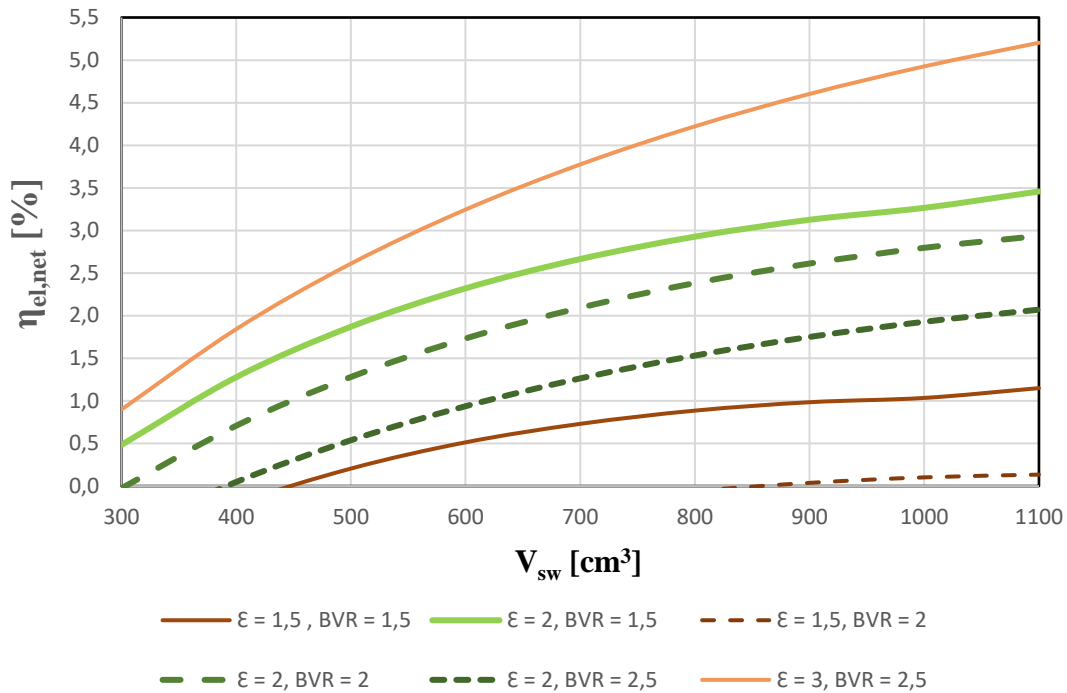
Graph 25 - Expander efficiency on V_{sw} and BVR, Var 2, constant leakage area

Heat output on swept volume



Graph 26 -Heat output on V_{sw} and BVR, Var 2, constant leakage area

Net electrical efficiency on swept volume



Graph 27 - Net electrical efficiency on V_{sw} and BVR, Var 2, constant leakage area

It is visible that achieving heat output of 200 – 250 kW while maintaining a reasonable efficiency is still impossible. Therefore, the required heat output will be doubled, to 400 – 500 kW_t, with the aim to place an ORC system with two parallel vane expanders as a bottoming cycle beneath the cycle in Variant 2.

The range of acceptable expander geometries is narrower than for Variant 1. Two expanders are proposed.

	Expander E	Expander F
BVR [-]	1,6	2,5
V_{sw} [cm³]	1100	950

Graph 28 - Defining the geometry of expanders for further testing in Variant 2, desired thermal output 400 - 500 kW

Expander E is expected to better utilise lower inlet pressures, while expander F is expected to achieve better overall efficiency at pressure ratios of over 2,5. Their respective geometries can be found in Appendix A.

Chapter 8: Obtaining the outputs for a range of working conditions for the examined expanders

8.1 Sensitivity analysis for Variant 1

The four expanders defined in Chapter 7.1 are tested under a wide range of conditions – temperatures between 180 °C and 600 °C and pressure ratios of 5 – 15 (0,5 MPa up to 15 MPa of inlet pressure, see Table 13 and section 7.1.2). Below are the four evaluated parameters of each expander – expander efficiency η_{exp} , net cycle electrical efficiency $\eta_{el,net}$, produced electric power and heat output Q_{out} . These are mapped against expander admission temperature T_{ad} and the cycle pressure ratio ϵ using MATLAB.

8.1.1 Expander A

Expander A is the smallest expander with a BVR of 3,2 and V_{sw} of 1300 cm². This means it works better with lower inlet pressures than the larger expanders, but the overall efficiencies are lower.

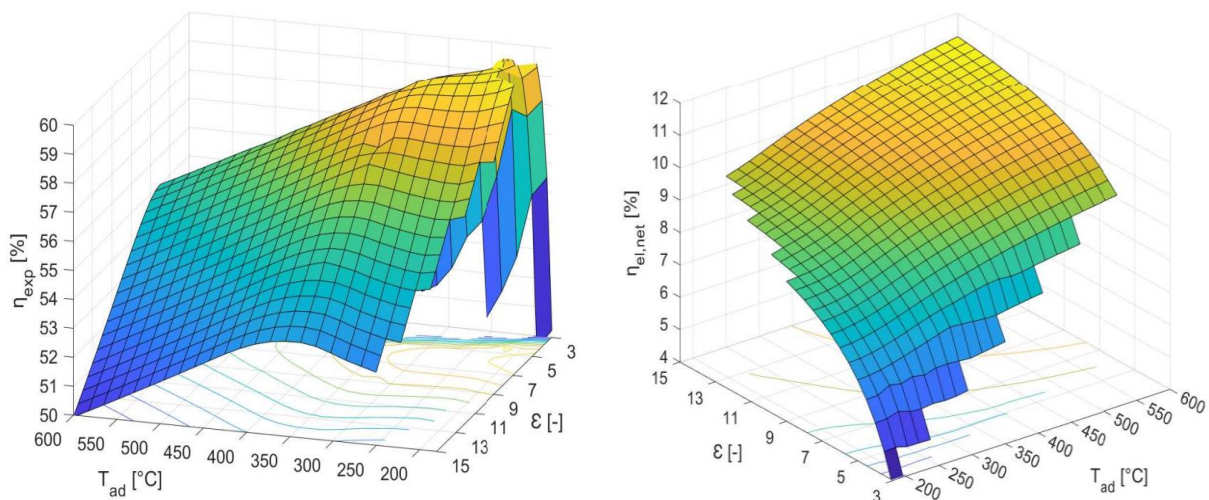


Figure 32 - Expander efficiency (left) and net electrical efficiency (right) of expander A

As outlined in previous chapters, the highest expander efficiency is achieved at low inlet parameters, whereas the overall electrical net efficiency is highest at high inlet parameters, despite the decreasing expander efficiency.

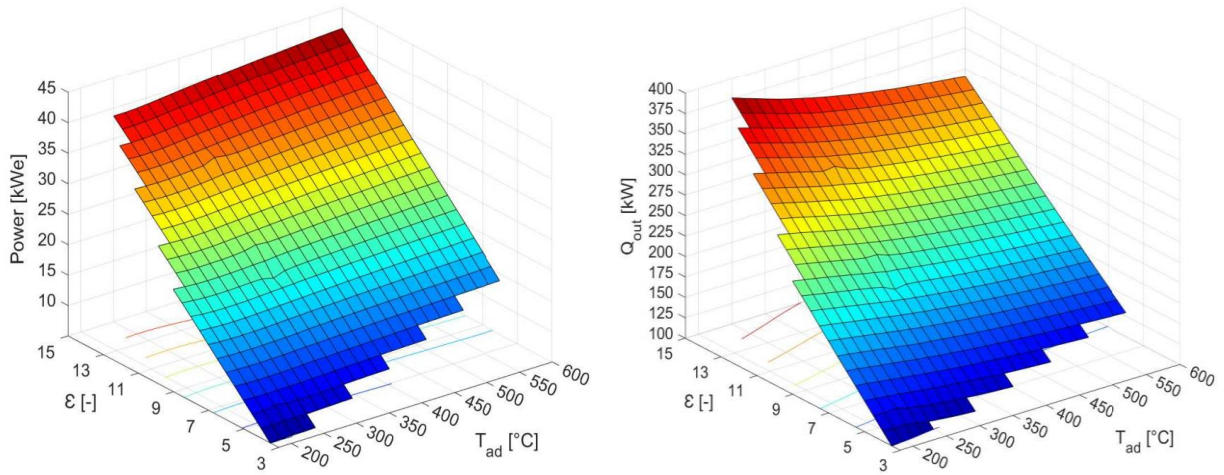


Figure 33 - Net electric power (left) and heat output (right) of expander A

As expected, the net power and heat output increase with increasing parameters. What perhaps wasn't apparent from the graphs in section 7.1, is that for a given inlet pressure, the net electric power increases with temperature, while for outputted heat, the opposite is true. It is important to note that for all of the expanders, the setting with the highest efficiency will not be applicable, as the corresponding heat output exceeds the upper threshold of 250 kW defined in earlier sections.

8.1.2 Expander B

This is the medium-sized expander with a BVR of 4,4 and V_{sw} of 1800 cm². As observed in section 7.1.3, the overall performance of the expander improves with increasing BVR and V_{sw} , with the net electrical efficiency roughly 1,5% higher than expander A.

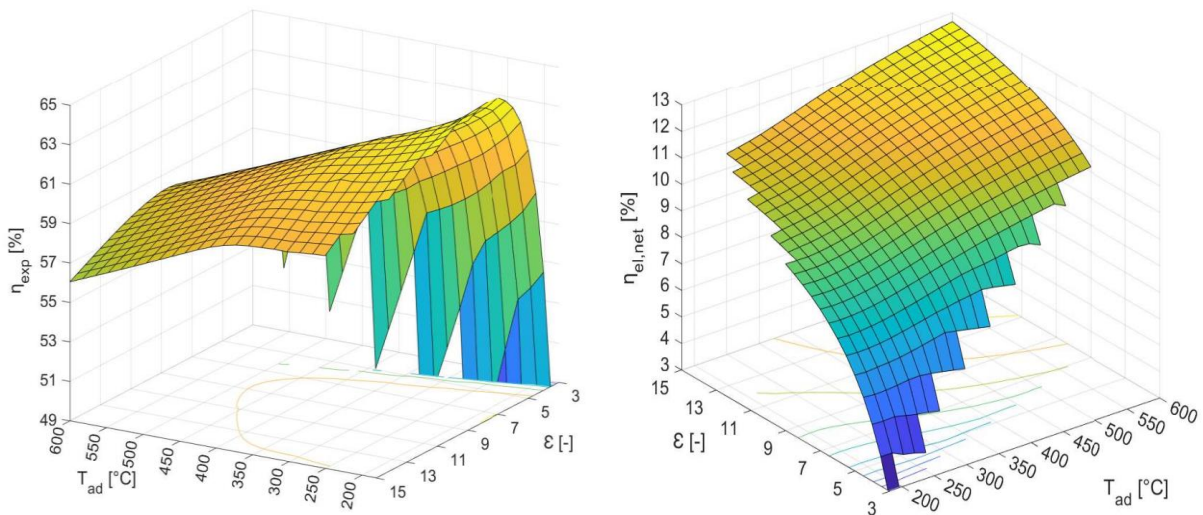


Figure 34 - Expander efficiency (left) and net electrical efficiency (right) of expander B

The maximum achieved power output is higher and the heat output lower than for expander A, which is better for us since a setting with higher efficiency can be now used.

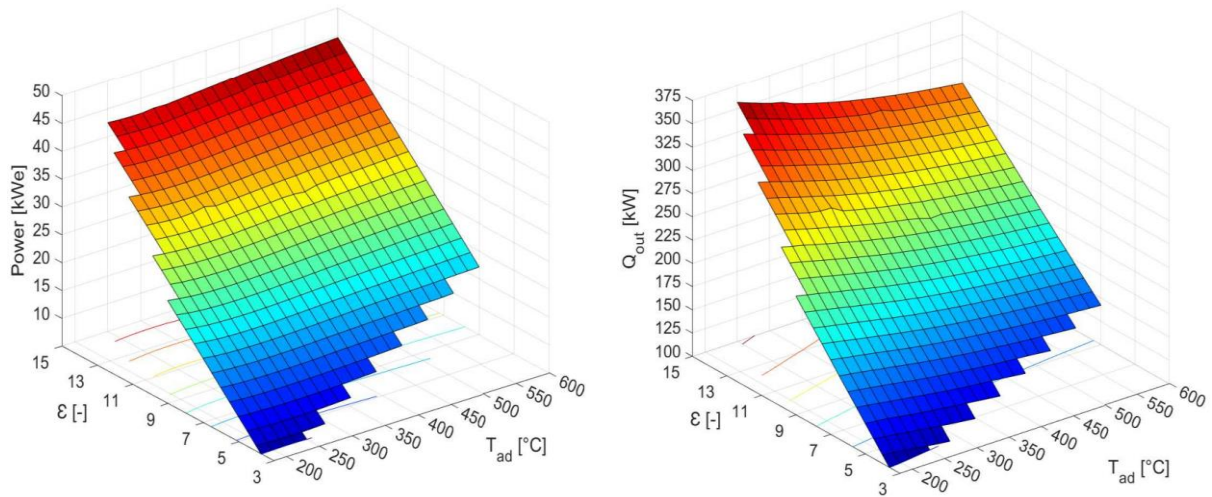


Figure 35 - Power output (left) and heat output (right) of expander B

8.1.3 Expander C

Expander C is the largest expander with a BVR of 6,2 and V_{sw} of 2000 cm³. While the maximum value for efficiency is very similar to those achieved by expander B, the expander efficiency across the entire range is better. It dips below 50% for only one combination of inlet conditions.

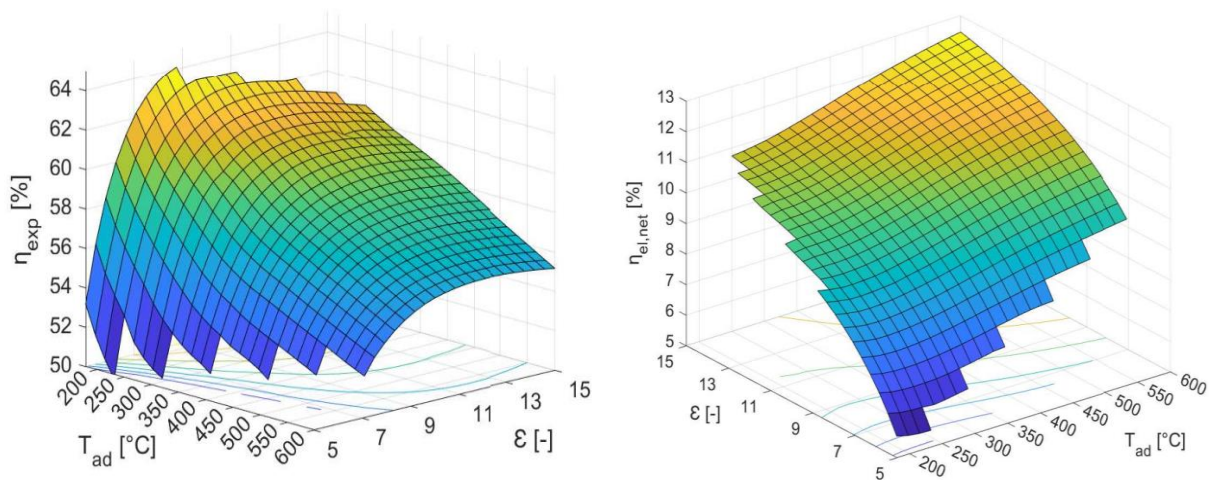


Figure 36 - Expander efficiency (left) and electrical efficiency (right) of expander C

Both the net electric power and outputted heat are around 10% lower than for expander B. This means that a configuration of inlet parameters with a higher net efficiency can be used while still keeping the cycle in the 200 – 250 kW heat output.

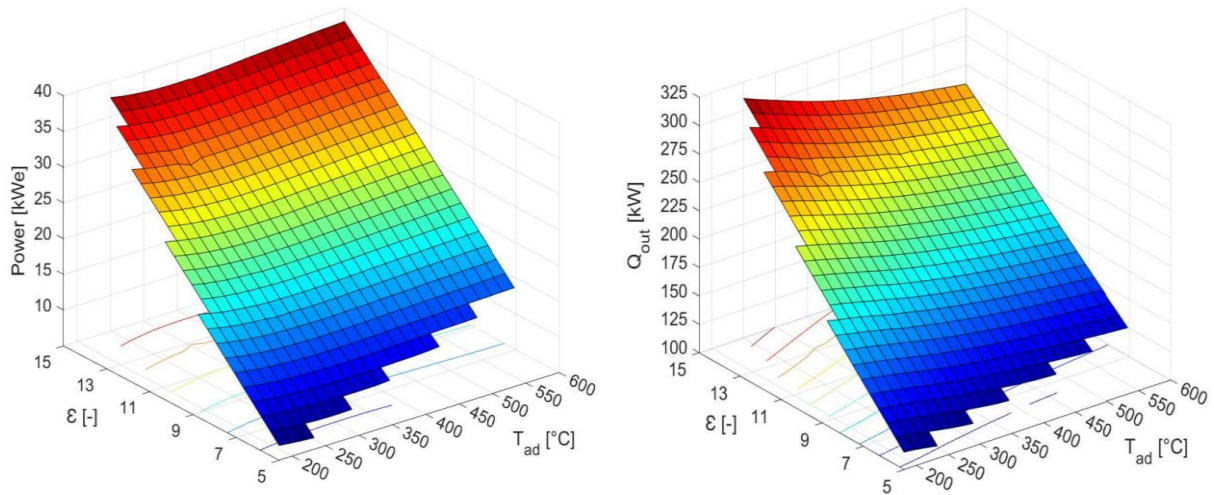


Figure 37 - Power output (left) and heat output (right) of expander C

8.1.4 Expander D

Expanders A – C had their geometries chosen to provide a compromise between BVR and V_{sw} and could therefore be calculated for a wide range of inlet conditions. However, expander D was chosen with a relatively low BVR of 3,5 and a high V_{sw} of 2000 cm³ to see how this affects the machine performance. The expectation of higher output parameters was fulfilled. This machine is the only one achieving expander efficiency over 65,5% and net electrical efficiency over 13%. The range of steam inlet conditions is significantly smaller due to a higher mass flow rate which can cause pressure drop below the saturation curve and thus becomes difficult for the iterative mechanism to calculate, as outlined in 6.4.2.

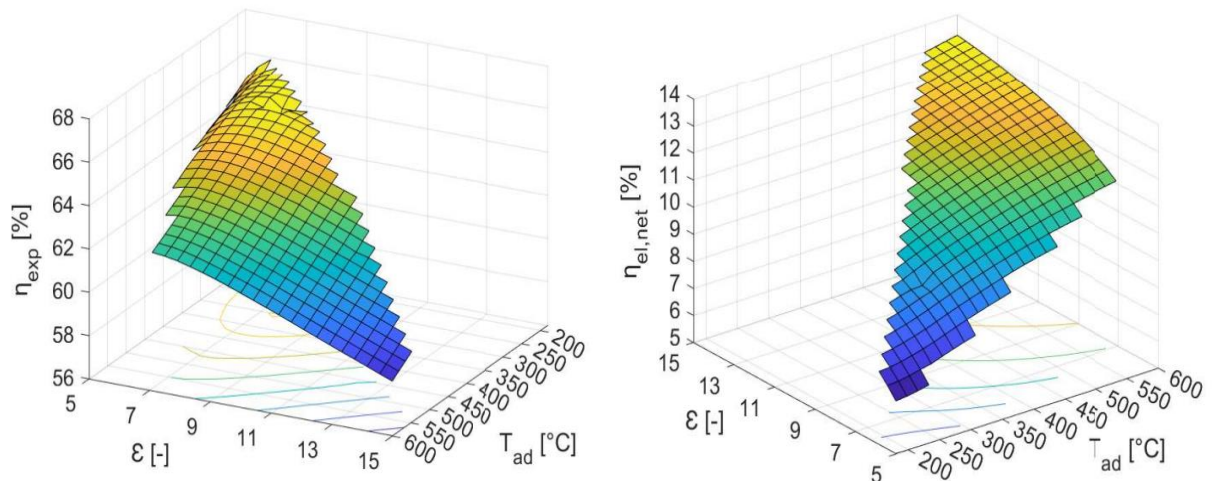


Figure 38 - Expander efficiency (left) and electrical efficiency (right) of expander D

The machine also achieves the highest net power output of over 55 kW. The maximum heat output, while higher than for expanders B and C, is lower than for expander A. Therefore, a combination of inlet steam parameters that satisfies the heat demand with a relatively high efficiency can be chosen.

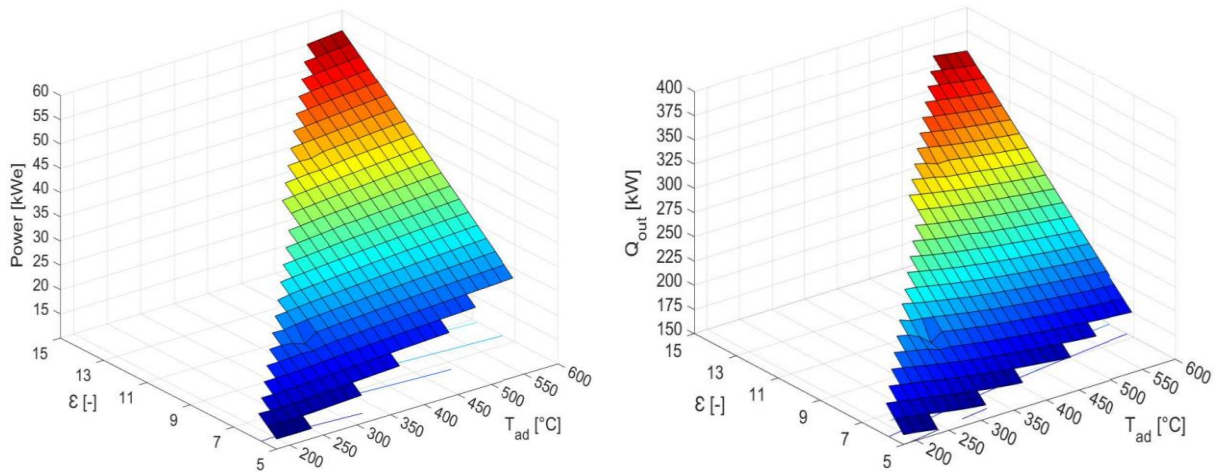


Figure 39 - Power output (left) and heat output (right) of expander D

It is also important to note that expander D is the second smallest expander after expander A, with 789 mm across the rotor and the starwheels.

8.1.5 Exhaust temperature, filling factor and losses

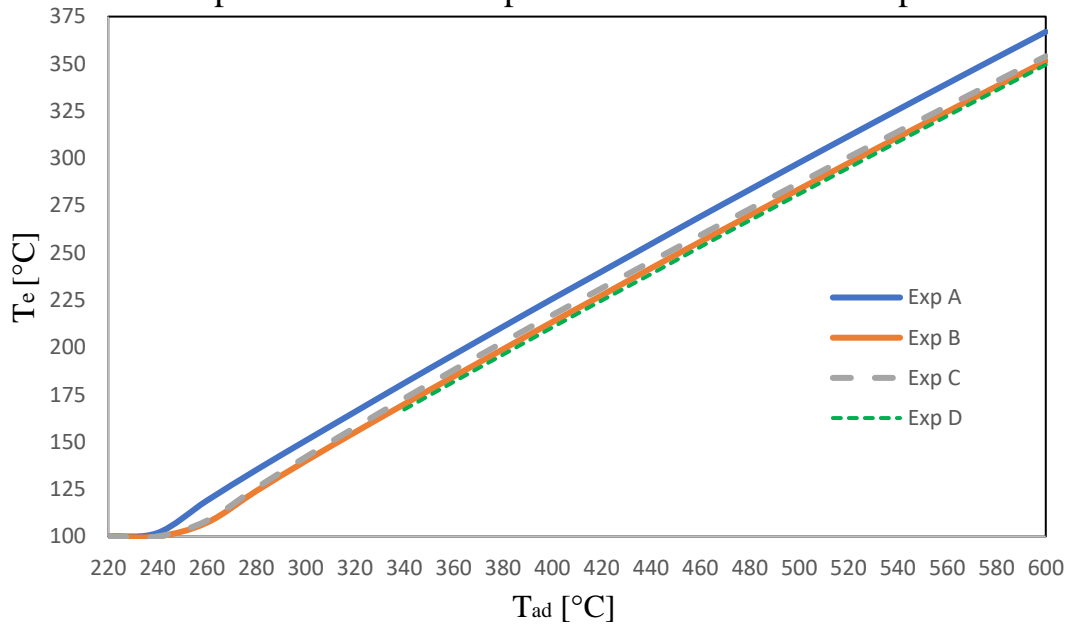
The efficiency of both the expander and the steam Rankine cycle, along with delivered electric power and heat output for each of the proposed expanders were evaluated in the previous sections. Several more indicative parameters are evaluated in this section to have a better idea about the expanders' performance and losses.

Exhaust temperature and ambient heat loss

Firstly, exhaust temperature is examined. Because of the unusually intensive superheating on the steam inlet, the fixed range of inlet pressures and the isentropic efficiencies of 50 – 65%, the expansion process mostly ends significantly in superheated steam. The exhaust temperature depends on both inlet parameters, but more on inlet temperature because of the wider temperature range. The dependence of exhaust temperature T_e of all four expanders on admission temperature T_{ad} is shown in the graph below, for a pressure ratio of 10.

As visible from the graph, some of the bottom values end up in wet steam, the quality however, is never lower $x = 0,95$, which, as learned in Chapters 4 and 5 is completely acceptable for the single-screw expander.

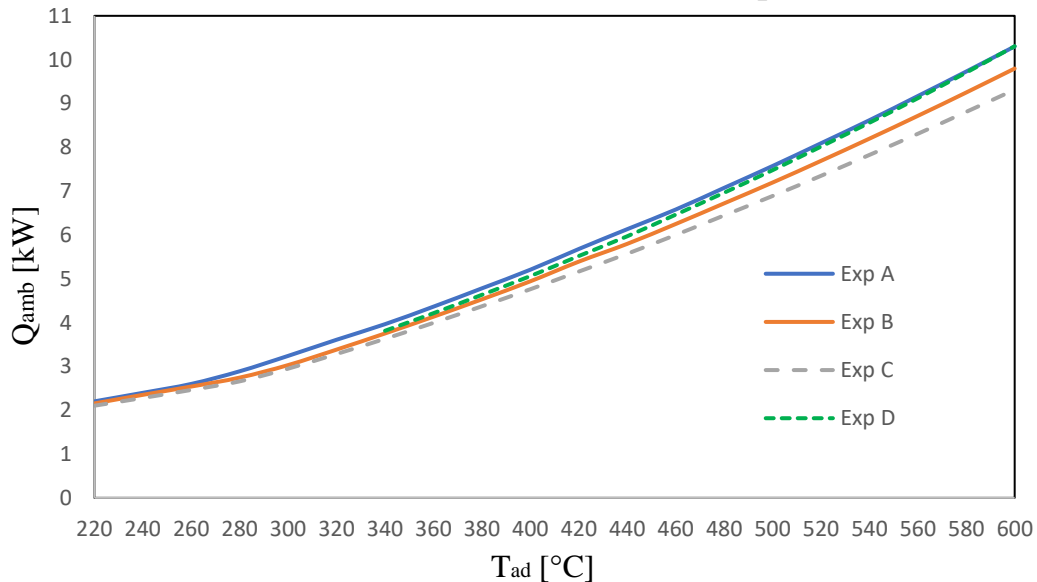
Expander exhaust temperature on admission temperature



Graph 29 - Exhaust steam temperature on admission temperature for $\epsilon = 10$

Q_{amb} is a loss associated with both the inlet pressure and temperature, but depends more heavily on the temperature. It is the heat emitted from the imaginary expander envelope to the environment which is at constant ambient temperature. The only inherit losses it contains are the heat transfers between the fluid and the envelope at the expander inlet and exhaust. But the mechanical losses are considered to transform completely into heat and are also included in this loss (see equation (16)).

Ambient heat losses on admission temperature



Graph 30 - Ambient heat losses on admission temperature for expanders A - D for $\epsilon = 10$

Filling factor and volumetric efficiency

Positive displacements machines can suffer from significant leakage and therefore their volumetric performance is often evaluated [83]–[85]. This is done by expressing the machine’s filling factor FF or volumetric efficiency η_{vol} . Filling factor is defined as the ratio of the actual mass flow rate and the mass flow rate that could be theoretically displaced by the expander.

$$FF = \frac{\dot{m}}{\rho_0 \frac{V_{sw}}{BVR} N} \quad (43)$$

Volumetric efficiency is defined as the ratio of the internal mass flow that participates in producing work and the complete mass flow including the leakage [110].

$$\eta_{vol} = \frac{\dot{m}_{int}}{\dot{m}} = \frac{\dot{m} - \dot{m}_{leak}}{\dot{m}} \quad (44)$$

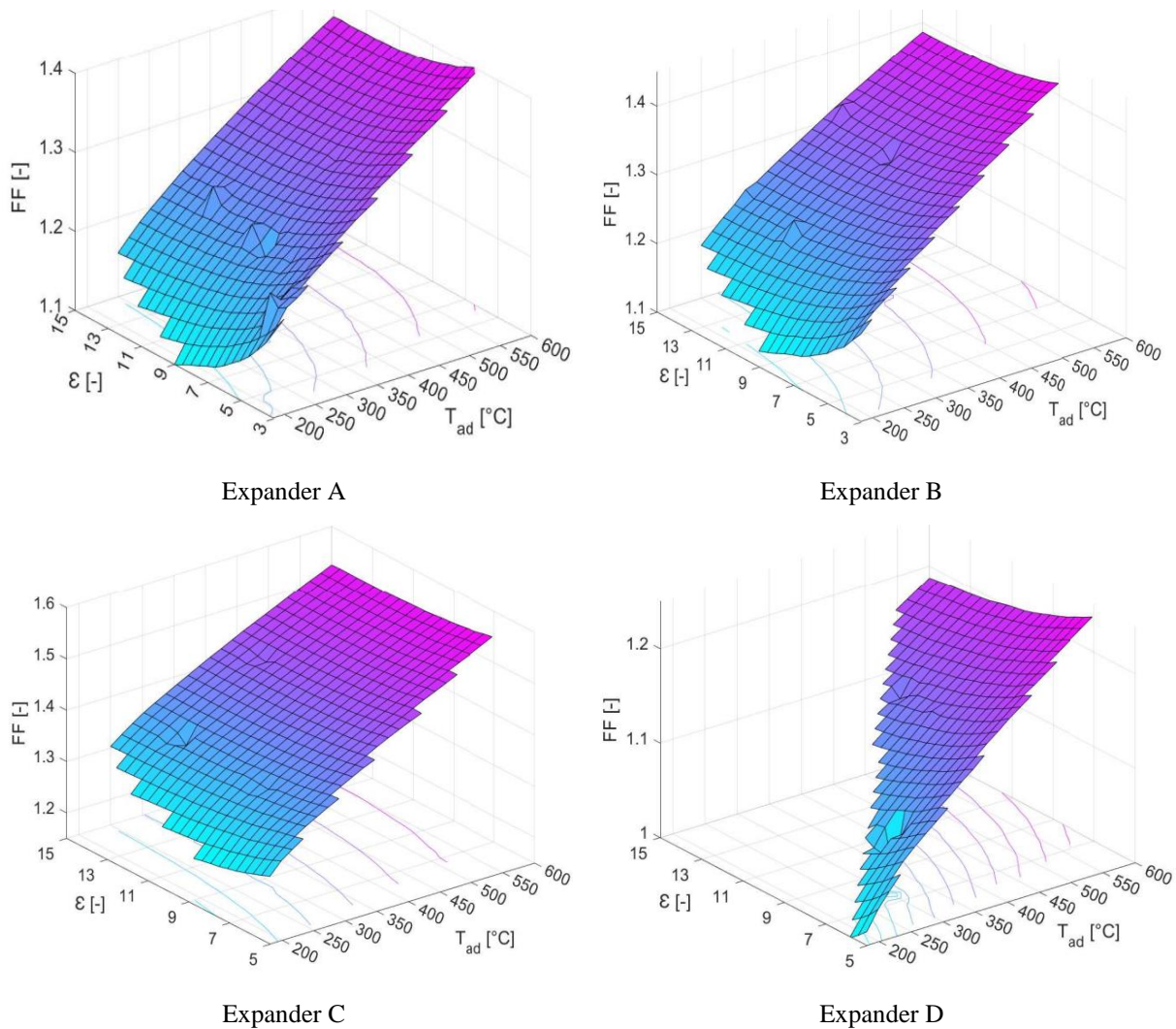


Figure 40 - Filling factor for the four expanders A – D

The filling factor rises with temperature but remains fairly constant for a given temperature level with increasing pressure ratio, which is consistent with experimental

findings obtained by the author of the used thermodynamic model in [110] and by Ziviani in [111]. Filling factor is useful for evaluating the performance of the expander because it increases with internal leakage and supply cooling down and decreases with the inlet pressure drop. Values both above and below 1 are possible.

Volumetric efficiency is useful for knowing the relative internal mass flow rate to the entire mass flow rate and therefore gives information about the leakage. It decreases with increasing inlet temperature and pressure.

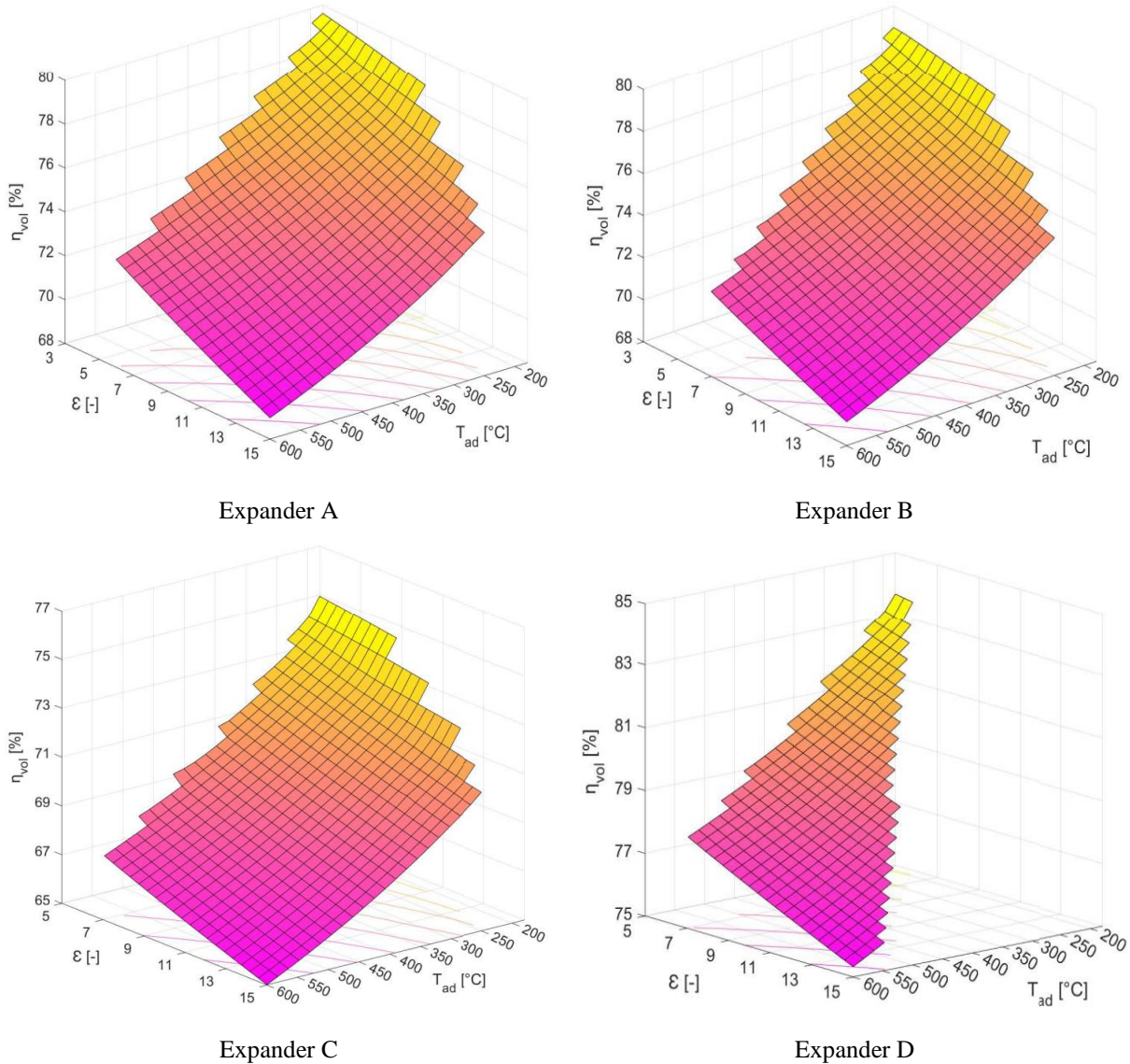


Figure 41 – Volumetric efficiency for the four expanders A – D

Expander C, the largest expander, has the worst volumetric performance out of all the studied machines, while expander D has the best one. Corresponding the data presented in sections 8.1.1 and 8.1.2, expanders A and B have a very similar volumetric performance.

8.2 Sensitivity analysis for Variant 2

Similar sensitivity analysis is performed for expanders proposed for Variant 2. In a more detailed analysis, the efficiency of utilising the heat from the heat sources should also

be evaluated as it would become highly relevant in this variant because the flue gasses will not be completely cooled down to regular exhaust temperatures. However, this falls outside the scope of this work and can be analysed in subsequent studies.

8.2.1 Expander E

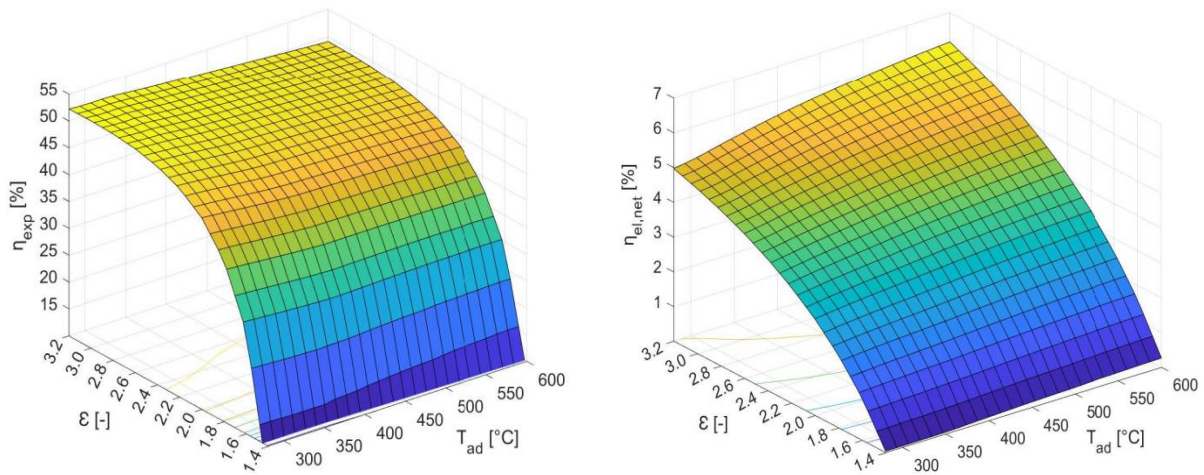


Figure 42 - Expander mechanical efficiency and cycle net electrical efficiency for expander E

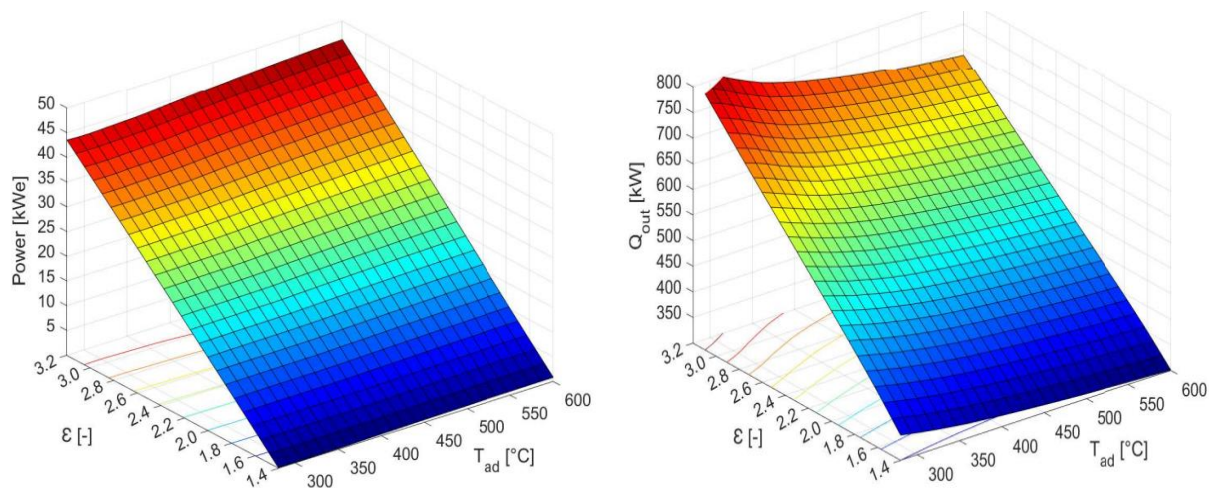


Figure 43 - Net electric power and heat output for expander E

While this expander can achieve relatively high efficiency and electric power output on the given range of steam inlet conditions, most of the more interesting values also produce more heat than desired. As predicted, this expander is more suitable for working with lower inlet pressure.

8.2.2 Expander F

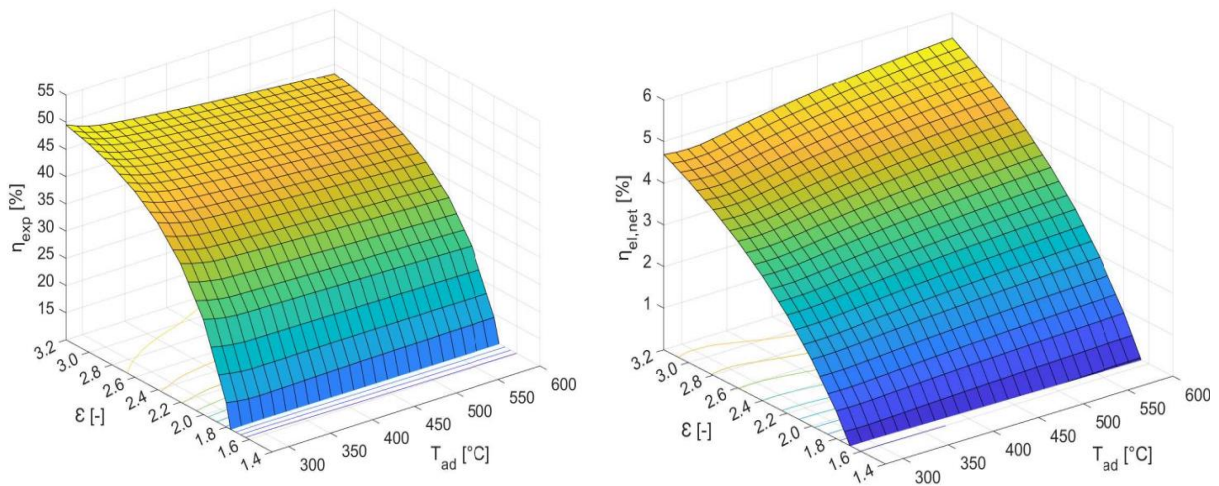


Figure 44 - Expander mechanical efficiency and net electrical efficiency for expander F

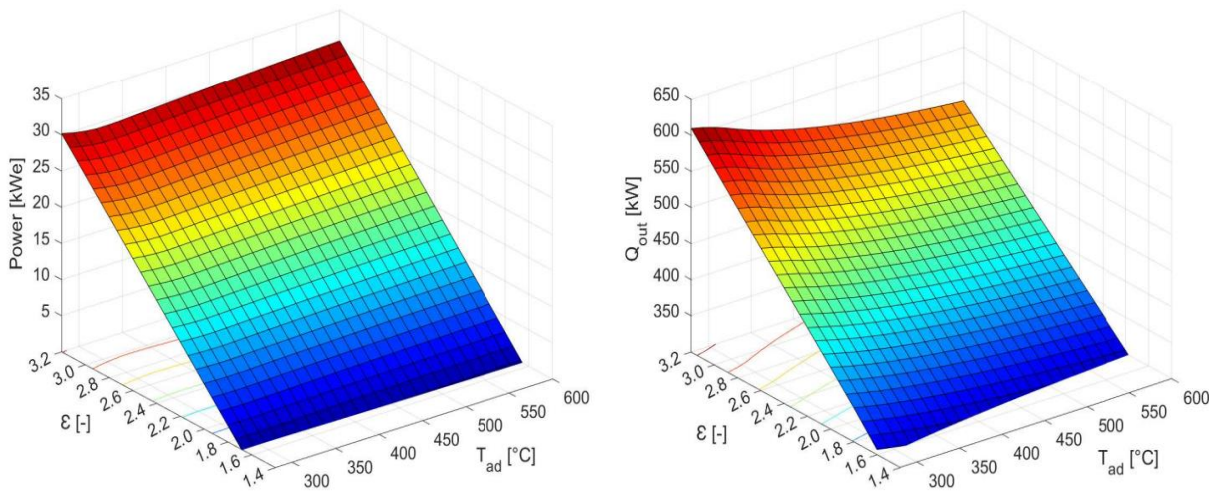


Figure 45 - Net electric power and heat output for expander F

The range of thermal output of this expander is much closer to the desired values. Peak electrical net efficiency is achieved only slightly above the upper threshold of 500 kW_t.

The dependence of heat losses and exhaust steam temperature on the inlet temperature was already established in 8.1. The volumetric performance of expanders E and F will now be evaluated.

8.2.3 Volumetric performance

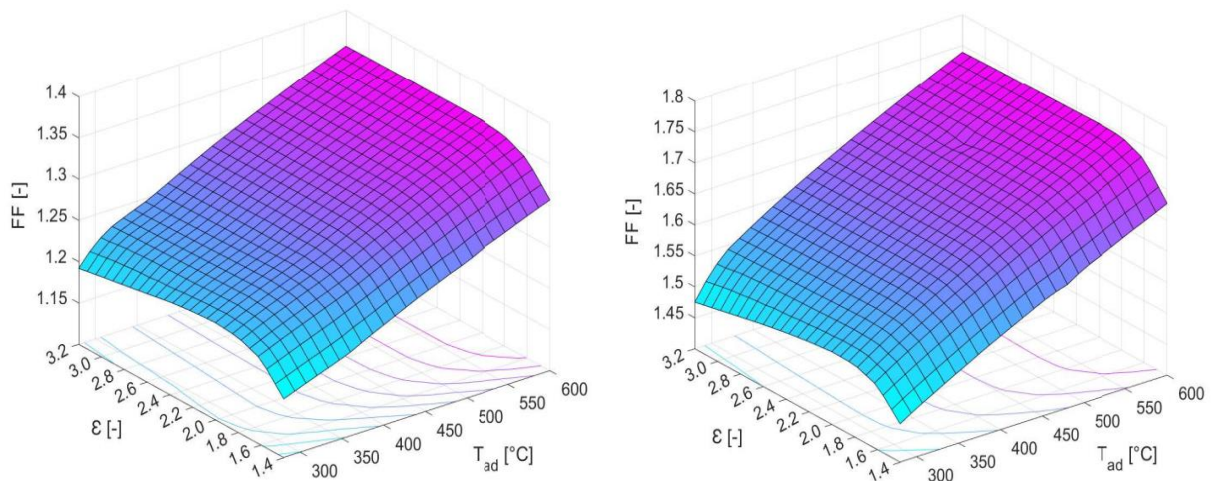


Figure 46 - Filling factor of expanders E (left) and F (right)

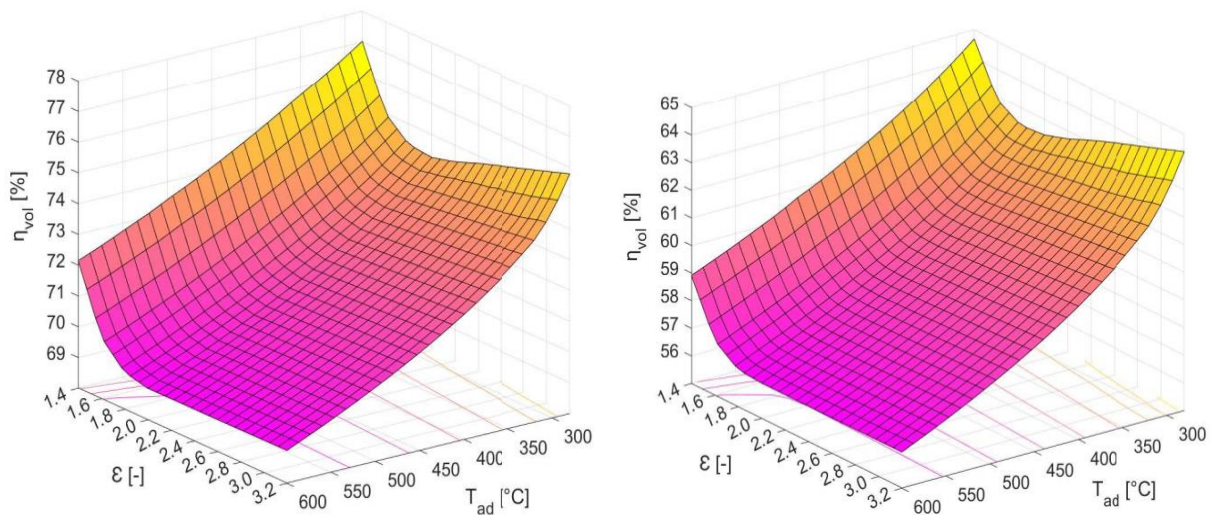


Figure 47 - Volumetric efficiency of expanders E (left) and F (right)

The volumetric performance of expander E is quite close to expanders examined for Variant 1, while expander F suffers from higher relative leakage. This is the reason for slightly lower expander efficiency across the entire range of values. The curve of the volumetric parameters is noticeably different than in Variant 1 and there is a pit in volumetric efficiency curve at a pressure ratio of around 2. Overall, the relative leakage goes up with temperature due to higher steam density and lower total mass flow rate.

8.3 Recommended ranges of inlet steam parameters

In this chapter, the data presented in 8.2 is evaluated and it is shown which inlet steam parameters correspond to the desired heat output of 200 – 250 kW (Var 1) and 400 – 500 kW (Var 2). It is also shown what power outputs and efficiencies can be expected for these inlet steam parameters.

8.3.1 Ranges of viable inlet conditions for Variant 1

Because the desired heat output can be achieved under a wide range of steam inlet conditions, the conditions are presented as approximate ranges, both graphically and numerically, rather than as specific values.

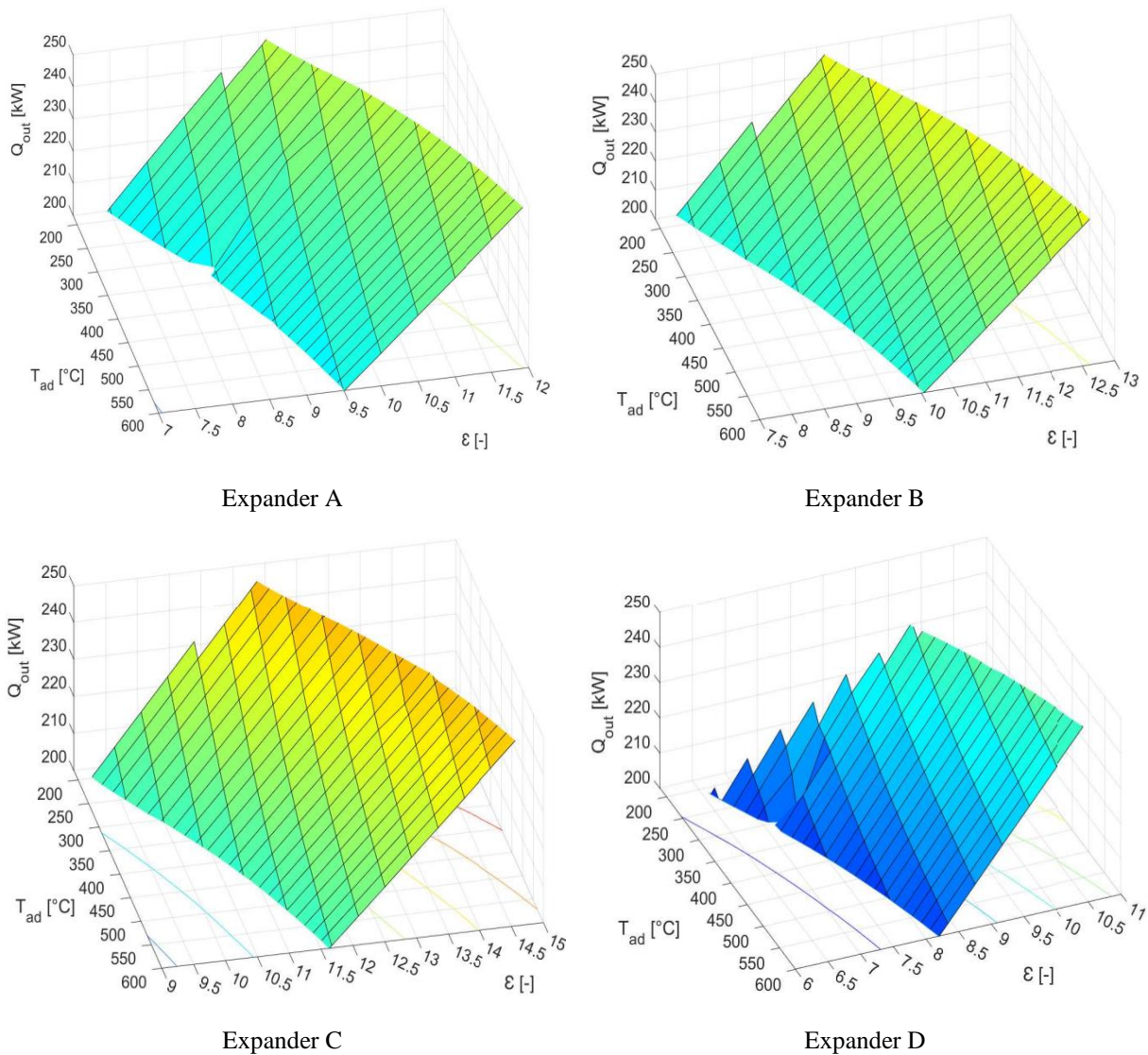


Figure 48 - Ranges of pressures and temperatures that satisfy the stated heat output for expanders A – D

The desired heat output can be achieved for all of the admission temperatures 180 – 600 °C by expanders A and B and for 220 – 600 °C by expanders C and D. The table below summarizes the ranges of pressure ratios for which the desired heat output can be achieved as well as the range of corresponding delivered electric power and efficiencies. The highest power delivery and highest net cycle efficiency are naturally achieved for $T_{ad} = 600$ °C and the highest corresponding pressure ratio.

	Expander A	Expander B	Expander C	Expander D
Pressure ratio range [-]	7,5 – 11,9	7,8 – 12,6	9,4 – 14,5	6,7 – 10,4
Net electric power range [kW]	17,35 – 32,29	20,03 – 36,52	20,70 – 36,66	18,76 – 36,89
Mass flow rate [g/s]	72 - 111	72 - 107	73 - 110	74 - 106
Expander efficiency range [%]	52,02 – 59,52	56,97 – 65,10	55,27 – 62,82	61,0 – 65,83
Net electric efficiency range [%]	7,88 – 10,94	8,73 – 12,36	9,25 – 12,38	8,42 – 12,43
Maximum electric efficiency for 200 kW heat output [%] *	10,54	11,66	11,70	11,66
Pressure ratio for 200 kW heat output at maximum efficiency [-]	9,5	10,0	11,9	8,2
Maximum electric efficiency for 250 kW heat output [%]	10,94	12,36	12,38	12,43
Pressure ratio for 250 kW heat output at maximum efficiency [-]	11,9	12,6	14,5	10,4

Table 24 - Overview of delivered electric power and efficiencies of expanders A - D for a heat output of 200 - 250 kW

* Maximum efficiency for both 200 and 250 kW_t is always achieved for the maximum temperature, 600 °C

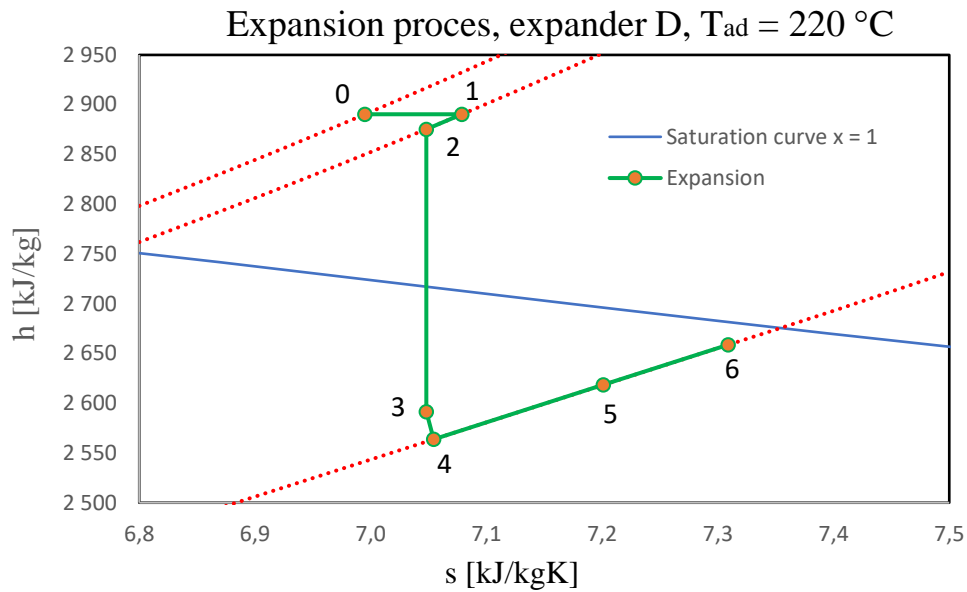
Despite the differences in geometries and performance on the entire range of inlet conditions, expanders B – D show very similar performance for the defined range of heat output of the cycle, with expander D coming out slightly on top with higher expander efficiency, higher net power output and slightly higher net electrical efficiency. Furthermore, its dimensions are significantly smaller than for expander B and C and size is an important factor for decentralised machines.

Expander A, the smallest expander, achieves roughly 1 – 1,5% lower net electrical efficiency than the other expanders, along with correspondingly lower power output. This expander should be chosen only if size was the most important factor.

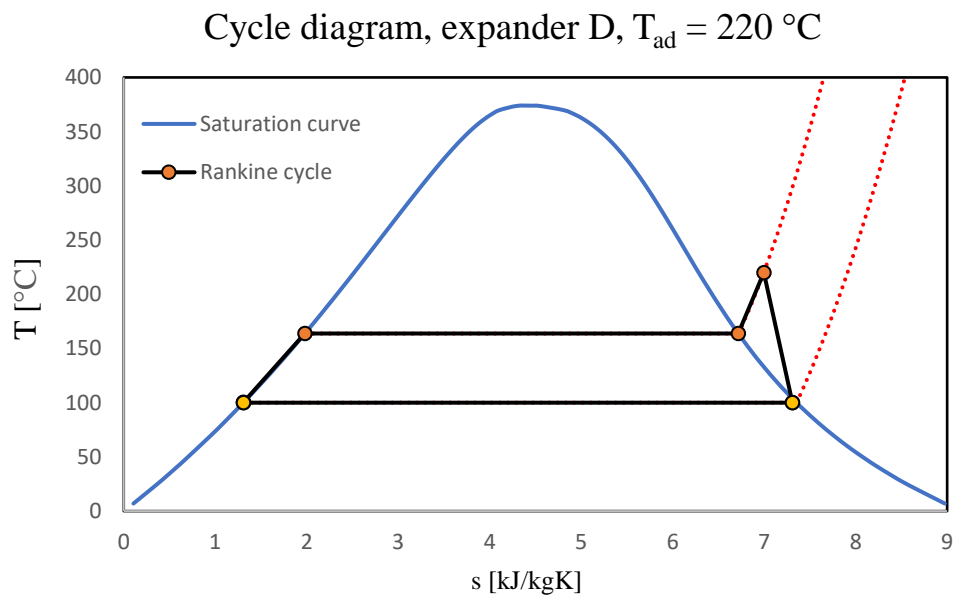
The performed sensitivity analysis conveys that it is sensible to design single-screw expanders with built-in volume ratio of around 3,5 and with a high corresponding swept volume. The drawback is that at lower admission temperatures, a narrower range of inlet steam conditions can be calculated using the presented thermodynamic model.

The cycle efficiency rises with the inlet temperature, as was shown at the very beginning of this work in Figure 3, despite the decreasing expander efficiency. These two factors seem to even out as the temperature is increased and the rise in the cycle efficiency becomes more and more marginal at temperatures over 450 °C. A techno-economic analysis would need to be conducted to determine the optimal operating conditions, respecting both the efficiency and the cost of the materials. This is highly relevant in micro-CHP systems,

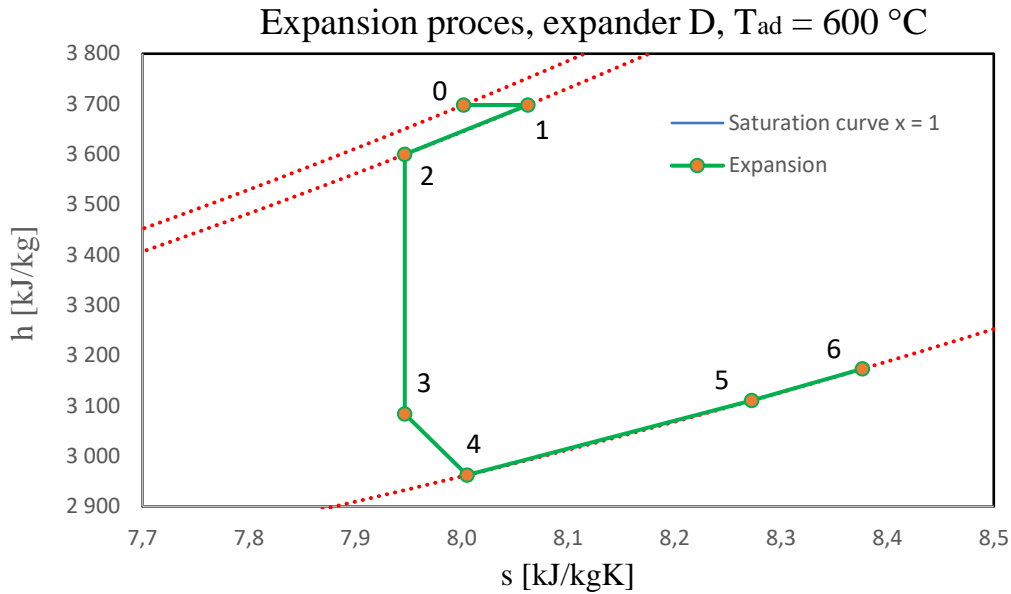
since electrical efficiency is often cited as secondary to other properties such as size, complexity or investment costs [27].



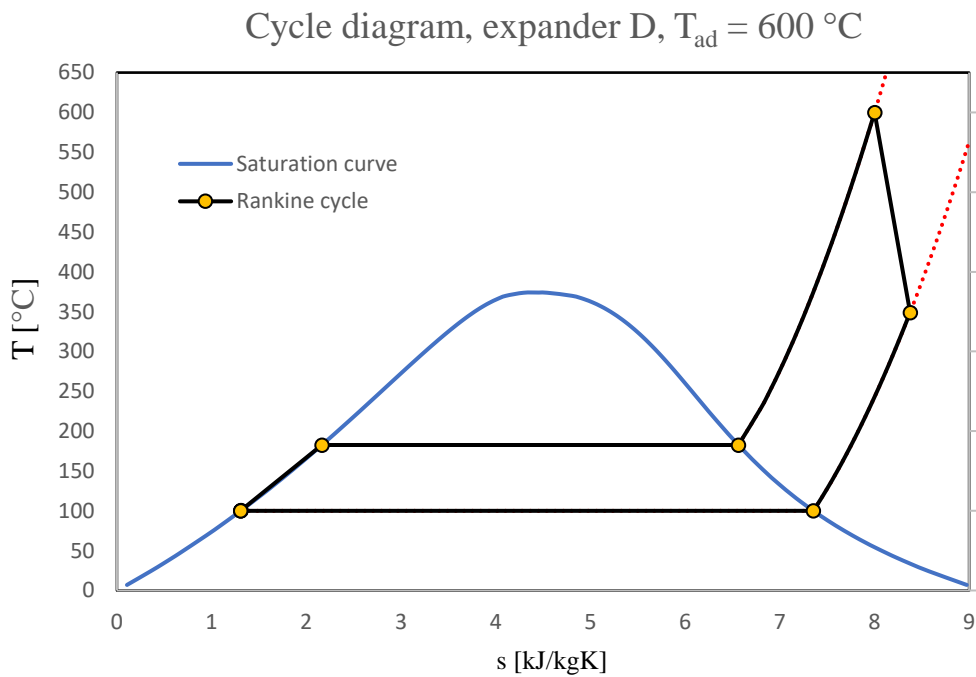
Graph 31 - h-s diagram of the expansion process for expander D at $T_{ad} = 220\text{ °C}$ and $\epsilon = 6,7$



Graph 32 - T-s diagram of the entire Rankine cycle for expander D at $T_{ad} = 220\text{ °C}$ and $\epsilon = 6,7$; expansion is simplified to a single curve



Graph 33 - h-s diagram of the expansion process for expander D at $T_{ad} = 600\text{ }^{\circ}\text{C}$ and $\epsilon = 10,4$



Graph 34 - T-s diagram of the entire Rankine cycle for expander D at $T_{ad} = 600\text{ }^{\circ}\text{C}$ and $\epsilon = 10,4$; expansion is simplified to a single curve

8.3.2 Ranges of viable inlet conditions for Variant 2

Similar summarization is performed for Variant 2 and inlet steam conditions for which thermal output in the range of 400 – 500 kW can be achieved are presented. Both expanders can work across the entire range of examined temperatures 280 – 600 °C.

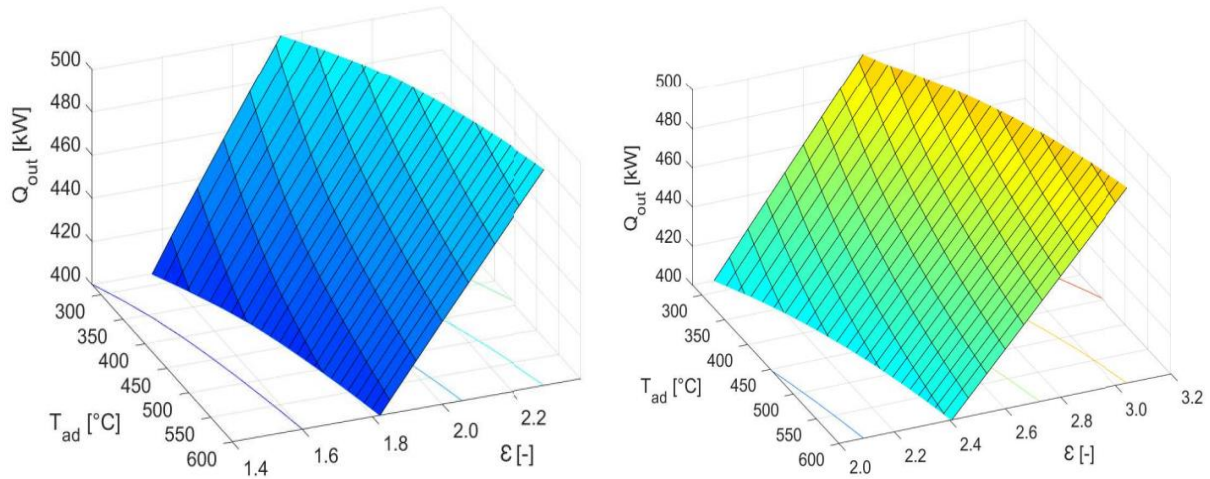


Figure 49 - Thermal output in the range of 400 - 500 kW for Rankine cycles with expanders E (left) and F (right)

	Expander E	Expander F
Pressure ratio range [-]	1,57 – 2,50	2,08 – 3,04
Net electric power range [kW]	4,38 – 23,75	7,93 – 27,66
Mass flow rate [g/s]	149 - 248	148 - 247
Expander efficiency range [%]	25,40 – 46,65	30,70 – 44,45
Net electric efficiency range [%]	1,05 – 4,38	1,92 – 5,10
Maximum electric efficiency for 400 kW heat output [%]	2,69	3,52
Pressure ratio for 400 kW heat output at maximum efficiency [-]	2,30	2,41
Maximum electric efficiency for 500 kW heat output [%]	4,38	5,10
Pressure ratio for 500 kW heat output at maximum efficiency [-]	2,50	3,04

Table 25 - Power output and efficiencies for expanders E and F on the given thermal output range

* Maximum efficiency for both 200 and 250 kW_t is always achieved for the maximum temperature, 600 °C

The mass flow rates for both expanders are almost exactly the same. Expander F can achieve higher overall efficiency than its counterpart despite its higher leakage owing to a built-in volume ratio that is better suited for the examined range of pressure ratios. This allows larger part of the expansion to occur isentropically, see eq. (11) and (12).

For this Variant, the degree of utilisation of the heat from the heat source (a boiler or a flue gas heat exchanger) should also be evaluated. However, as this falls outside the scope of this work, it is omitted here and readdressed in the closing chapters.

Expansion proces, expander F, $T_{ad} = 280\text{ }^{\circ}\text{C}$

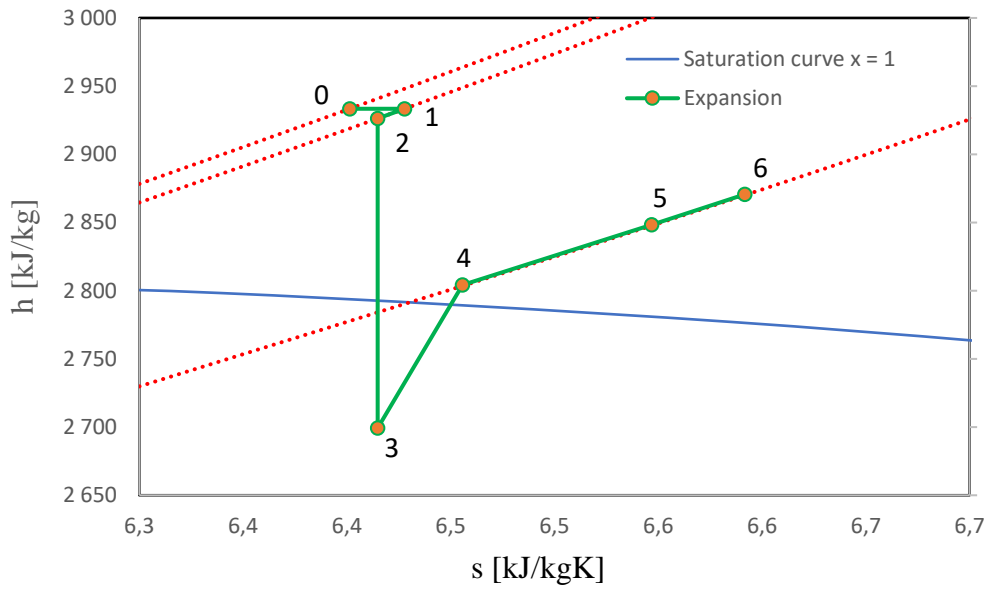


Figure 50 - Expansion process for expander F at admission temperature $280\text{ }^{\circ}\text{C}$ and pressure ratio 2,08

Cycle diagram, expander F, $T_{ad} = 280\text{ }^{\circ}\text{C}$

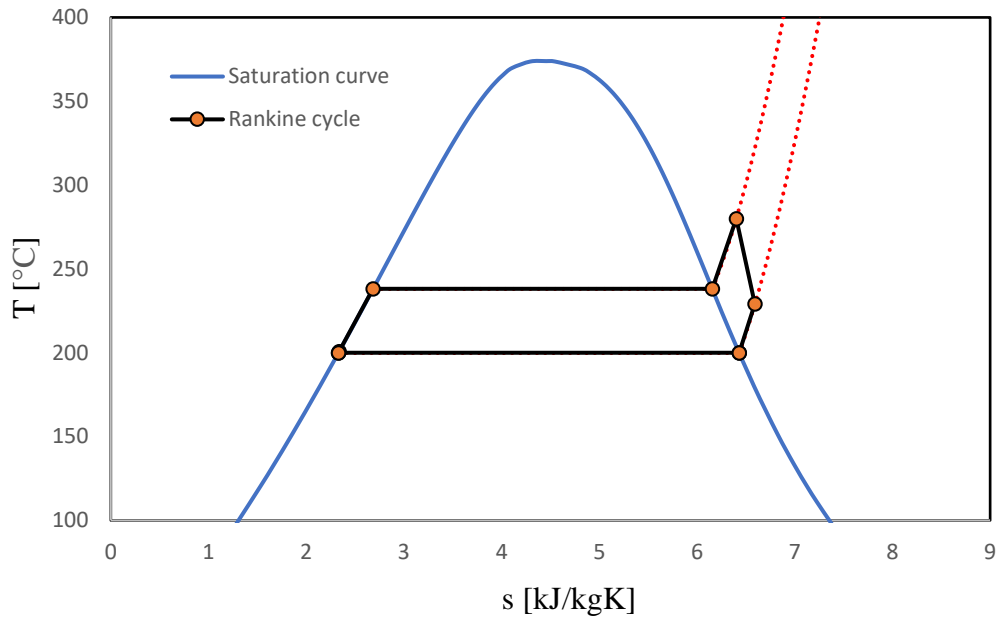


Figure 51 - T-s diagram of Rankine cycle with expander F at admission temperature $280\text{ }^{\circ}\text{C}$ and pressure ratio 2,08

Expansion proces, expander F, $T_{ad} = 600\text{ }^{\circ}\text{C}$

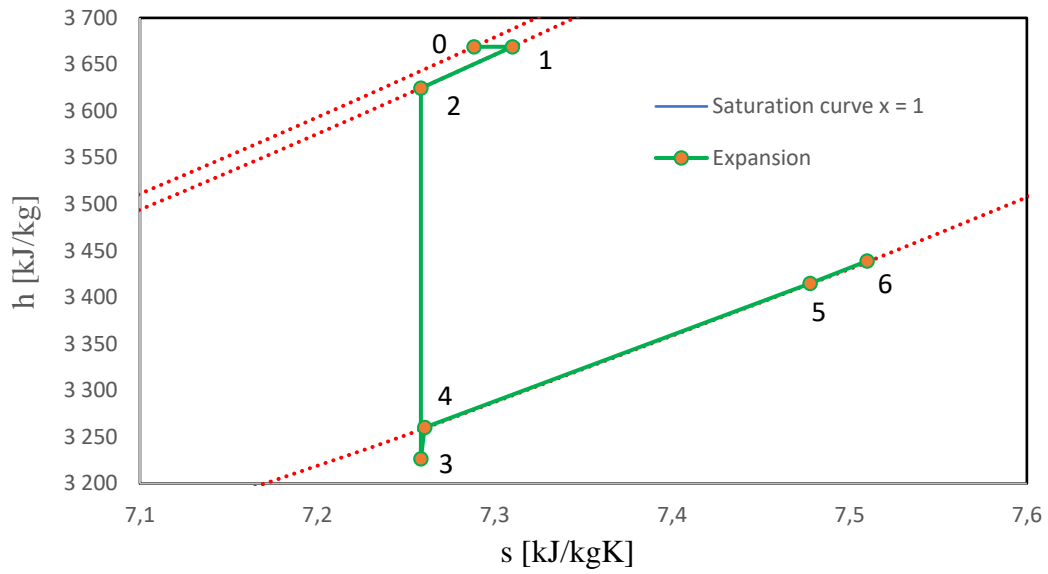


Figure 52 - Expansion process for expander F at admission temperature $600\text{ }^{\circ}\text{C}$ and pressure ratio 3,04

Cycle diagram, expander F, $T_{ad} = 600\text{ }^{\circ}\text{C}$

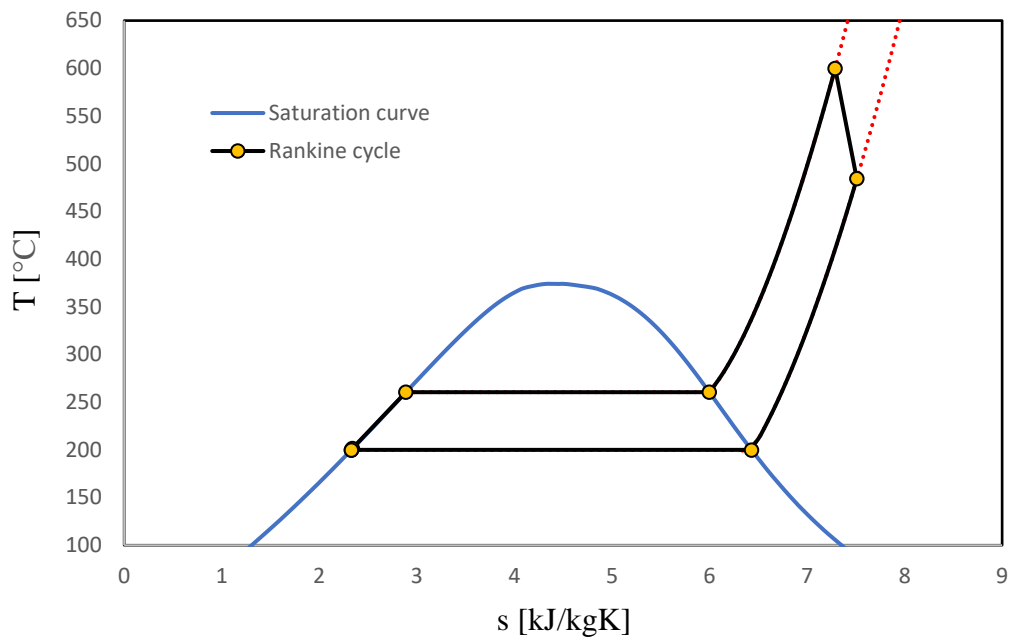


Figure 53 - T-s diagram of Rankine cycle with expander F at admission temperature $600\text{ }^{\circ}\text{C}$ and pressure ratio 3,04

Chapter 9: Evaluation of performance and perspectives of studied expanders

9.1 Comparison of obtained results with commercial and research projects

The single-screw expanders proposed for Variant 1, where steam condensates at atmospheric pressure, can achieve similar or better expansion efficiency than their twin-screw counterparts summarized in Chapter 4, Table 9. The newly opened high temperature area has been examined and at 600 °C, the proposed Rankine cycle can achieve net electrical efficiency of up to 12,43% delivering up to 36,9 kW of net electric power while providing 250 kW of useful heat. This is over double the net efficiency of the smaller ORC unit WAVE 120 with a thermal power output of 113 kW [17] or the ORC units offered by Enogia [16]. Even at lower temperatures that do not require new generations of durable materials, the cycle can achieve efficiency of 8 – 10 % if the expander is designed correctly. However, when compared to other biomass technologies presented in Chapter 2, it is still within the range of efficiencies achieved by other tested biomass technologies. In particular, the internal combustion engines integrated with biomass gasification technology can achieve greater electrical efficiencies, although this comes at the cost of a much more complex system. Furthermore, the area of low-power steam cogeneration is still largely unexplored and significant research and testing still needs to be done before the technology can be considered feasible.

9.2 Possibilities of connecting a steam Rankine cycle with a bottoming ORC

Section 8.3 examined single-screw expander utilised in a Rankine cycle where the steam condensates at a temperature of 200 °C. This temperature was proposed with the idea of combining the RC with a bottoming ORC based on the WAVE 120 unit, but with two parallel vane expanders. This method was chosen because of poor performance of the expander in Variant 2 for a lower cycle heat output of 200 – 250 kW (see 7.2.4).

By itself, this Rankine cycle can achieve maximum net electrical efficiency of 5,10 %. Unlike in Variant 1, high temperatures are necessary to produce electric power with a reasonable efficiency. In this discussion, the bottoming ORC is assumed to have the same performance as the WAVE 120 unit. The ORC mass-flow is assumed to distribute equally into both of the vane expanders. All of the output heat from the topping RC is considered to transfer completely into the bottoming cycle (except for the ambient losses from the expander envelope, see energy balance of the expander in eq. (16)). The overall electrical and CHP efficiency of this system can then be obtained in the following steps:

$$P_{el,net,ORC} = Q_{out,RC} \cdot \eta_{el,net,ORC} \quad (45)$$

$$\eta_{el,net,system} = \frac{P_{el,net,RC} + P_{el,net,ORC}}{Q_{in}} \quad (46)$$

$$Q_{th,system} = Q_{th,ORC} = Q_{out,RC} \cdot \eta_{th,ORC} \quad (47)$$

$$\eta_{CHP,system} = \frac{P_{el,net,RC} + P_{el,net,ORC} + Q_{th,ORC}}{Q_{in}} \quad (48)$$

Expander F is considered for both cases due to its better overall performance at its peak electrical efficiency for both cases. Net electrical and thermal efficiency of the bottoming ORC are assumed to be equal to those of WAVE 120, therefore 5,12 % and 83,88 % respectively [17].

	Rankine cycle thermal output [kW]	
	400	500
System thermal input [kW]	430,84	542,47
System power output [kW]	35,67	53,26
System electrical efficiency [%]	8,28	9,82
System thermal output [kW]	335,32	419,15
System overall peak CHP efficiency [%]	86,15	87,13

Table 26 - Parameters and performance of two variants of a Rankine cycle with a bottoming ORC

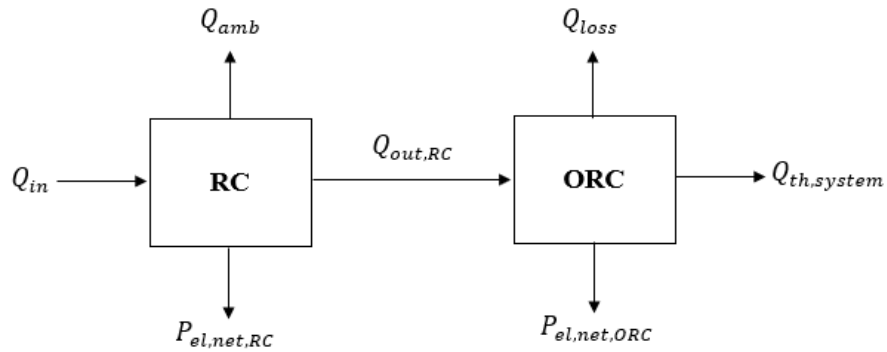


Figure 54 - Energy balance and flow in the entire system RC + bottoming ORC

Q-T diagram of heat exchange between the topping and bottoming cycle

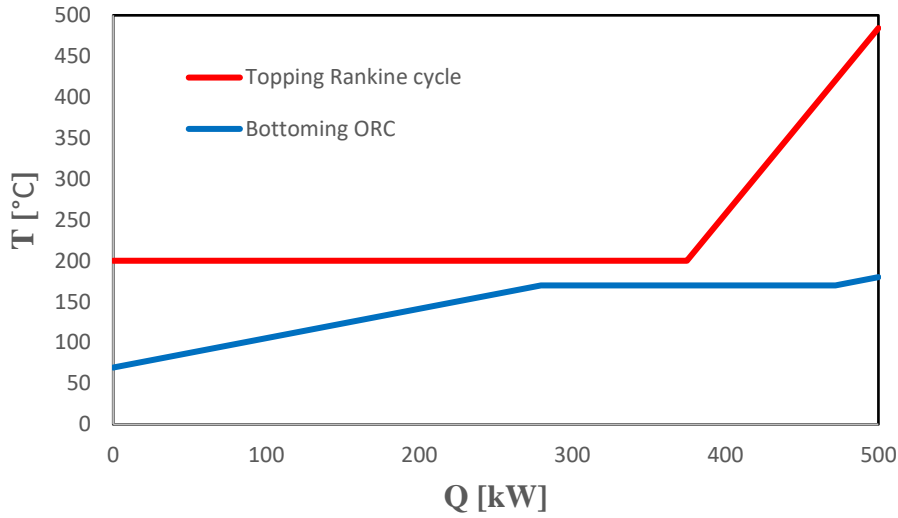


Figure 55 - Q-T diagram of heat exchange between the steam cycle and the ORC, thermal input into the ORC is 500 kW. Parameters of the ORC cycle were obtained from [17].

The diagram in Figure 55 displays the heat transfer between the two cycles in a counterflow heat exchanger. The temperature differences are quite high, especially on the right-hand side of the diagram, which would create exergy losses. The following relations for exergy efficiency of this heat exchange can be expressed with formulas from [129] :

$$E = \int_0^Q \left(1 - \frac{T_0}{T}\right) \delta Q \quad (49)$$

$$\eta_{ex,hx} = \frac{E_{ORC}}{E_{RC}} \quad (50)$$

where E_{ORC} is the exergy transfer into the organic Rankine cycle, E_{RC} is the exergy transferred from the steam Rankine Cycle and T_0 is the dead state temperature in Kelvins. The exergy efficiency of the heat transfer between the topping and the bottoming cycle could be increased by:

- selecting different condensing temperature of the RC and different evaporation temperature of the ORC.
- increasing the superheating in the ORC.

It should be noted that higher exergy efficiency would not necessarily produce more desirable results. For example, higher superheating of the ORC would lead to a lower mass flow rate in the cycle (assuming the heat input is firmly set), thus possibly decreasing the actual power output.

The degree to which the heat from the heat source is utilised is another factor. It was touched upon only briefly in 8.2. but it is important when designing a real application of a cycle. Lower steam condensing temperature would lead to better utilisation of the heat source.

By doubling the thermal output, this system may no longer be applicable in some of the micro systems described in the beginning of this work. Modifications described

throughout this section are necessary to scale it back down while retaining reasonable performance. These modifications should be subjected to analysis and optimization to determine the most desirable configuration.

This chapter contains rough calculation and estimate of the potential of combining the steam and the ORC cycle. The nature of the heat exchange between them and their optimization should be investigated in greater detail in future works.

9.3 Defining boundary conditions and recommendations for subsequent conceptual studies

The goal of this work is to establish a foundation in the field of micro- and small-scale cogeneration from biomass by utilizing steam technologies. Future authors are welcome to build upon and discuss the knowledge presented here. There are multiple pathways for subsequent conceptual studies that can stem from this work:

- **Boundary conditions optimization** – the boundary conditions of both examined variants were firmly set by the desired condensation temperatures. But since the expansion mostly ends in superheated steam, the minimum temperature differences in the heat exchangers could likely be respected with lower steam condensation temperatures in both variants. In Variant 2, different evaporation pressure or superheating in the ORC could also be chosen. The high steam condensing pressure in Variant 2 caused poor performance of the expander even after modifying the leakage relations of the model. A new variant with condensation temperature at 150 – 195 °C should be examined. Correctly optimizing these parameters holds the potential to improving the expander performance, the cycle efficiency, but also increasing the heat source utilisation (see 9.2.).
- **Improving the accuracy of the used models** – as outlined in 6.4.2, some assumptions were made regarding the single-screw expander geometry. These can become sources of errors when predicting the behaviour of the expansion machine. To improve this, a complex leakage model could be implemented to better assess the size of the leakage area. Furthermore, CAD models of the defined expanders can be constructed to validate the geometry model and to accurately obtain the suction port area for each configuration of the single-screw machine. This approach can eventually lead to prototype manufacturing and testing.
- **Simulating other types of volumetric expanders** – in this work, the single-screw expander was chosen after carefully researching the available expanders and their limitations. However, other expansion machines have the potential to be utilised in a low power steam unit. Namely the twin-screw and piston expander have been implemented in steam cycles at larger scale and should be researched further in the context of micro-scale steam CHPs.

- **Heat transfer calculation and condenser design** – heat transfer between the condensing steam and cooling water (RC in Variant 1) and between the condensing steam and organic working fluid (RC in Variant 2) should be calculated and optimized. This calculation will then serve as the foundation for a conceptual design of the condenser.

- **Evaluating and optimizing the utilisation efficiency** – as outlined in 8.2, analysing the heat source utilisation efficiency should be another objective for further research. Specifically in Variant 2, the flue gases will not be cooled down to the standard temperatures of 120 – 180 °C [130]. This will decrease the amount of utilised heat from the heat source and make the entire system less feasible if this heat is not utilised elsewhere.

- **Techno-economic analysis** – employing high temperature steam can increase the cycle efficiency. On the other hand, designing, testing, and constructing the proposed CHP units could prove economically challenging. In section 8.1, it was explained that as the steam inlet temperature increases, the rise in cycle electrical efficiency becomes milder. A fundamental question is whether utilizing a very high steam temperature could be justified in the context of increased investment costs. A techno-economic study could be performed to assess the optimal operating conditions, as well as the feasibility and economic potential.

Conclusion

The research part of this work focused on three main subjects. Micro- and small-scale biomass CHP technologies, materials for utilising steam at high temperatures and finally on different types of volumetric expanders, their characteristics, and possible applications. It was explained that biomass is a highly perspective type of fuel that is CO₂ neutral, cost-efficient and locally available. Next, it was found that thanks to advances in material engineering, higher steam inlet temperatures of up to 600 °C can be achieved. Based on this detailed research, the single-screw expander was chosen as a viable expansion machine for a low-power steam CHP unit.

Two mathematical models were selected to predict the performance and geometry of the single-screw expander. Two variants of Rankine cycle were then defined as main areas of interest, both with different CHP perspectives. Upon analysing the impact of the expander geometry on its behaviour and performance, several different single-screw expanders were proposed for further examination.

This was done by performing a sensitivity analysis, where a wide scale of inlet temperatures and cycle pressure ratios was tested on the selected expanders. Their performance was summarized and evaluated. Expander efficiency ranging from 52,02 to 65,10 % and net electrical cycle efficiency of 7,88 – 12,43 % can be achieved under the given conditions for a steam cycle condensing at atmospheric pressure. Another variant where the heat output from the steam cycle is utilized by an ORC based on the WAVE 120 unit was proposed and its rough potential estimated. This cycle operates with expander efficiency 25,40 – 46,65% and net electrical cycle efficiency 1,05 – 5,10 %. The results obtained throughout this work were compared with similar technologies and a rough assessment of the potential of the proposed cycles was evaluated. It is important to note that simply plugging the computed expander efficiency into a model steam cycle will yield slightly inaccurate results because of the more complicated energy balance of the thermodynamic model.

The stand-alone steam cycle technology in Variant 1 attained better net efficiencies than some of the micro- and small-scale ORCs offered on the market. Combining the steam cycle examined in Variant 2 with a bottoming ORC based on the WAVE 120 unit can increase the overall system electrical efficiency, but the thermal output is roughly four times higher. With electrical efficiency < 10 %, the technology may be less competitive in this range. Optimization of both cycles can make the system more efficient and scale it down. However, further investigation and testing needs to be made before the technology can be proclaimed feasible and competitive. Little information is available about utilising high parameter steam in low-power applications. Therefore, while the presented concepts have potential, more research and testing must be made. Possible areas of further study are highlighted towards the end of the work.

List of Figures

Figure 1 - Scheme of a simple RC	1
Figure 2 - T-s diagram of a simple RC	1
Figure 3 - Efficiency of the RC on steam temperature and pressure from 370 up to 450 C. The condensation pressure is 10 kPa. The dotted line displays the optimum pressure for each temperature [3].....	2
Figure 4 - Supercritical steam Rankine cycle with single reheat [43]	9
Figure 5 - Thermo-physical properties of ferritic and austenitic steels and nickel alloys [41]	10
Figure 6 - Maximum working temperatures of different materials based on operating pressure [41].....	13
Figure 7 - Types of expanders [65].....	14
Figure 8 - Different types of volumetric expanders sorted by their rotor motion [64]	15
Figure 9 - An experimental swash-plate piston configuration [72]	16
Figure 10 - The rolling piston	17
Figure 11 - Example cross section of a twin-screw expander [81].....	18
Figure 12 - Operating principle of the twin-screw. A - suction; B and C - expansion; D - discharge	18
Figure 13 – Cylindrical-plate, the most common configuration of the single-screw expander [85].....	19
Figure 14 - Expansion process of the single screw expander. a) suction, b) expansion, c) end of expansion and discharge [80]	19
Figure 15 - Operating principle of the scroll expander [95]	21
Figure 16 - Working principle of the rotary vane. 1- inlet; 2-3 - expansion; 4- exhaust [97] .	22
Figure 17 - Selection map for pistons and turbomachines [108]	25
Figure 18 - Power output of installed volumetric expanders in ORC systems [67]	26
Figure 19 - Different configurations of the SSE based on the shape and number of rotors [114].....	29
Figure 20 - Compared performance of a SSE when organic fluids and water are used as working fluid [113].....	29
Figure 21 - Filling factor and volumetric efficiency on inlet pressure (working fluid is R245fa) [110].....	30

Figure 22 - Leakage paths within a single-screw expander – fitting (L7 – L9), meshing (L1 – L5) and splitting (L6) [85]	31
Figure 23 - Schematic of the screw expander model [110]	33
Figure 24 - Inputs and outputs of the SSE model	34
Figure 25 - Under- and over-expansion in the p-V diagram [110]	36
Figure 26 - Flowchart of the iterative calculation of the expansion	38
Figure 27 - Scheme of the inputs and desired outputs of the geometry model.....	39
Figure 28 - Main geometric parameters of the SSE [80]	40
Figure 29 - Schematic view of the rotor meshing, suction and discharge side [80]	40
Figure 30 - Representation of Vg1 and Vg2 volumes [80].....	42
Figure 31 - Schematic of RC + ORC combined cycle system tested in [126].....	43
Figure 32 - Expander efficiency (left) and net electrical efficiency (right) of expander A	67
Figure 33 - Net electric power (left) and heat output (right) of expander A	68
Figure 34 - Expander efficiency (left) and net electrical efficiency (right) of expander B	68
Figure 35 - Power output (left) and heat output (right) of expander B.....	69
Figure 36 - Expander efficiency (left) and electrical efficiency (right) of expander C	69
Figure 37 - Power output (left) and heat output (right) of expander C.....	70
Figure 38 - Expander efficiency (left) and electrical efficiency (right) of expander D.....	70
Figure 39 - Power output (left) and heat output (right) of expander D.....	71
Figure 40 - Filling factor for the four expanders A – D.....	73
Figure 41 – Volumetric efficiency for the four expanders A – D.....	74
Figure 42 - Expander mechanical efficiency and cycle net electrical efficiency for expander E	75
Figure 43 - Net electric power and heat output for expander E.....	75
Figure 44 - Expander mechanical efficiency and net electrical efficiency for expander F	76
Figure 45 - Net electric power and heat output for expander F	76
Figure 46 - Filling factor of expanders E (left) and F (right).....	77
Figure 47 - Volumetric efficiency of expanders E (left) and F (right)	77
Figure 48 - Ranges of pressures and temperatures that satisfy the stated heat output for expanders A – D.....	78
Figure 49 - Thermal output in the range of 400 - 500 kW for Rankine cycles with expanders E (left) and F (right).....	82
Figure 50 - Expansion process for expander F at admission temperature 280 °C and pressure ratio 2,08	83

Figure 51 - T-s diagram of Rankine cycle with expander F at admission temperature 280 °C and pressure ratio 2,08	83
Figure 52 - Expansion process for expander F at admission temperature 600 °C and pressure ratio 3,04	84
Figure 53 - T-s diagram of Rankine cycle with expander F at admission temperature 600 °C and pressure ratio 3,04	84
Figure 54 - Energy balance and flow in the entire system RC + bottoming ORC	86
Figure 55 - Q-T diagram of heat exchange between the steam cycle and the ORC, thermal input into the ORC is 500 kW. Parameters of the ORC cycle were obtained from [17].	87

List of Tables

Table 1 - Overview of main CHP technologies and their characteristics [5] [6] [8].....	4
Table 2 - Overview of current commercial biomass CHP technologies with power output up to 50 kW _e	6
Table 3 - Research and development regarding micro-CHP biomass technologies.....	7
Table 4 - Components and their candidate materials for a A-USC plant as a result of the COMTES700 and AD700 programmes [47]	10
Table 5 - Mechanical properties of several low-alloyed steels. The properties may vary depending on the type of heat treatment process applied [41][50].....	11
Table 6 - Mechanical properties of several high-alloyed martensitic steels. The properties may vary depending on the type of heat treatment process applied [52][53][54][55].....	11
Table 7 - Mechanical properties of several high-alloyed martensitic steels. The properties may vary depending on the type of heat treatment process applied [41][56][57]	12
Table 8 - Results from studies and investigations of piston expanders	17
Table 9 - results from studies and investigations of screw expanders.....	20
Table 10 - Specifications of various experimental and commercial scroll expanders.....	22
Table 11 - Specifications of various experimental and commercial vane expanders	23
Table 12 - Comparison of different volumetric expander types. Based on information summarized in previous chapters. Some parameters taken from [64] and [65].....	24
Table 13 - Boundary conditions for cycle properties of two variants of examined Rankine cycles.....	44
Table 14 - Expander properties and coefficients	45
Table 15 - Assumed geometry coefficients of the expanders [80]	45
Table 16 - Conditions for determining influence of BVR, T = 220 °C, Var 1	49
Table 17 - Conditions for determining influence of BVR for Var 1, T = 450 °C	51
Table 18 - Parameters for determining the influence of swept volume on the performance for Var 1.....	54
Table 19 - Selected expanders and their swept volumes and volume ratios for Var 1	56
Table 20 - Boundary conditions for a second iteration of BVR evaluation for Var 2.....	57
Table 21 - Boundary conditions for determining the influence of swept volume on the expander performance, Var 2.....	59

Table 22 - Boundary conditions for testing the losses for both variants	60
Table 23 - Boundary conditions for determining the influence of BVR on the expander behaviour, Var 2, constant leakage area	63
Table 24 - Overview of delivered electric power and efficiencies of expanders A - D for a heat output of 200 - 250 kW	79
Table 25 - Power output and efficiencies for expanders E and F on the given thermal output range.....	82
Table 26 - Parameters and performance of two variants of a Rankine cycle with a bottoming ORC	86
Table 27 - Geometry parameters of designed expanders. See Figure 28 for visualization. ..	108

List of graphs

Graph 1 - Expander efficiency on BVR, $T = 220\text{ }^{\circ}\text{C}$, Var 1	49
Graph 2 - Outputted heat on BVR, $T = 220\text{ }^{\circ}\text{C}$, desired range of outputs highlighted, Var 1 ..	50
Graph 3 – Net electric power electric power on BVR, $T = 220\text{ }^{\circ}\text{C}$, Var 1	50
Graph 4 - Electrical efficiency of the cycle on BVR, $T = 220\text{ }^{\circ}\text{C}$, Var 1	51
Graph 5 - Expander efficiency on BVR for Var 1, $T = 450\text{ }^{\circ}\text{C}$	52
Graph 6 - Heat output on BVR, $T = 450\text{ }^{\circ}\text{C}$, with the desired range highlighted, Var 1	52
Graph 7 - Electric power on BVR for Var 1, $T = 450\text{ }^{\circ}\text{C}$	53
Graph 8 - Electrical efficiency on BVR for Var 1, $T = 450\text{ }^{\circ}\text{C}$	53
Graph 9 - Heat output on swept volume for Var 1	54
Graph 10 - Power output on swept volume for Var 1	55
Graph 11 - Power output on swept volume and volume ratio for Var 1	55
Graph 12 - Expander efficiency on BVR for Var 2	58
Graph 13 - Heat output on BVR for Var 2, $T = 450\text{ }^{\circ}\text{C}$	58
Graph 14 - Outputted heat on V_{sw} for different BVRs, Var 2	59
Graph 15 - Expander efficiency on V_{sw} for different BVRs, Var 2	59
Graph 16 - Dependence of various losses on pressure ratios for Var 1 and Var 2	60
Graph 17 - Relative leakage flow rate on pressure ratio, Var 2	61
Graph 18 - Comparison of the relative leakage flow with and without the correction coefficient, Var 1	62
Graph 19 - Comparison of the relative leakage flow with and without the correction coefficient, Var 2	62
Graph 20 - Expander efficiency on BVR, Var 2, constant leakage area	63
Graph 21 - Thermal output on BVR, Var 2, constant leakage area, desired range of heat outputs highlighted	63
Graph 22 - Net electric power output on BVR, Var 2, constant leakage area	64
Graph 23 - Net electrical efficiency on BVR, Var 2, constant leakage area	64
Graph 24 - Boundary conditions for determining the influence of both V_{sw} and BVR on the expander and cycle, Var 2, constant leakage area	64
Graph 25 - Expander efficiency on V_{sw} and BVR, Var 2, constant leakage area	65
Graph 26 -Heat output on V_{sw} and BVR, Var 2, constant leakage area	65

Graph 27 - Net electrical efficiency on V_{sw} and BVR, Var 2, constant leakage area.....	66
Graph 28 - Defining the geometry of expanders for further testing in Variant 2, desired thermal output 400 - 500 kW	66
Graph 29 - Exhaust steam temperature on admission temperature for $\epsilon = 10$	72
Graph 30 - Ambient heat losses on admission temperature for expanders A - D for $\epsilon = 10$...	72
Graph 31 - h-s diagram of the expansion process for expander D at $T_{ad} = 220$ °C and $\epsilon = 6,7$	80
Graph 32 - T-s diagram of the entire Rankine cycle for expander D at $T_{ad} = 220$ °C and $\epsilon = 6,7$; expansion is simplified to a single curve	80
Graph 33 - h-s diagram of the expansion process for expander D at $T_{ad} = 600$ °C and $\epsilon = 10,4$	81
Graph 34 - T-s diagram of the entire Rankine cycle for expander D at $T_{ad} = 600$ °C and $\epsilon = 10,4$; expansion is simplified to a single curve	81

Bibliography

- [1] O. Badr, S. Naik, P. W. O’Callaghan, and S. D. Probert, “Expansion machine for a low power-output steam Rankine-cycle engine,” *Appl. Energy*, vol. 39, no. 2, pp. 93–116, 1991, doi: 10.1016/0306-2619(91)90024-R.
- [2] R. Stobart and R. Weerasinghe, “Heat recovery and bottoming cycles for SI and CI engines - A perspective,” *SAE Tech. Pap.*, vol. 2006, no. 724, 2006, doi: 10.4271/2006-01-0662.
- [3] A. A. Taimoor, M. E. Siddiqui, and S. S. A. Aziz, “Thermodynamic analysis of partitioned combined cycle using simple gases,” *Appl. Sci.*, vol. 9, no. 19, 2019, doi: 10.3390/app9194190.
- [4] N. V. Khartchenko and V. M. Khartchenko, *Advanced Energy Systems*, 2nd editio. New York: CRC Press, 2014.
- [5] Vattenfall, “Moorburg CHP Plant,” [Online]. Available: <https://powerplants.vattenfall.com/moorburg/>.
- [6] R. Beith, *Small and micro combined heat and power (CHP) systems*. Cambridge, UK: Woodhead Publishing, 2011.
- [7] C. H. and P. P. U.S. Environmental Protection Agency, “Catalog of CHP Technologies Section 4. Technology Characterization - Steam Turbines,” 2015, [Online]. Available: https://www.epa.gov/sites/production/files/2015-07/documents/catalog_of_chp_technologies_section_4_technology_characterization_-_steam_turbines.pdf.
- [8] R. Padinger, S. Aigenbauer, C. Schmidl, and J. D. Bentzen, “Best practise report on decentralized biomass fired CHP plants and status of biomass fired small-and micro scale CHP technologies,” *IEA Bioenergy*, vol. 32, no. 2019, pp. 1–83, 2019.
- [9] SmartCHP, “Cogeneration crucial in delivering the Fit for 55 package.” [https://www.smartchp.eu/cogeneration-as-a-key-solution-to-deliver-the-fit-for-55-package-objectives/#:~:text=The CODE2 project \(Cogeneration Observatory,and low-carbon energy sources](https://www.smartchp.eu/cogeneration-as-a-key-solution-to-deliver-the-fit-for-55-package-objectives/#:~:text=The CODE2 project (Cogeneration Observatory,and low-carbon energy sources).
- [10] J. Mascuch, V. Novotny, V. Vodicka, and Z. Zeleny, “Towards development of 1-10 kW pilot ORC units operating with hexamethyldisiloxane and using rotary vane expander,” *Energy Procedia*, vol. 129, pp. 826–833, 2017, doi: 10.1016/j.egypro.2017.09.196.
- [11] C. Wouters, E. S. Fraga, and A. M. James, “Residential Microgrid Design Optimisation under Uncertain μ CHP Characteristics,” *Comput. Aided Chem. Eng.*, vol. 38, pp. 1491–1496, Jan. 2016, doi: 10.1016/B978-0-444-63428-3.50253-8.
- [12] D. G. Thombarse, “Stirling Engine: Micro-CHP System for Residential Application,” in *Encyclopedia of Materials: Science and Technology*, 2nd editio., 2008, pp. 1–8.
- [13] L. Dong, H. Liu, and S. Riffat, “Development of small-scale and micro-scale biomass-fuelled CHP systems - A literature review,” *Appl. Therm. Eng.*, vol. 29, no. 11–12, pp. 2119–2126, 2009, doi: 10.1016/j.applthermaleng.2008.12.004.
- [14] J. Mascuch, V. Novotny, V. Vodicka, Z. Zeleny, and J. Spale, “Set-Up and Pilot Operation of an in-House Developed Biomass Orc Mchp in the Czech Republic,” *Orc2019*, pp. 1–9, 2019.
- [15] CNN, “Europe’s scramble for gas could cause the next energy shortage.” <https://edition.cnn.com/2022/05/30/energy/lng-global-winter-shortage-europe/index.html>.

- [16] “Enogia ORC.” <https://enogia.com/en/orc-3/>.
- [17] J. Mascuch, J. Spale, V. Vodicka, Z. Zeleny, and V. Novotny, “Scaling-Up a Biomass Fired Micro-Chp Orc for Better Performance Towards Commercialization,” *6th Int. Semin. ORC power Syst.*, pp. 1–10, 2021.
- [18] Kaymacor, “Kaymacor ORChidea,” [Online]. Available: <https://www.kaymacor.com/products>.
- [19] Winno Energy, “Gaisfication unit.” <https://www.winnoenergy.com/smallchp.html>.
- [20] NewEnCo, “Biomass CHP.” <https://www.newenco.co.uk/biomass-chp>.
- [21] Froling, “Froling CHP 50.” <https://www.froeling.com/en/products/heat-and-electricity/wood-combined-heat-and-power-chp.html>.
- [22] Microgen, “Microgen Stirling engine.” <https://www.microgen-engine.com/>.
- [23] O. Energy, “Power generation.” <https://www.orcan-energy.com/en/applications-power-generation.html>.
- [24] VEP, “Green Steam + Neumot.” <http://www.vep.at/en/wirtschaftliche-stromerzeugung.php>.
- [25] “Genoastirling.” <http://www.genoastirling.com/>.
- [26] “Stirling-tech,” [Online]. Available: <http://stirling-tech.com/biogen/>.
- [27] E. Macchi and M. Astolfi, *Organic Rankine Cycle (ORC) Power Systems: Technologies and Applications*. Duxfor, UK: Woodhead Publishing, 2016.
- [28] D. Mertzis, P. Mitsakis, S. Tsiakmakis, P. Manara, A. Zabaniotou, and Z. Samaras, “Performance analysis of a small-scale combined heat and power system using agricultural biomass residues: The SMART-CHP demonstration project,” *Energy*, vol. 64, pp. 367–374, 2014, doi: 10.1016/j.energy.2013.11.055.
- [29] D. I. of M. Research, “Thermoelect CHP.” https://www.dlr.de/wf/en/desktopdefault.aspx/tabid-5940/9557_read-53804/.
- [30] M. Jradi, J. Li, H. Liu, and S. Riffat, “Micro-scale ORC-based combined heat and power system using a novel scroll expander,” *Int. J. Low-Carbon Technol.*, vol. 9, no. 2, pp. 91–99, 2014, doi: 10.1093/ijlct/ctu012.
- [31] B. Energy, “Hot air turbine.” <https://bluebox.energy/779-2/mono/>.
- [32] I. Borisov and A. Khalatov, “The biomass fueled micro-scale CHP unit with stirling engine and two-stage vortex combustion chamber,” *Heat Mass Transf.*, 2022, [Online]. Available: <https://doi.org/10.1007/s00231-021-03165-z>.
- [33] E. Cardozo and A. Malmquist, “Performance comparison between the use of wood and sugarcane bagasse pellets in a Stirling engine micro-CHP system,” *Appl. Therm. Eng.*, vol. 159, no. June, p. 113945, 2019, doi: 10.1016/j.applthermaleng.2019.113945.
- [34] Uniflow, “Uniflow Generator.” <https://www.uniflowpower.com/>.
- [35] M. Badami and M. Mura, “Preliminary design and controlling strategies of a small-scale wood waste Rankine Cycle (RC) with a reciprocating steam engine (SE),” *Energy*, vol. 34, no. 9, pp. 1315–1324, 2009, doi: 10.1016/j.energy.2009.04.031.
- [36] M. Francesconi, G. Pasini, R. Lensi, and M. Antonelli, “Externally fired micro gas turbine for biomass application using automotive components,” *AIP Conf. Proc.*, vol. 2191, no. December, 2019, doi: 10.1063/1.5138813.
- [37] C. Mărculescu, V. E. Cenușă, and F. N. Alexe, “Analysis on using biomass lean syngas in micro gas turbines,” *IOP Conf. Ser. Earth Environ. Sci.*, vol. 40, no. 1, 2016, doi: 10.1088/1755-1315/40/1/012036.
- [38] Xcel Energy, “Current projects.” <https://mi.my.xcelenergy.com/s/energy-portfolio/biomass>.
- [39] Bladon, “BLADON microturbine gensets for a greener future.” <https://www.bladonmt.com/blog/bladon-micro-turbine-gensets-for-a-greener-future>.
- [40] I. Opreș, V. E. Cenușă, M. Norișor, G. Darie, F. N. Alexe, and S. Costinaș, “Parametric

- optimization of the thermodynamic cycle design for supercritical steam power plants,” *Energy Convers. Manag.*, vol. 208, no. December 2019, p. 112587, 2020, doi: 10.1016/j.enconman.2020.112587.
- [41] A. Di Gianfrancesco, *Materials for Ultra-Supercritical and Advanced Ultra-Supercritical Power Plants*. Duxfor, UK: Elsevier Ltd., 2017.
- [42] M. Piwowarski, “Optimization of steam cycles with respect to supercritical parameters,” *Polish Marit. Res.*, vol. 16, no. Special, pp. 45–51, 2009, doi: 10.2478/v10012-008-0043-3.
- [43] T. Engineering, “What is Supercritical Rankine Cycle – Definition.” <https://www.thermal-engineering.org/what-is-supercritical-rankine-cycle-definition/>.
- [44] “Pushing the steam cycle boundaries.” <https://www.powerengineeringint.com/coal-fired/pushing-the-steam-cycle-boundaries/>.
- [45] R. Blum, “High-efficiency coal-fired power plants.”
- [46] “COMTES700: a rig for the over 50s.” <https://www.modernpowersystems.com/features/featurecomtes700-a-rig-for-the-over-50s>.
- [47] K. Nicol, *Status of advanced ultra-supercritical pulverised coal technology*, no. October. 2013.
- [48] A. Shibli, *Coal Power Plant Materials and Life Assessment - Developments and Applications*, Elsevier L. Cambridge, UK, 2014.
- [49] M. P. Systems, “T24 revisited.” <https://www.modernpowersystems.com/features/featuret24-revisited-7971348/>.
- [50] P. R. Kannan, V. Muthupandi, B. Arivazhagan, and K. Devakumaran, “Microstructure and Mechanical Properties of Heat-treated T92 Martensitic Heat Resistant Steel,” *High Temp. Mater. Process.*, vol. 36, no. 8, pp. 771–778, 2017, doi: 10.1515/htmp-2016-0030.
- [51] O. Mohamed, A. Khalil, and J. Wang, “Modeling and control of supercritical and ultra-supercritical power plants: A review,” *Energies*, vol. 13, no. 11, 2020, doi: 10.3390/en13112935.
- [52] H. Li and D. Mitchell, “Microstructural characterization of P91 steel in the virgin, service exposed and post-service re-normalized conditions,” 2013. [Online]. Available: <https://ro.uow.edu.au/cgi/viewcontent.cgi?referer=https://www.google.com/&httpsredir=1&article=2837&context=eispapers>.
- [53] M. Piping, “P92 Steel: Allowable Stress, Tensile, Yield – Temperature Chart,” [Online]. Available: <http://www.metalspiping.com/p92-steel-allowable-stress-tensile-yield-temperature-chart.html>.
- [54] “European Steel and Alloy Grades,” [Online]. Available: http://www.steelnumber.com/en/steel_composition_eu.php?name_id=81.
- [55] J. Kasl and D. Jandová, “Metallography of CB2 steel used for cast turbine components,” *Mater. Sci. Forum*, vol. 782, no. April 2015, pp. 179–185, 2014, doi: 10.4028/www.scientific.net/MSF.782.179.
- [56] Special Metals, “Inconel Alloy X-750.” <https://www.specialmetals.com/assets/smc/documents/alloys/inconel/inconel-alloy-x-750.pdf>.
- [57] Haynes Intl, “Haynes 282 Alloy principal features,” [Online]. Available: <http://haynesintl.com/docs/default-source/pdfs/new-alloy-brochures/high-temperature-alloys/brochures/282-brochure.pdf?sfvrsn=20>.
- [58] T. Achter, R. Quinkertz, M. Baca, and S. Ag, “Increased efficiency and flexibility of large coal-fired power plants applied to 350-MW-class units,” in *Power-Gen Asia 2016*, 2016, pp. 1–21.

- [59] L. C. Enríquez, J. Muñoz-antón, and J. M. M. Peñalosa, “Supercritical Steam power cycle for Line-Focus Solar Power Plants Supercritical Steam power cycle for Line-Focus Solar Power Plants,” no. January 2015, pp. 2–8, 2014, doi: 10.13140/2.1.4031.7769.
- [60] I. A. Fernández, M. R. Gómez, J. R. Gómez, and Á. B. Insua, “Review of propulsion systems on LNG carriers,” *Renew. Sustain. Energy Rev.*, vol. 67, no. January, pp. 1395–1411, 2017, doi: 10.1016/j.rser.2016.09.095.
- [61] V. Medica-Viola, V. Mrzljak, N. Anđelić, and M. Jelić, “Analysis of low-power steam turbine with one extraction for marine applications,” *Nase More*, vol. 67, no. 2, pp. 87–95, 2020, doi: 10.17818/NM/2020/2.1.
- [62] “Cyclone Power.” <http://cyclonepower.com/>.
- [63] G. Negreanu, V. Berbece, L. Mihaescu, I. Oprea, I. Pisa, and D. Andreescu, “Thermal power plant for energy willow use: design, performances,” in *3rd International Conference on Thermal Equipment, Renewable Energy and Rural Development*, 2014, no. June, doi: 10.13140/2.1.1796.9609.
- [64] M. Imran, M. Usman, B. S. Park, and D. H. Lee, “Volumetric expanders for low grade heat and waste heat recovery applications,” *Renew. Sustain. Energy Rev.*, vol. 57, pp. 1090–1109, 2016, doi: 10.1016/j.rser.2015.12.139.
- [65] A. P. Weiß, “Volumetric Expander vs. Turbine - Which is the better choice for small ORC Plants?,” *Eff. Br. mindfulness Interv. acute pain Exp. An Exam. Individ. Differ.*, vol. 1, no. September 2013, pp. 1–36, 2013.
- [66] N. Ivanova, V. Gugleva, M. Dobрева, I. Pehlivanov, S. Stefanov, and V. Andonova, “Expanders for Organic Rankine Cycle Technology,” *Intech*, vol. i, no. tourism, p. 13, 2016.
- [67] V. Vodička, “Optimalizace lamelového expandéru pro tepelné oběhy nízkých výkonů,” Dissertation, CTU Prague, 2019.
- [68] O. Badr, P. W. O’Callaghan, M. Hussein, and S. D. Probert, “Multi-vane expanders as prime movers for low-grade energy organic Rankine-cycle engines,” *Appl. Energy*, vol. 16, no. 2, pp. 129–146, 1984, doi: 10.1016/0306-2619(84)90060-6.
- [69] E. Dick, *Fundamentals of Turbomachines*. Springer International Publishing, 2015.
- [70] V. Vodicka, L. Guillaume, J. Mascuch, and V. Lemort, “Testing and Modeling a Vane Expander Used in an Orc Working With Hexamethyldisiloxane (Mm),” *Proc. 3rd Int. Semin. ORC Power Syst. ASME ORC 2015*, no. Mm, pp. 1–10, 2015.
- [71] J. Mascuch, V. Novotny, J. Spale, V. Vodicka, and Z. Zeleny, “Experience from set-up and pilot operation of an in-house developed biomass-fired ORC microcogeneration unit,” *Renew. Energy*, vol. 165, pp. 251–260, 2021, doi: 10.1016/j.renene.2020.11.021.
- [72] J. F. Oudkerk, R. Dickes, O. Dumont, and V. Lemort, “Experimental performance of a piston expander in a small- scale organic Rankine cycle,” *IOP Conf. Ser. Mater. Sci. Eng.*, vol. 90, no. 1, 2015, doi: 10.1088/1757-899X/90/1/012066.
- [73] O. Dumont, R. Dickes, and V. Lemort, “Experimental investigation of four volumetric expanders,” *Energy Procedia*, vol. 129, no. September, pp. 859–866, 2017, doi: 10.1016/j.egypro.2017.09.206.
- [74] Z. Zhang, Y. Ma, M. Li, and L. Zhao, “Recent advances of energy recovery expanders in the transcritical CO₂ refrigeration cycle,” *HVAC R Res.*, vol. 19, no. 4, pp. 376–384, 2013, doi: 10.1080/10789669.2013.784644.
- [75] D. Seher, T. Lengenfelder, J. Gerhardt, N. Eisenmenger, M. Hackner, and I. Krinn, “Waste Heat Recovery for Commercial Vehicles with a Rankine Process,” *21st Aachen Colloq. Automob. Engine Technol.*, pp. 1–15, 2012.
- [76] O. Dumont, A. Parthoens, R. Dickes, and V. Lemort, “Experimental investigation and optimal performance assessment of four volumetric expanders (scroll, screw, piston

- and roots) tested in a small-scale organic Rankine cycle system,” *Energy*, vol. 165, no. June, pp. 1119–1127, 2018, doi: 10.1016/j.energy.2018.06.182.
- [77] T. Hua, M. Yitai, L. Minxia, G. Haiqing, and L. Zhongyan, “Influence of a non-condensable gas on the performance of a piston expander for use in carbon dioxide trans-critical heat pumps,” *Appl. Therm. Eng.*, vol. 31, no. 11–12, pp. 1943–1949, 2011, doi: 10.1016/j.applthermaleng.2011.02.041.
- [78] R. Weerasinghe and S. Hounsham, “Small Engines as Bottoming Cycle Steam Expanders for Internal Combustion Engines,” *J. Combust.*, vol. 2017, 2017, doi: 10.1155/2017/1742138.
- [79] H. Öhman and P. Lundqvist, “Screw expanders in ORC applications, review and a new perspective,” *3rd Int. Semin. ORC Power Syst. Oct. 12-14, Brussels, Belgium*, no. October, 2015, doi: 10.13140/RG.2.1.3137.3523.
- [80] D. Ziviani, E. A. Groll, J. E. Braun, and M. De Paepe, “Review and update on the geometry modeling of single-screw machines with emphasis on expanders,” *Int. J. Refrig.*, vol. 92, pp. 10–26, 2018, doi: 10.1016/j.ijrefrig.2018.05.029.
- [81] “Screw expander.” <https://greensecure.org/screw-expander/>.
- [82] P. Iodice, G. Langella, and A. Amoresano, “Exergetic analysis of a new direct steam generation solar plant using screw expanders,” *Energies*, vol. 13, no. 3, 2020, doi: 10.3390/en13030720.
- [83] A. Giuffrida, “A semi-empirical method for assessing the performance of an open-drive screw refrigeration compressor,” *Appl. Therm. Eng.*, vol. 93, pp. 813–823, 2016, doi: 10.1016/j.applthermaleng.2015.10.023.
- [84] D. Ziviani, I. Bell, M. De Paepe, and M. Van Den Broek, “Comprehensive model of a single screw expander for ORC-systems,” *22nd Int. Compress. Eng. Conf. Purdue*, pp. 1–10, 2014.
- [85] L. Shen *et al.*, “Theoretical and experimental analyses of the internal leakage in single-screw expanders,” *Int. J. Refrig.*, vol. 86, pp. 273–281, 2018, doi: 10.1016/j.ijrefrig.2017.10.037.
- [86] P. Platell, “Displacement expanders for small scale cogeneration,” Stockholm Royal Institute of Technology, 1993.
- [87] “fj-opcon.” <http://www.fj-opcon.com/en/Product/detail/id/5>.
- [88] “jxhdep.” <http://www.jxhdep.com/en/newsInfo.asp?pid=4>.
- [89] T. Biederman and S. L. City, “Geothermal ORC Systems using Large Screw Expanders,” pp. 1–8, 2014.
- [90] B. Carey, “Total Flow Power Generation From Geothermal Resources Using a Helical Screw Expander,” *Proc. New Zeal. Geotherm. Work.*, pp. 127–132, 1983.
- [91] H. Tang, H. Wu, X. Wang, and Z. Xing, “Performance study of a twin-screw expander used in a geothermal organic Rankine cycle power generator,” *Energy*, vol. 90, pp. 631–642, 2015, doi: 10.1016/j.energy.2015.07.093.
- [92] W. He, Y. Wu, Y. Peng, Y. Zhang, C. Ma, and G. Ma, “Influence of intake pressure on the performance of single screw expander working with compressed air,” *Appl. Therm. Eng.*, vol. 51, no. 1–2, pp. 662–669, 2013, doi: 10.1016/j.applthermaleng.2012.10.013.
- [93] S. Lemort, V. Guillaume, L. Legros, A. Declaye, S. Quilín, “A COMPARISON OF PISTON, SCREW AND SCROLL EXPANDERS FOR SMALL-SCALE RANKINE CYCLE SYSTEMS Thermodynamics Laboratory, University of Liège, Campus du Sart Tilman, B49, STATE OF THE ART,” *3rd Int. Conf. Microgeneration Relat. Technol.*, 2013.
- [94] BraytonEnergy LLC, “Rotary screw Brayton Cycle Engine.” <https://www.braytonenergy.net/our-projects/2-kw-recuperated-brayton/>.
- [95] T. SAITOH, N. YAMADA, and S. WAKASHIMA, “Solar Rankine Cycle System

- Using Scroll Expander,” *J. Environ. Eng.*, vol. 2, no. 4, pp. 708–719, 2007, doi: 10.1299/jee.2.708.
- [96] M. Hijriawan, N. A. Pambudi, D. S. Wijayanto, M. K. Biddinika, and L. H. Saw, “Experimental analysis of R134a working fluid on Organic Rankine Cycle (ORC) systems with scroll-expander,” *Eng. Sci. Technol. an Int. J.*, no. xxxx, 2021, doi: 10.1016/j.jestch.2021.06.016.
- [97] K. J. Harada, “Development of a Small Scale Scroll Expander,” *Zhurnal Eksp. i Teor. Fiz.*, pp. 1–142, 2010.
- [98] “11 kW Semi-Hermetic Steam Scroll Expander.” <https://airsquared.com/projects/11-kw-semi-hermetic-steam-scroll-expander/>.
- [99] H. J. Kim, J. M. Ahn, I. Park, and P. C. Rha, “Scroll expander for power generation from a low-grade steam source,” *Proc. Inst. Mech. Eng. Part A J. Power Energy*, vol. 221, no. 5, pp. 705–712, 2007, doi: 10.1243/09576509JPE392.
- [100] J. Dieckmann and TIAX LLC, “Waste Heat-to-Power Using Scroll Expander for Organic Rankine Bottoming Cycle,” 2017.
- [101] J. C. Chang, C. W. Chang, T. C. Hung, J. R. Lin, and K. C. Huang, “Experimental study and CFD approach for scroll type expander used in low-temperature organic Rankine cycle,” *Appl. Therm. Eng.*, vol. 73, no. 2, pp. 1444–1452, 2014, doi: 10.1016/j.applthermaleng.2014.08.050.
- [102] P. Iodice, G. Langella, and A. Amoresano, “Energy performance and numerical optimization of a screw expander–based solar thermal electricity system in a widerange of fluctuating operating conditions,” *Int. J. Energy Res.*, no. 03, pp. 1858–1874, 2020.
- [103] G. F. Robertson, “Experimental and analytical study of a steam vane expander,” 1977.
- [104] M. Mahardika, “Experimental and CFD analysis of rotary multi vane expander for small capacity generation,” *MATEC Web Conf.*, vol. 204, pp. 1–6, 2018, doi: 10.1051/mateconf/201820406007.
- [105] W. Suankramdee, T. Thongtip, and S. Aphornratana, “Experimental study of a sliding vane expander in a micro-scale ORC system for utilizing low-grade heat,” *Energy Procedia*, vol. 138, pp. 823–828, 2017, doi: 10.1016/j.egypro.2017.10.085.
- [106] F. Fatigati, M. Di Bartolomeo, and R. Cipollone, “Dual intake rotary vane expander technology: Experimental and theoretical assessment,” *Energy Convers. Manag.*, vol. 186, no. October 2018, pp. 156–167, 2019, doi: 10.1016/j.enconman.2019.02.026.
- [107] G. Żywica, T. Kaczmarczyk, and E. Ichnatowicz, “Expanders for dispersed power generation: maintenance and diagnostics problems,” *Trans. Inst. Fluid-Flow Mach.*, vol. 131, no. 131, pp. 173–188, 2016.
- [108] Barber-Nichols, “How to Select Turbomachinery For Your Application,” 1999.
- [109] D. Ziviani *et al.*, “PDSim: Demonstrating the capabilities of an open-source simulation framework for positive displacement compressors and expanders,” *Int. J. Refrig.*, vol. 110, pp. 323–339, 2020, doi: 10.1016/j.ijrefrig.2019.10.015.
- [110] A. Giuffrida, “Improving the semi-empirical modelling of a single-screw expander for small organic Rankine cycles,” *Appl. Energy*, vol. 193, pp. 356–368, 2017, doi: 10.1016/j.apenergy.2017.02.015.
- [111] D. Ziviani *et al.*, “Characterizing the performance of a single-screw expander in a small-scale organic Rankine cycle for waste heat recovery,” *Appl. Energy*, vol. 181, pp. 155–170, 2016, doi: 10.1016/j.apenergy.2016.08.048.
- [112] X. Zhang, Z. Li, J. Wang, Y. Wu, and C. Ma, “Performance Improvement of KCS (Kalina Cycle System) 34 by Replacing Throttle Valve With Single-Screw Expander,” *Front. Energy Res.*, vol. 9, no. October, pp. 1–11, 2021, doi: 10.3389/fenrg.2021.741704.
- [113] J. Wang, Y. Zhang, W. Wang, and Y. Zhang, “Comparative analysis of electric power

- and steam loss rate between single flash and binary geothermal power system with single screw expander,” *Adv. Mater. Res.*, vol. 354–355, pp. 325–328, 2012, doi: 10.4028/www.scientific.net/AMR.354-355.325.
- [114] D. Ziviani, I. H. Bell, M. De Paepe, and M. Van Den Broek, “Update on single-screw expander geometry model integrated into an open-source simulation tool,” *IOP Conf. Ser. Mater. Sci. Eng.*, vol. 90, no. 1, 2015, doi: 10.1088/1757-899X/90/1/012064.
- [115] I. H. Bell *et al.*, “PDSim: A general quasi-steady modeling approach for positive displacement compressors and expanders,” *Int. J. Refrig.*, vol. 110, pp. 310–322, 2020, doi: 10.1016/j.ijrefrig.2019.09.002.
- [116] D. Ziviani, A. Desideri, V. Lemort, M. De Paepe, and M. Van Den Broek, “Low-order models of a single-screw expander for organic Rankine cycle applications,” *IOP Conf. Ser. Mater. Sci. Eng.*, vol. 90, no. 1, 2015, doi: 10.1088/1757-899X/90/1/012061.
- [117] “SCORG alto.” <https://scorg.info/>.
- [118] “SCCAD - development and application of a software package for the design of screw compressors.” <https://www.swmath.org/software/18556>.
- [119] “KaSim - simulations, screw type machine.” <https://www.osti.gov/etdeweb/biblio/20780758>.
- [120] V. Lemort, S. Quoilin, C. Cuevas, and J. Lebrun, “Testing and modeling a scroll expander integrated into an Organic Rankine Cycle,” *Appl. Therm. Eng.*, vol. 29, no. 14–15, pp. 3094–3102, 2009, doi: 10.1016/j.applthermaleng.2009.04.013.
- [121] J. Muye, G. Praveen Kumar, J. C. Bruno, R. Saravanan, and A. Coronas, “Modelling of scroll expander for different working fluids for low capacity power generation,” *Appl. Therm. Eng.*, vol. 159, no. June, 2019, doi: 10.1016/j.applthermaleng.2019.113932.
- [122] “Github - ibell/pdsim.” <https://github.com/ibell/pdsim>.
- [123] “Github / PDSim / Issues.” <https://github.com/ibell/pdsim/issues/72>.
- [124] M. Rathán, “Carnotovy baterie využívající odpadní teplo - analýza a optimalizace konfigurací a parametrů systému,” Thesis, CTU Prague, 2021.
- [125] A. M. Pantaleo, S. Camporeale, and B. Fortunato, “Small scale biomass CHP: Techno-economic performance of steam vs gas turbines with bottoming ORC,” *Energy Procedia*, vol. 82, pp. 825–832, 2015, doi: 10.1016/j.egypro.2015.11.819.
- [126] X. Zhang, L. Wu, X. Wang, and G. Ju, “Comparative study of waste heat steam SRC, ORC and S-ORC power generation systems in medium-low temperature,” *Appl. Therm. Eng.*, vol. 106, pp. 1427–1439, 2016, doi: 10.1016/j.applthermaleng.2016.06.108.
- [127] P. Capaldi, “A high efficiency 20 kWe microcogeneration unit based on a turbocharged automotive gas engine,” *Appl. Therm. Eng.*, vol. 109, pp. 803–808, 2016, doi: 10.1016/j.applthermaleng.2016.03.019.
- [128] X. Wang, X. Liang, Z. Hao, and R. Chen, “Comparison of electrical and mechanical water pump performance in internal combustion engine,” *Int. J. Veh. Syst. Model. Test.*, vol. 10, no. 3, pp. 205–223, 2015, doi: 10.1504/IJVSMT.2015.070155.
- [129] Y. Cengel and M. Boles, *Thermodynamics: an engineering approach*, 6th ed. McGraw-Hill, 2007.
- [130] Y. V. Shatskikh, A. I. Sharapov, and I. G. Byankin, “Analysis of Deep Heat Recovery from Flue Gases,” *J. Phys. Conf. Ser.*, vol. 891, no. 1, 2017, doi: 10.1088/1742-6596/891/1/012188.

List of appendices

- Appendix A** **Geometry of designed expanders**
- Appendix B** **Single-screw expander geometry model**
(electronic appendix)
- Appendix C** **Single-screw expander thermodynamic model 1**
(version 1, determining the influence of BVR on performance;
electronic appendix)
- Appendix D** **Single-screw expander thermodynamic model 2**
(version 2, determining the influence of V_{sw} on performance;
electronic appendix)
- Appendix E** **Single-screw expander thermodynamic model 3**
(version 3, sensitivity analysis for a given expander geometry;
electronic appendix)
- Appendix F** **Script for generating 3D surface graphs**
(electronic appendix)

Appendix A Geometry of designed expanders

Expander label	A	B	C	D	E	F
Parameter						
Z_{sr}	6					
Z_{sw}	11					
i	1,83					
D_{sr} [mm]	239,06	327,53	398,52	301,18	140,72	192,22
D_{sw} [mm]	246,40	329,63	396,34	306,86	165,02	201,94
$D_{sw,in}$ [mm]	82,13	109,88	198,17	102,29	55,01	67,31
w_t [mm]	35,82	49,08	59,72	45,13	21,09	28,80
λ_d [-]	1,03	1,01	0,99	1,02	1,17	1,05
$d_{sr,sw}$ [mm]	191,25	262,02	318,81	240,94	112,57	153,78
λ_{opt} [-]	0,80					
β_s [°]	54,40	53,40	52,89	53,92	59,23	55,17
β^* [°]	8,36	8,56	8,67	8,46	7,34	8,20
β_{in}^* [°]	51,72	53,06	35,08	52,36	45,08	50,67
β_d [°]	38,08	37,38	37,03	37,75	41,46	38,62
L_s [mm]	100,17	132,32	158,05	124,00	70,89	82,88
L_d [mm]	75,98	100,07	119,33	93,92	54,63	63,02
L^* [mm]	29,88	40,94	49,81	37,65	17,59	24,03
$L_{rot,eff}$ [mm]	176,16	232,39	277,38	217,93	125,52	145,90
α_{sw} [°]	90					
γ [°]	32,73					
β_{open} [°]	27,24	28,03	28,44	27,62	23,43	26,63
β_{close} [°]	38,92	40,05	40,63	39,46	33,47	38,04
ξ [-]	0,02					
a [mm]	71,72	98,26	119,55	90,35	42,21	57,67
BVR [-]	3,0	4,4	6,2	3,5	1,6	2,5
V_{sw} [cm ³]	1300	1800	2000	2000	1100	950
$W_{exp,conf}$ [mm]	628,89	853,68	1033,97	788,74	390,16	509,49

Table 27 - Geometry parameters of designed expanders. See Figure 28 for visualization.